

Langmuir-probe measurement through the plasma grid aperture of hydrogen negative ion source

Engrhyt Rattanawongnara¹,

Masaki Osakabe^{2,1}, Katsuyoshi Tsumori^{2,1}, Haruhisa Nakano^{2,3}, Kenichi Nagaoka^{2,3}, and Yasuhiko Takeiri²

¹Grad. University for Advanced Studies (SOKENDAI), ²National Institute for Fusion Science, ³Nagoya University

4 October 2022 @ NIBS 2022 (Padova, Italy)

Neutral Beam Injection (NBI) is an essential tool for plasma heating and current drive

- To satisfy the Lawson criteria of fusion plasmas, we need to realize high performance plasmas of $T_i=10\text{keV}$ and $n_i=10^{20} [\text{m}^{-3}]$ with external plasma heating. In addition, current drive by external power injection is necessary in tokamak device.
- In order to fulfill these requirements, NBI can be robustly applied as an external power source.
- Realization of efficient NBI system is one of the key issues in realizing efficient fusion power plant.

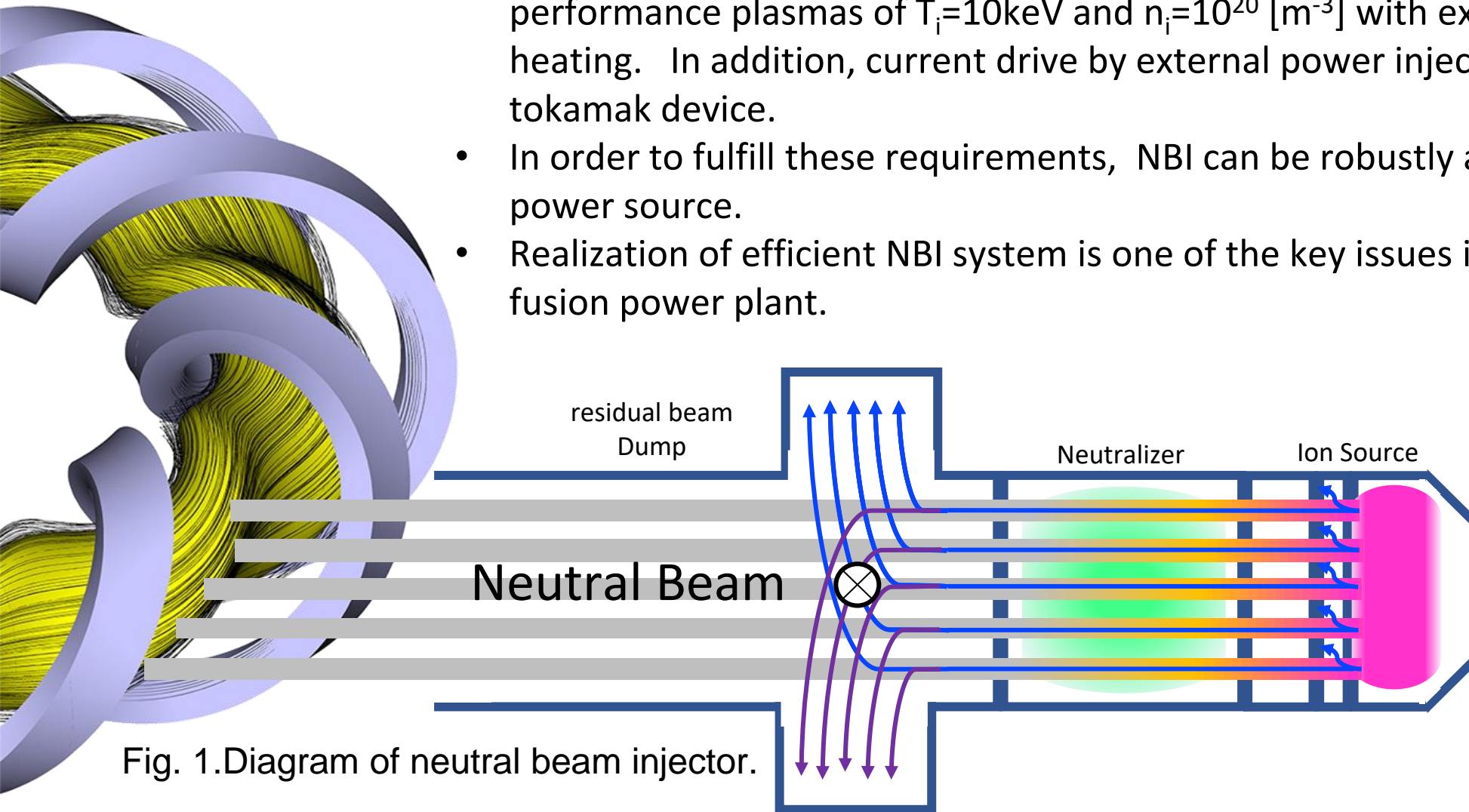


Fig. 1. Diagram of neutral beam injector.

Beam Extraction Boundary

- In the vicinity of the beam extraction aperture called “extraction area”, a meniscus is formed as a boundary between plasma and beam regions as shown in Fig. 2.
- Beamlet focusing is strongly affected by the meniscus shape, which depends on the variations of negative-ion density and applied extraction voltage

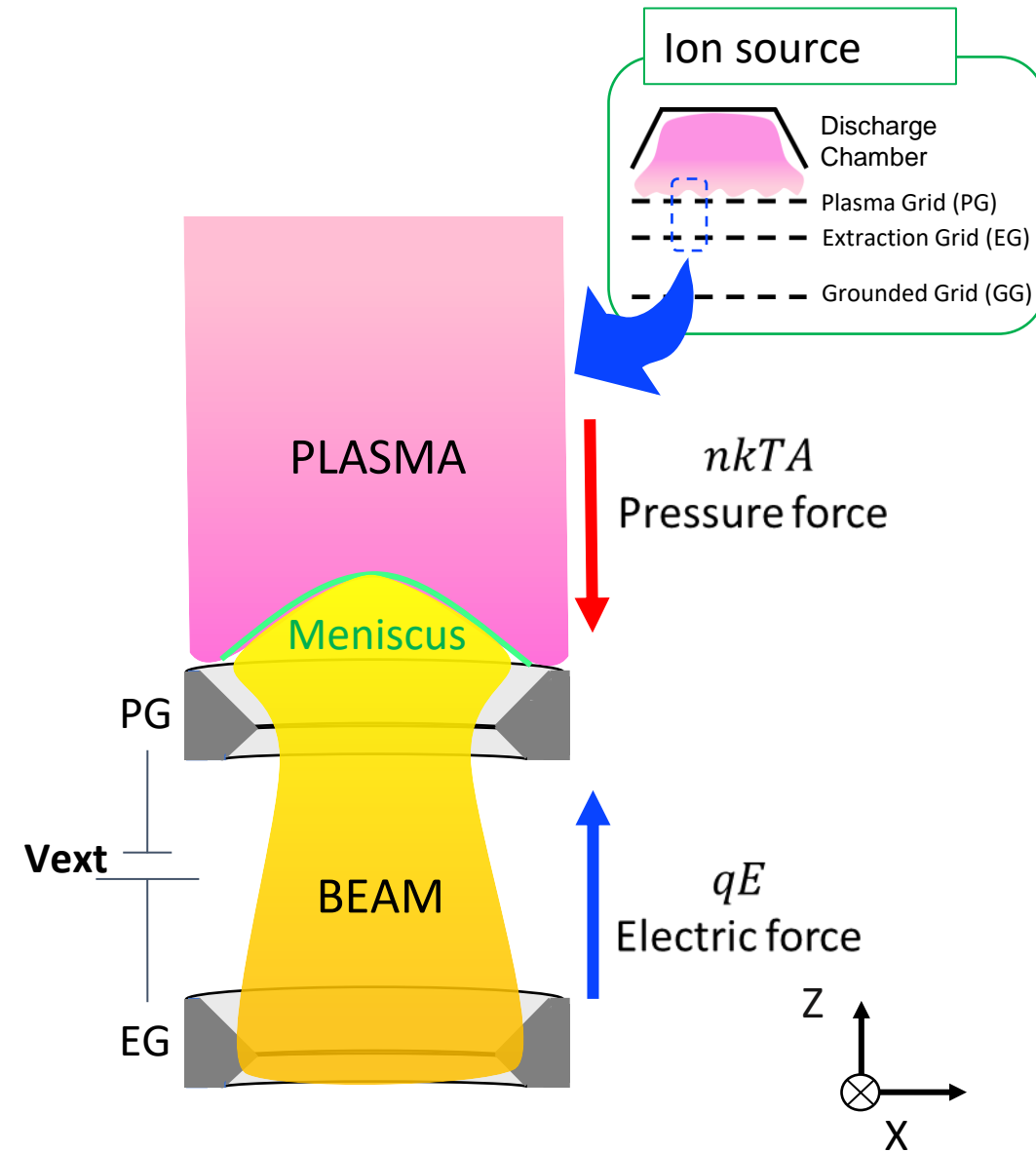


Fig. 2. Definition of the meniscus in the vicinity of the PG aperture.

Negative ion plasma

- Negative ion plasma consists of negative ion, positive ion and electron. Mainly, negative ion and positive ion conserve charge neutrality properties.
- Negative ion plasma is produced on the PG surface with lowered work function by adsorption of caesium atoms on the surface.
- The shielding mechanism to electrostatic fields in the negative-ion rich plasma can be different from ordinary plasma. This affects the formation and shape of the meniscus.

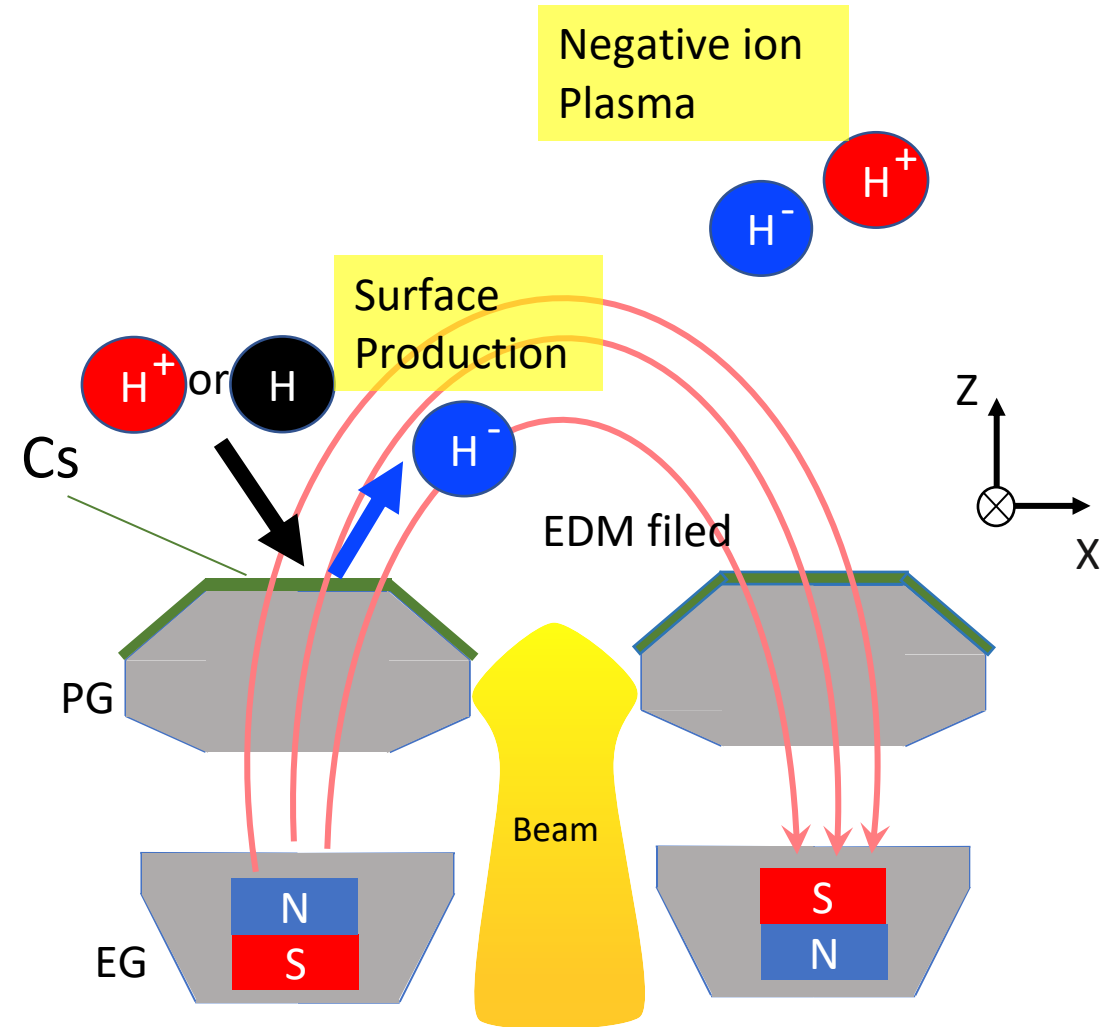


Fig. 3. Mechanism of negative ion production.

Experiment Setup

Research and development Negative ion source at NIFS (NIFS-RNIS)

- Ion Source : filament-arc type
- Input discharge power: $\sim 50\text{kW}$
- Plasma density: $\sim 2 \times 10^{17} \text{ m}^{-3}$
- Puffing gas: H_2
- Typical Operational Pressure: $\sim 0.8 \text{ Pa}$
- Cs seeding is applied for high negative-ion current operation
- Grid system:
Plasma grid(PG), Extraction Grign(EG), and Grounded Grid (GG)
- Bias voltage: $\sim 0.4\text{V}$
- Extraction voltage: 0-500V in this experiment

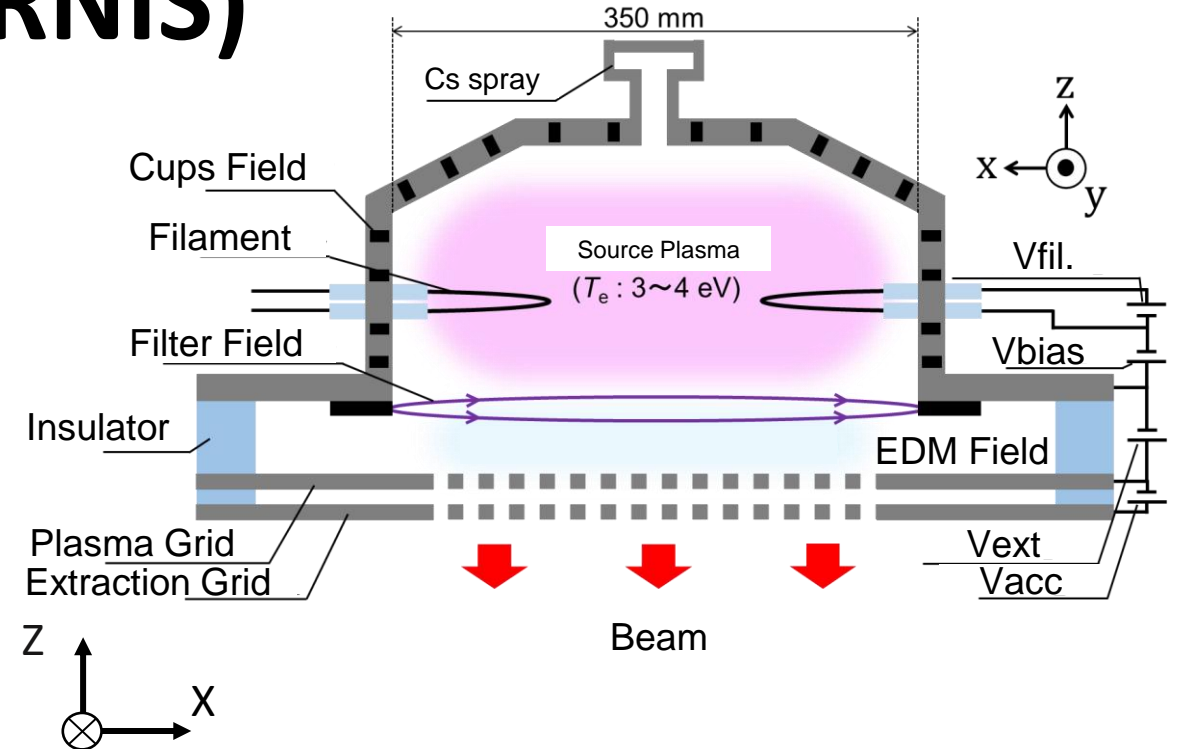


Fig. 4. Cross Section of NIFS-RNIS

Langmuir Probe (LP) Measurement is applied near/inside the beam extraction hole

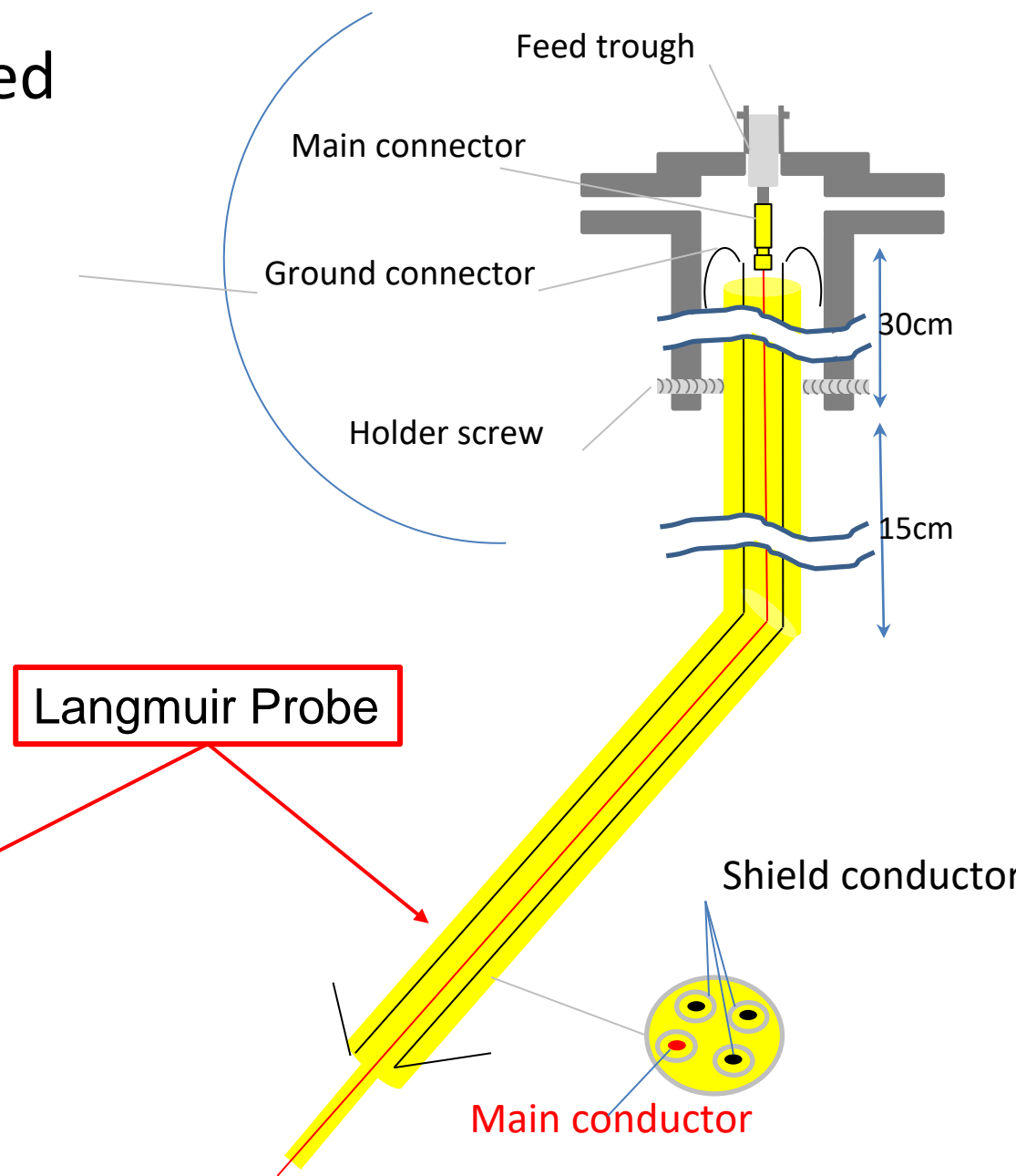
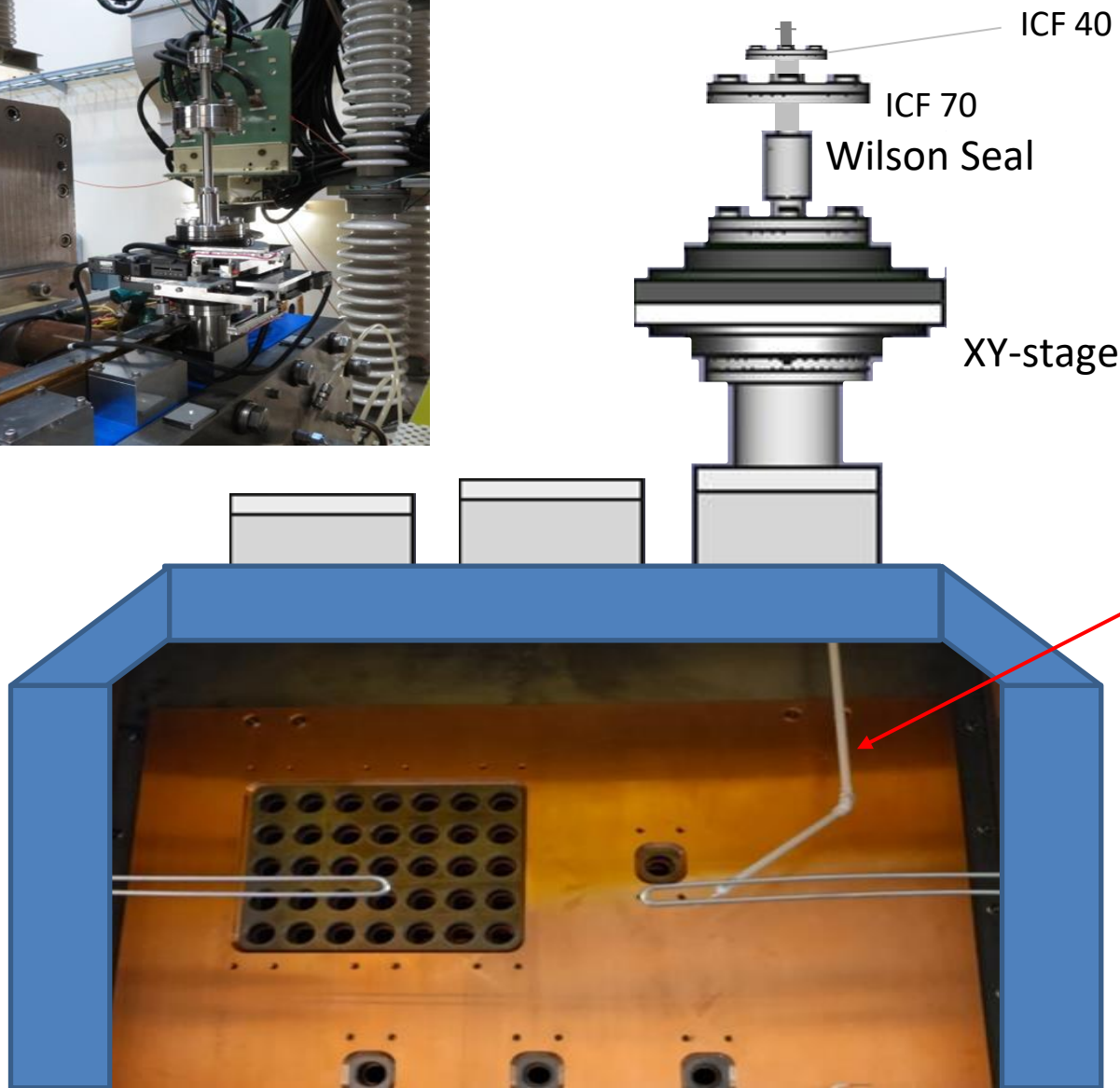
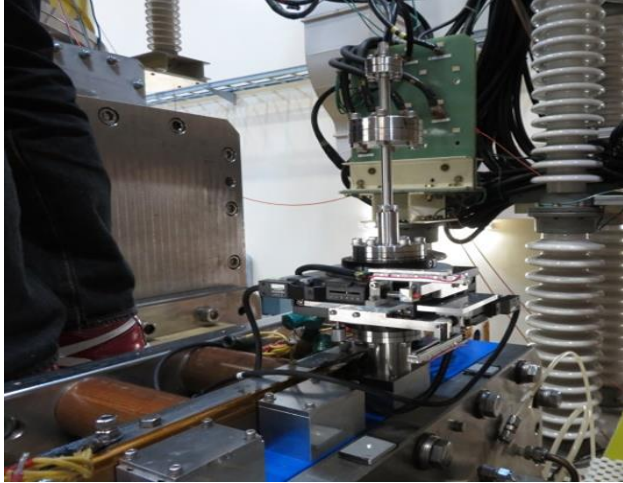
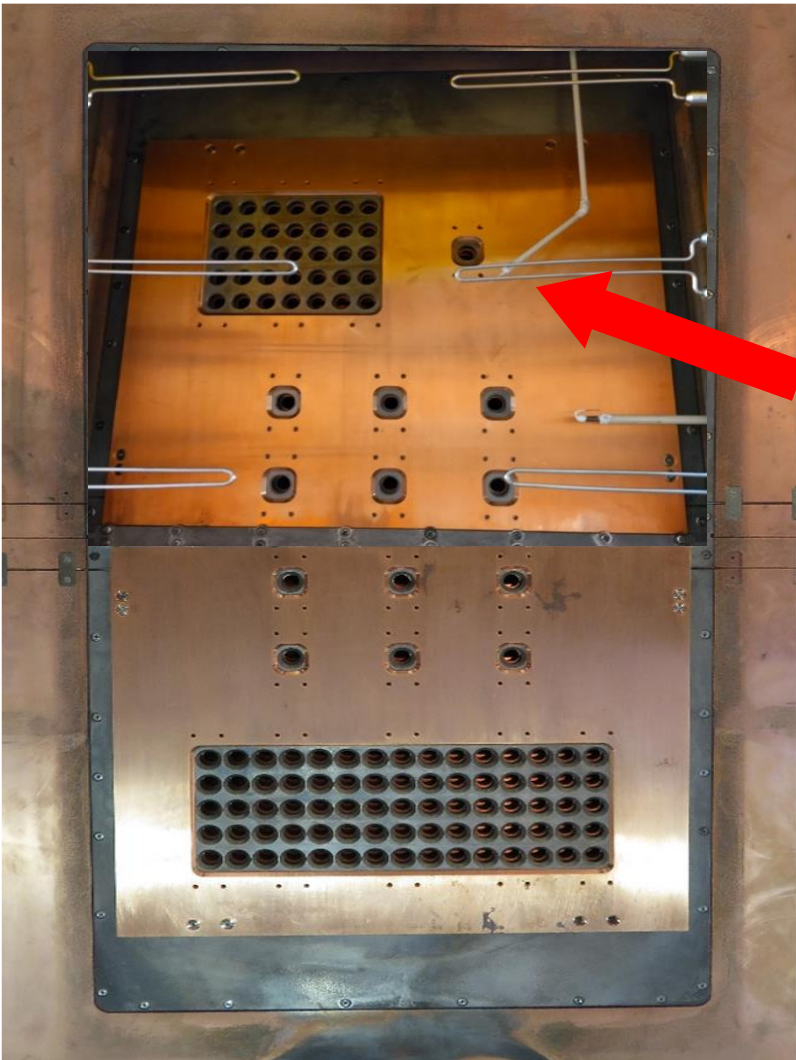
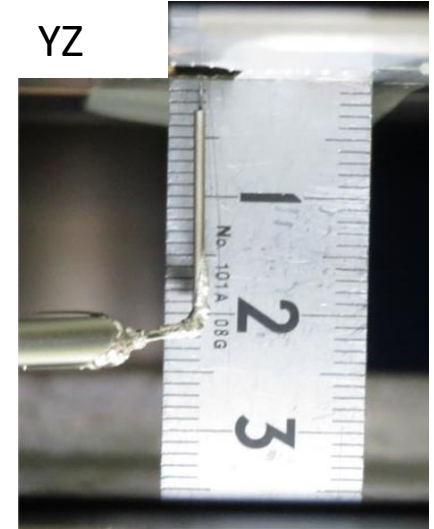
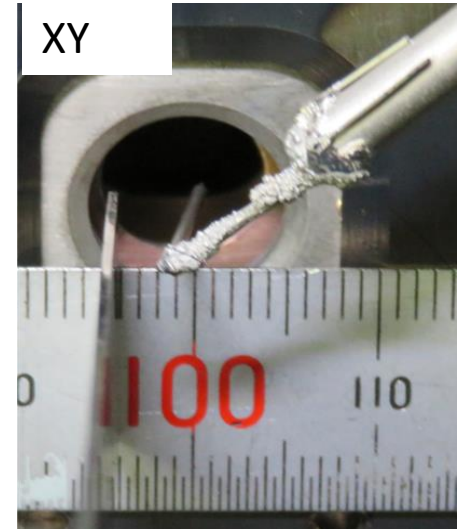
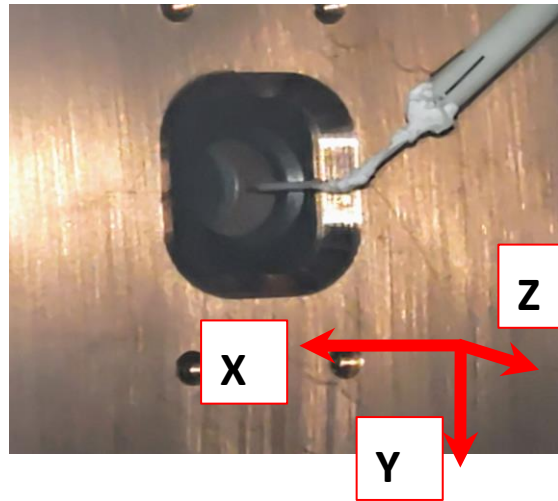


Fig. 5. Schematic drawing of LP system

Probe Geometry



Meniscus Langmuir Probe



Position of probe tip is measured with position sensor .
We set orientation of the tip to
X positive is horizontally left.
Z positive is the upstream side of the beam direction.

Fig. 6. Probe location and calibration.

Measurement Region for Probe position scan

Because mechanical movement is slow, the measurement point are changed after discharge finish.

From the figure 7, asterisk in red is a map for data analysis point and in blue is quality check the discrepancy from begin and finish of the batch.

The resolution in x direction is higher than z because we focus on precision of movement in z direction of plasma and avoid plasma parameter fluctuation by rejecting abnormal point and get more resolution when the point is valid.

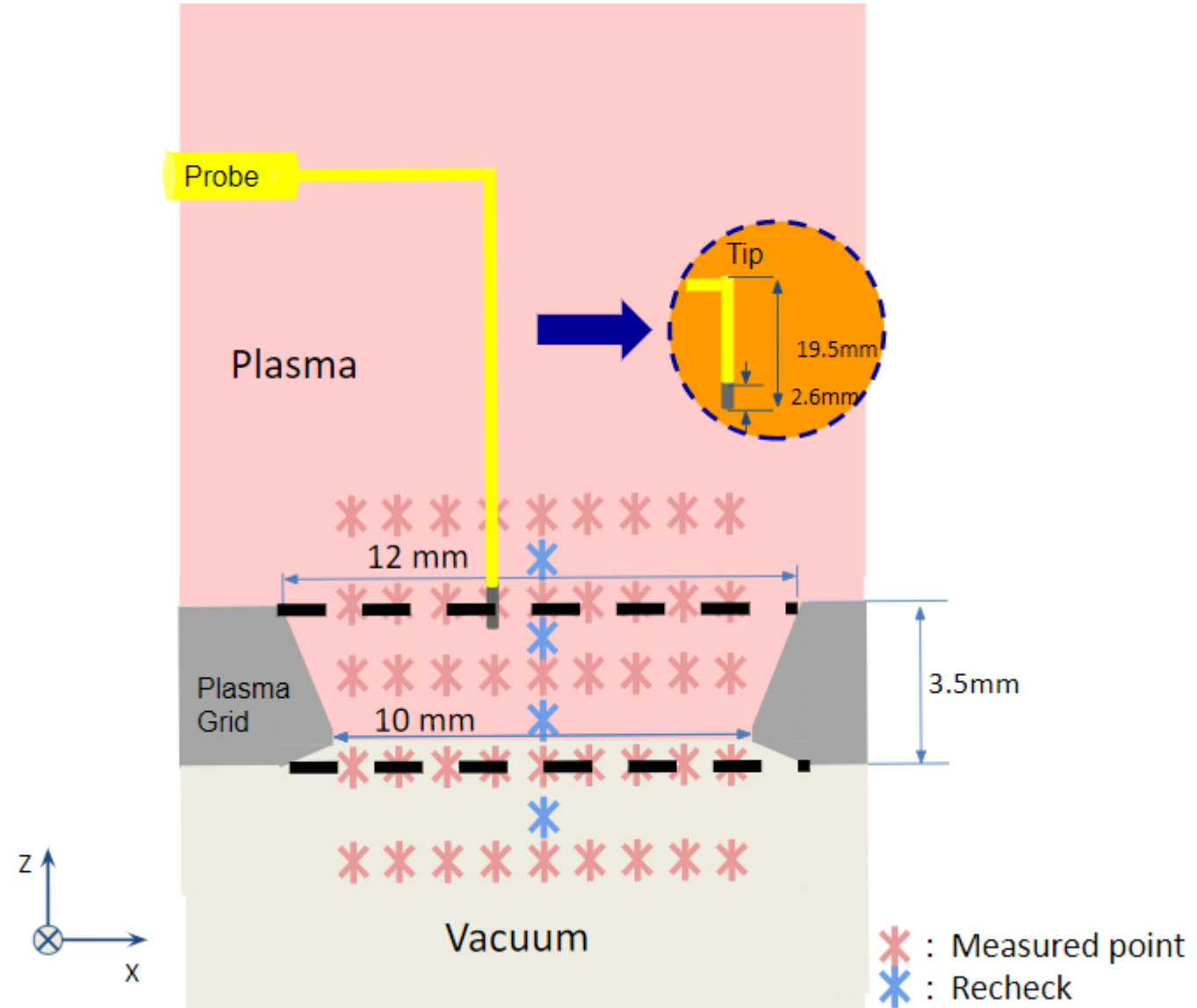
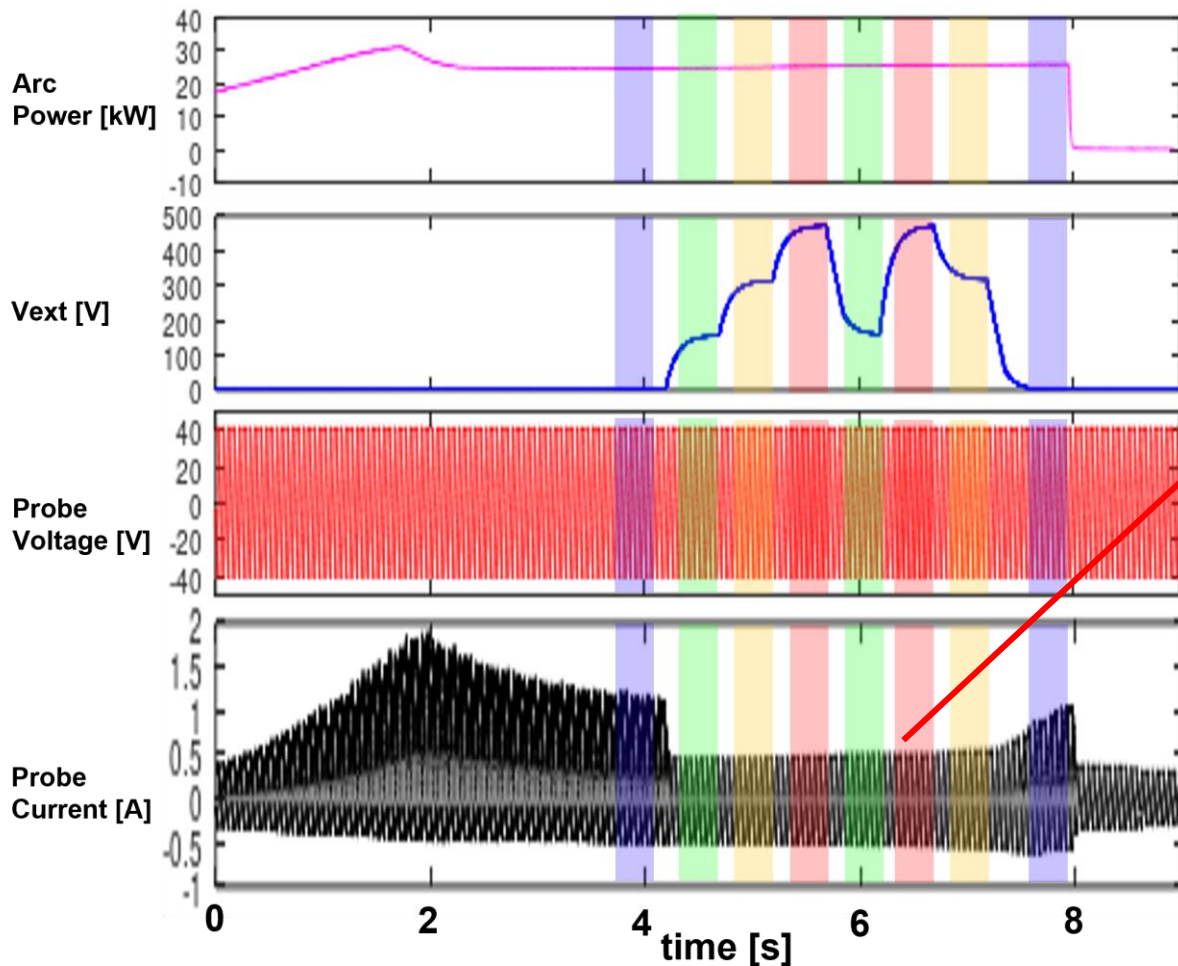


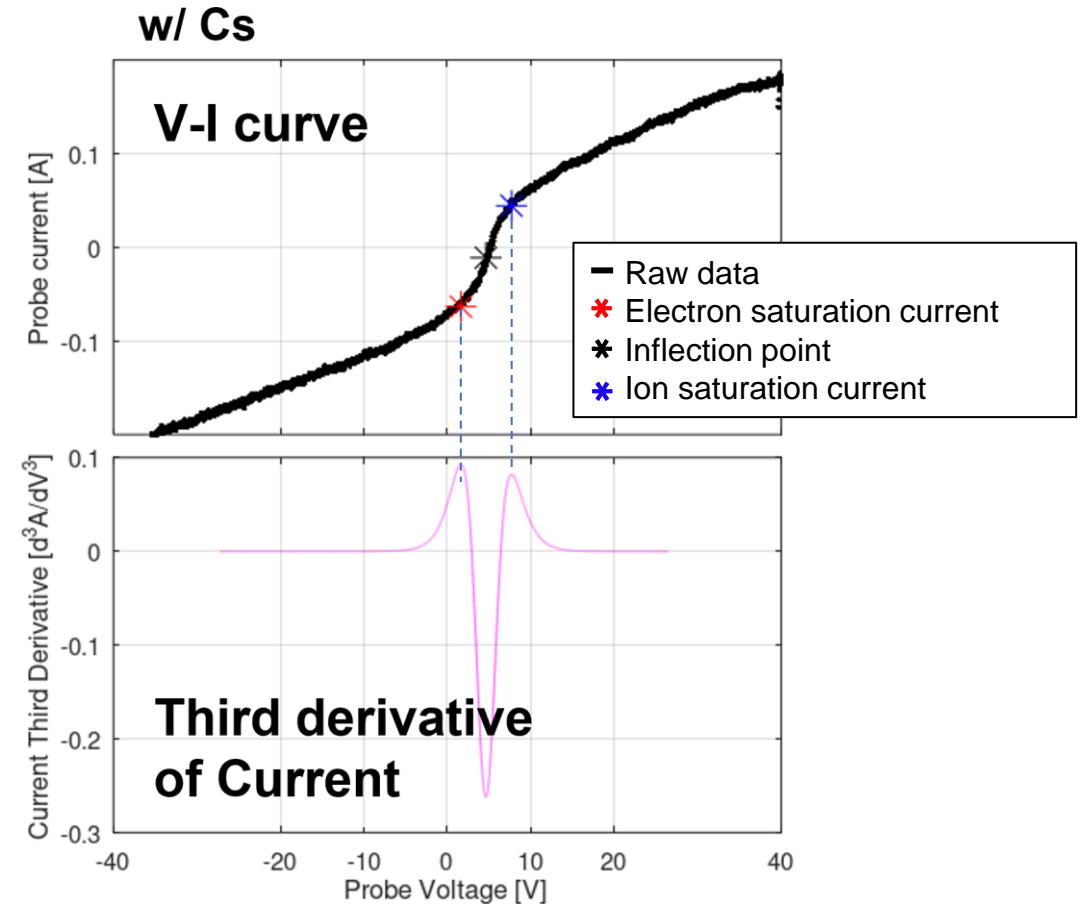
Fig. 7. Diagram of measurement point.

Typical discharge waveforms and Langmuir probe signals



Probe bias was swept for diagnostic through out the discharge.

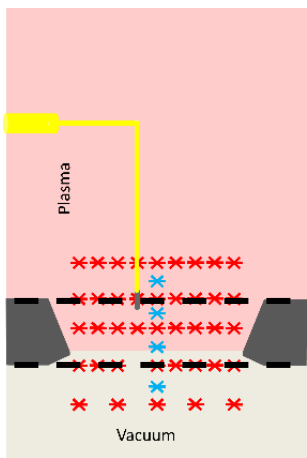
The color hatches indicate groups of sampling for each V_{ext} level.



The V-I curves are fitted to specific curve (explain in appendix). The function will track position of the retard region. Third derivative of the curve is calculated from the fitted function. The positive peak of third derivative on lower and higher probe bias voltage is use as saturation voltage for negative charge saturation current and positive charge saturation current.

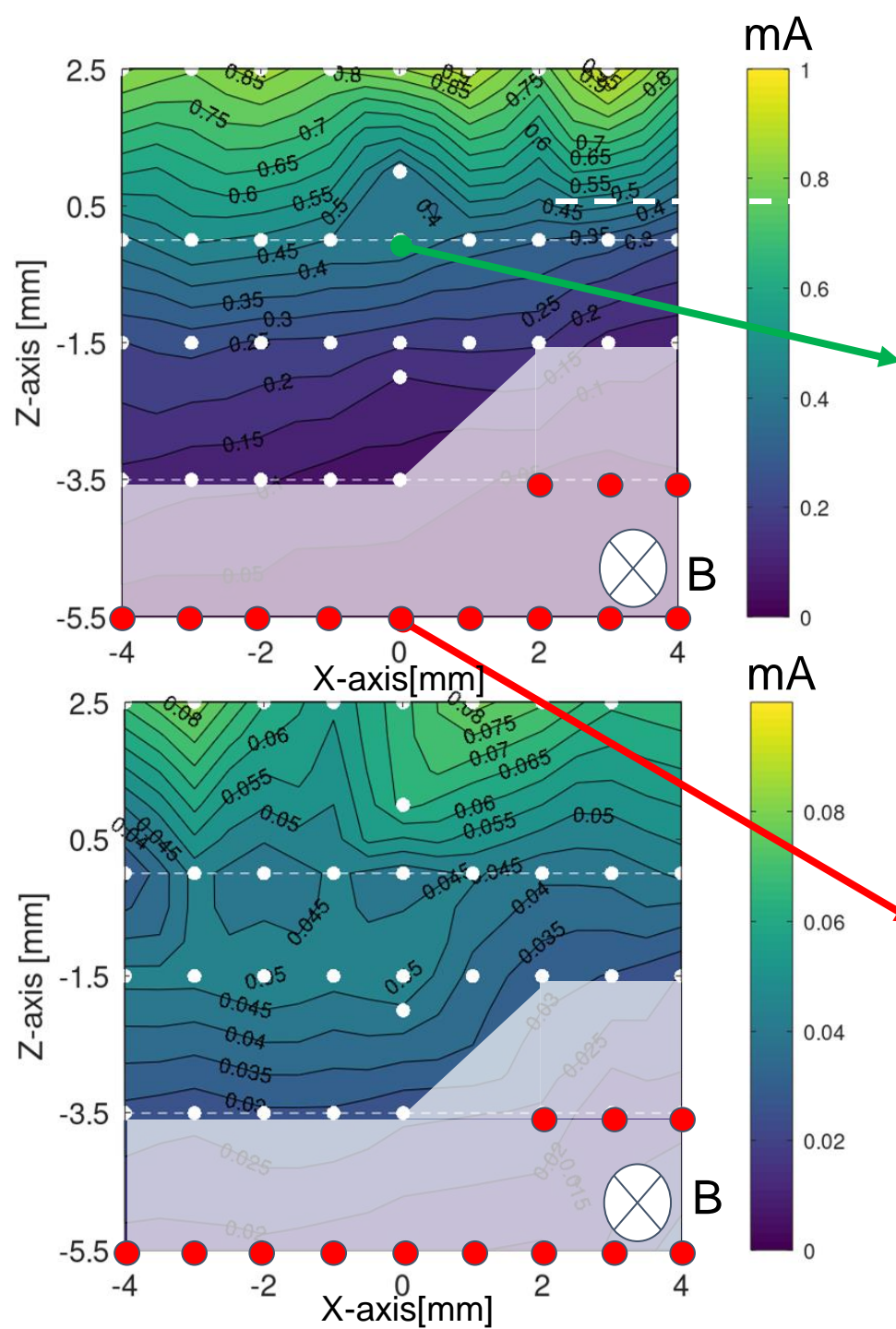
Preliminary analysis on saturation current measurement through a beam extraction hole

Extraction OFF ($V_{\text{ext}}=0\text{V}$, w/ Cs)

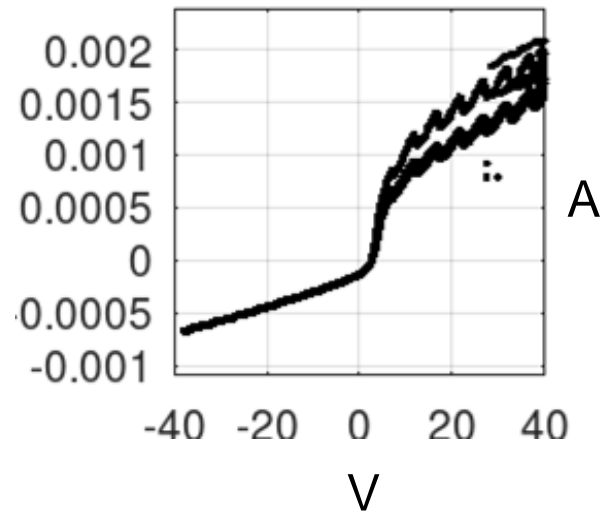


Negatively Charged Saturation Current

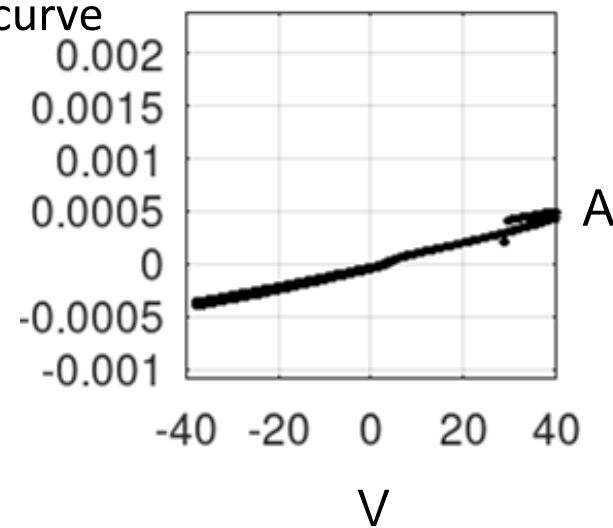
Positively Charged Saturation Current



Normal IV \circ
curve



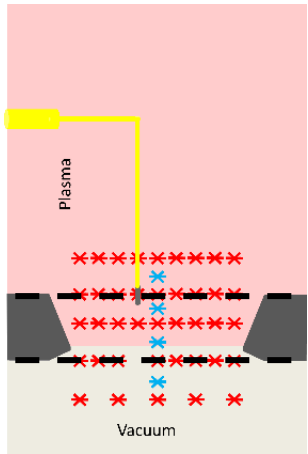
Anomaly IV \bullet
curve



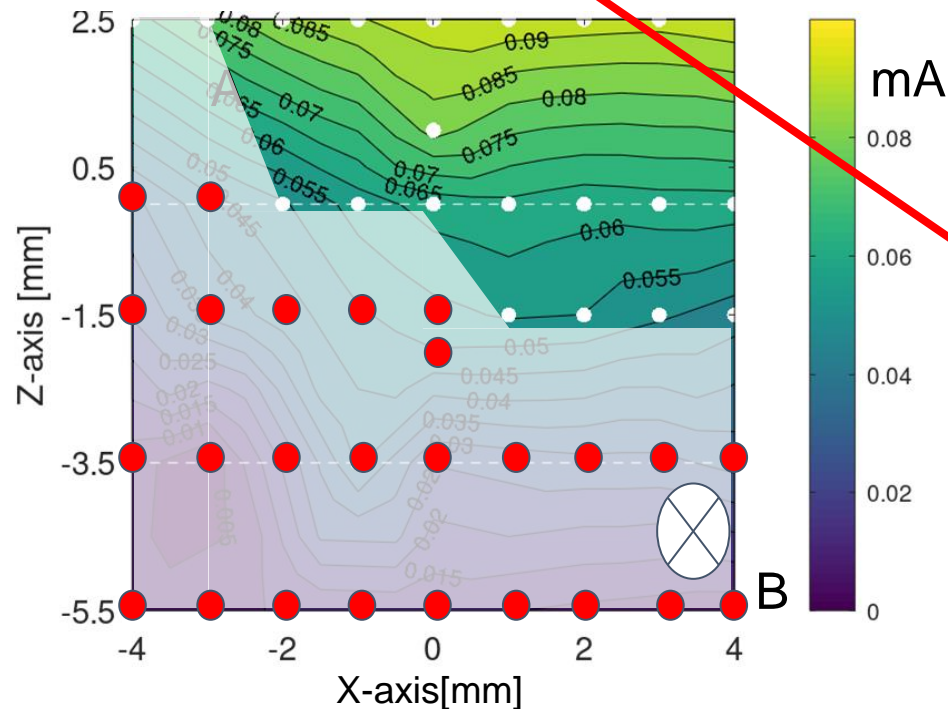
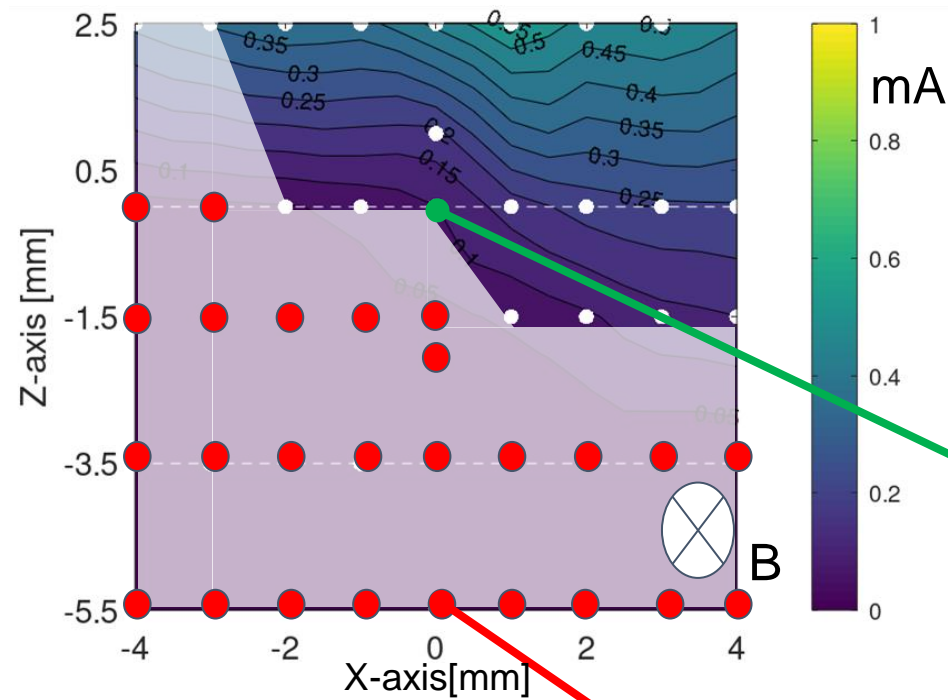
Extraction ON

($V_{\text{ext}}=450\text{V}$, w/ Cs)

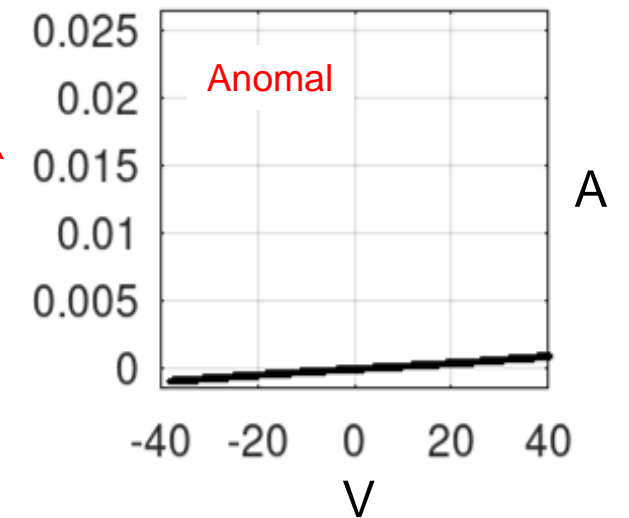
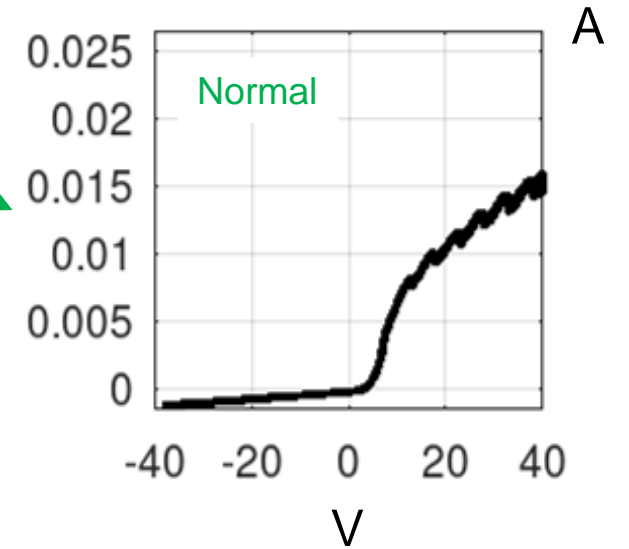
Negatively Charged Saturation Current



Positively Charged Saturation Current

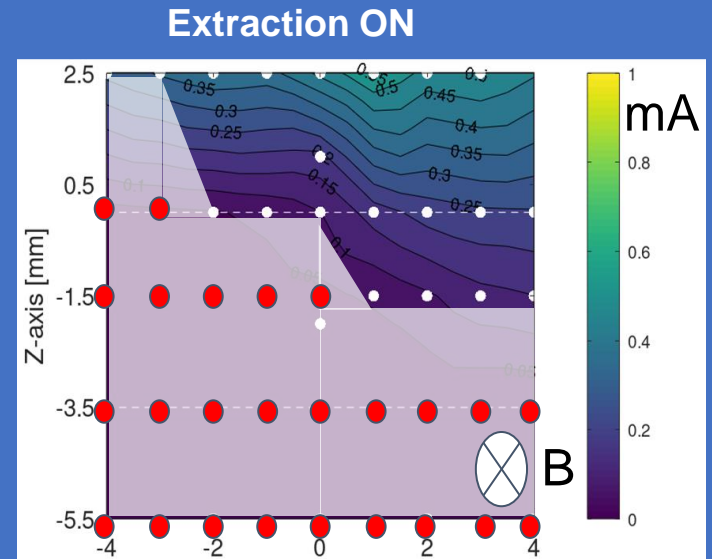
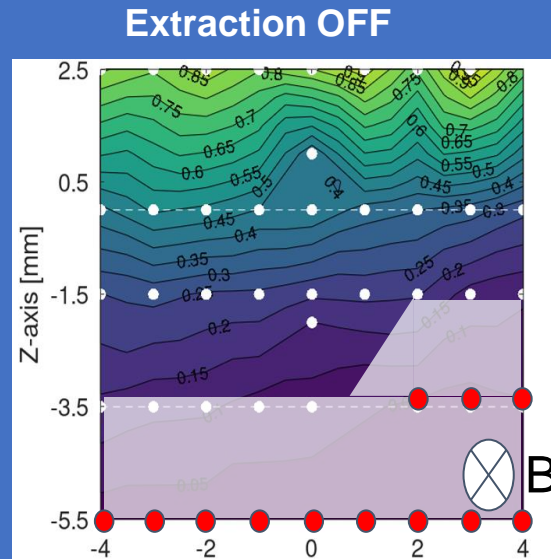


- Normal V-I curve observed
- Anomaly V-I curve observed

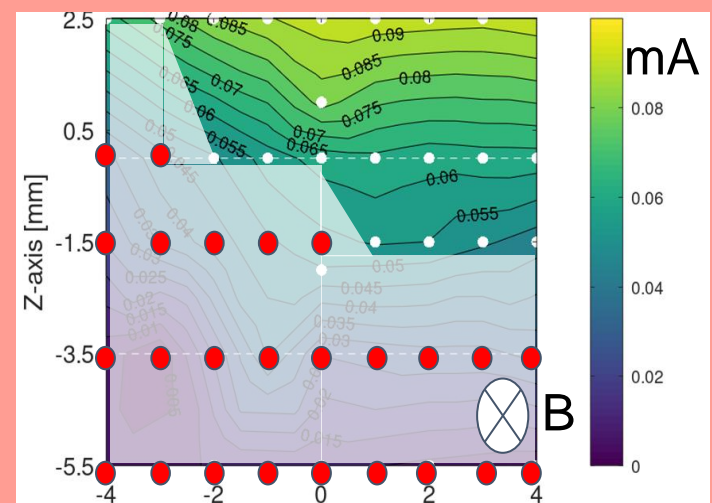
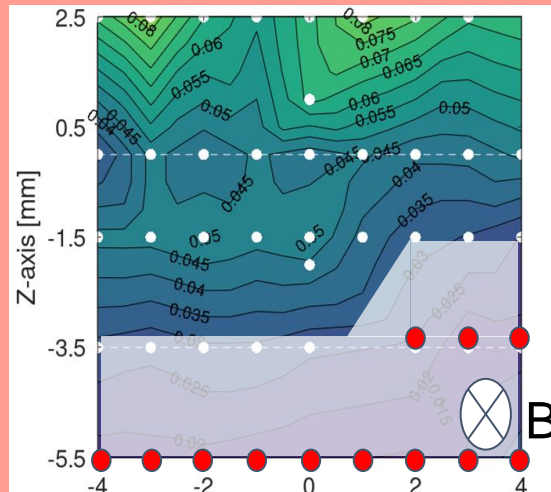


Comparison of Saturation currents with/without Extraction voltage

Negatively Charged Saturation Current

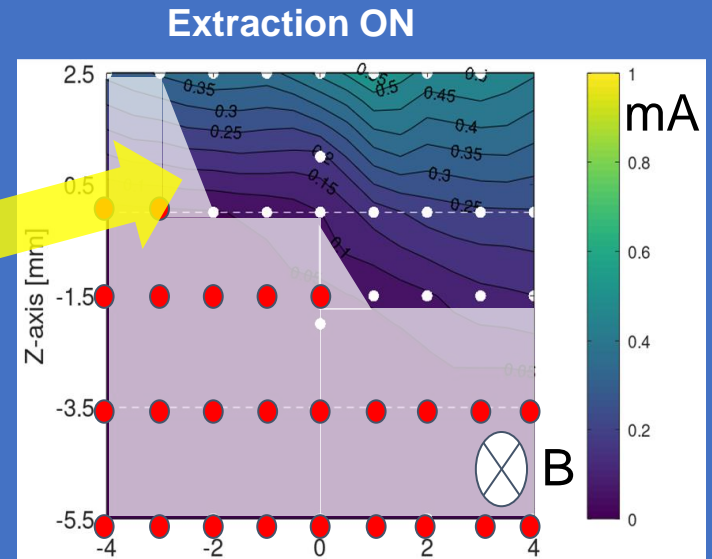
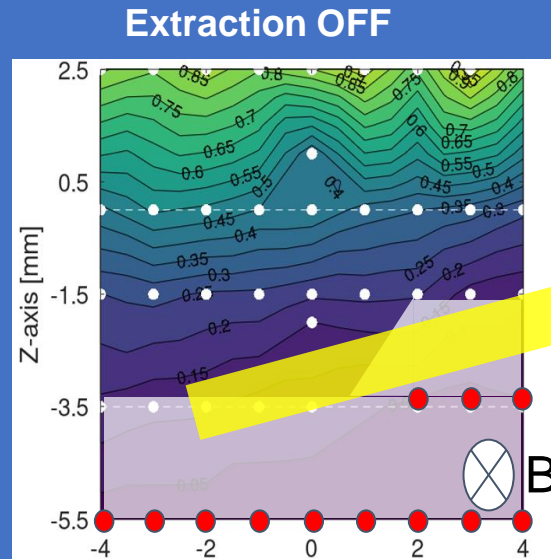


Positively Charged Saturation Current

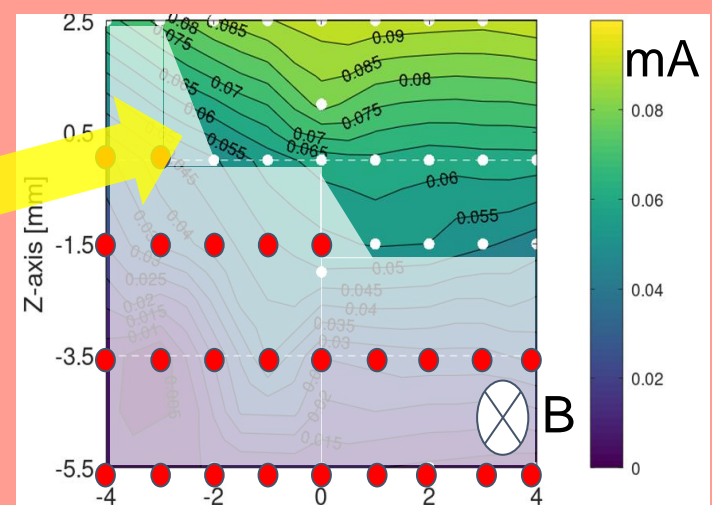
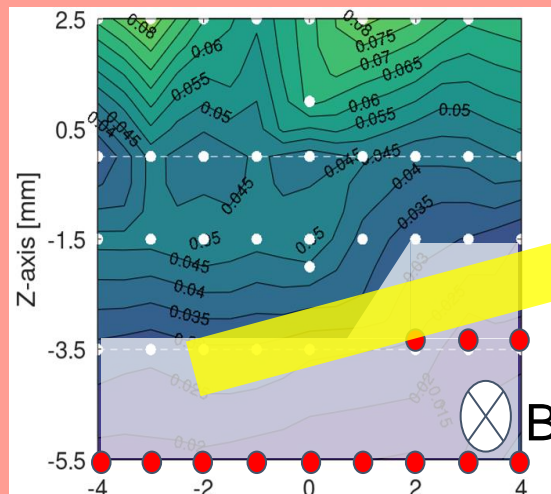


Anomaly region was expanded with the application of an extraction voltage

Negatively Charged Saturation Current

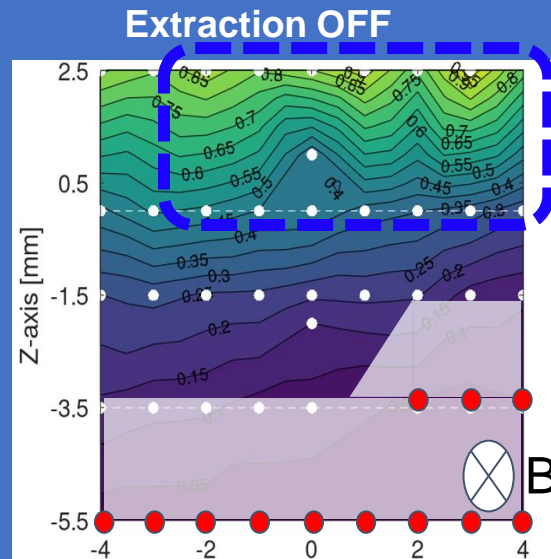


Positively Charged Saturation Current

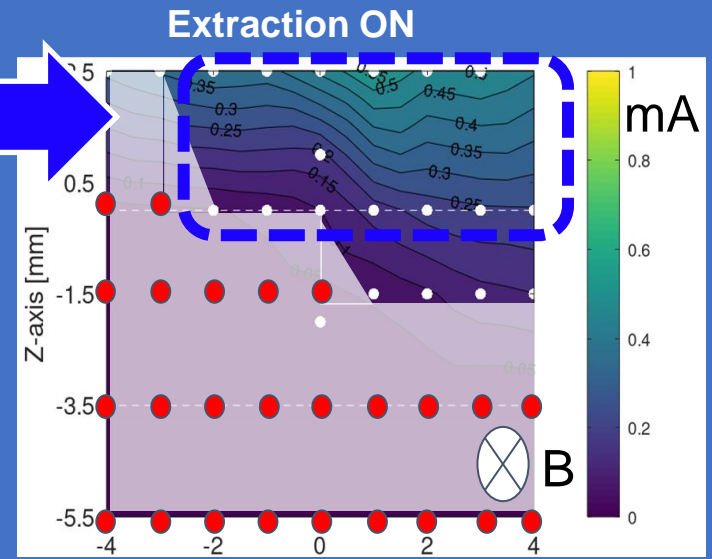


Decrease of negatively charged particles and **increase of positively charged particles** were observed with the application of extraction voltage

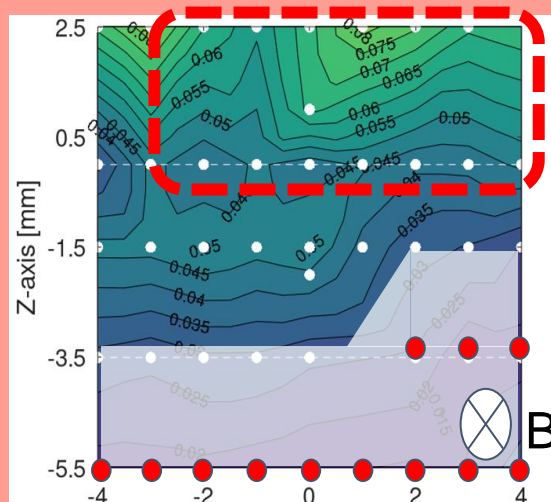
Negatively Charged Saturation Current



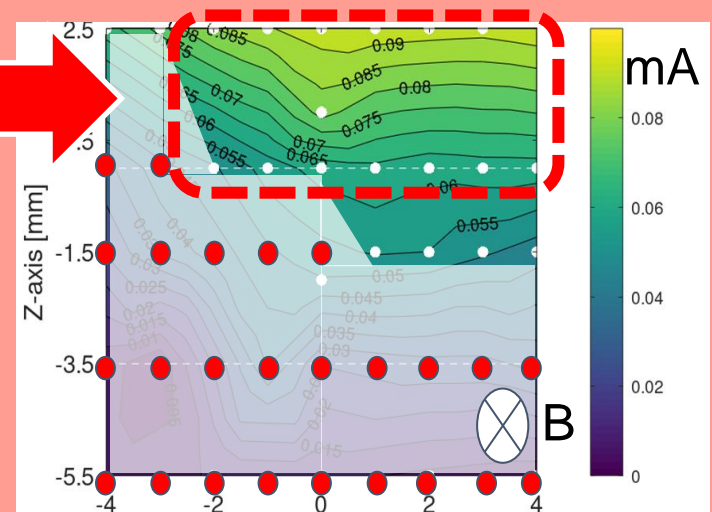
Decrease



Positively Charged Saturation Current



Increase



Summary

1. We conducted the Langmuir probe measurement through plasma grid aperture.
2. Analytical method was developed for evaluation of the saturation current from I - V curve in the negative ion plasma.
3. Preliminary measurement of plasma distribution is demonstrated in this research.

Future Plan

- The 3D spatial scan of the LP measurement will be performed to investigate the shape of plasma-beam boundary (meniscus) and the non-uniformity of negative ion densities inside the beam extraction aperture.
- The measurement of the LP will be performed at higher extraction voltage in order to observe the influence of the extraction electric field to the meniscus formation, more clearly.

Appendix 1 drift of plasma

Movement of plasma due to ExB drift

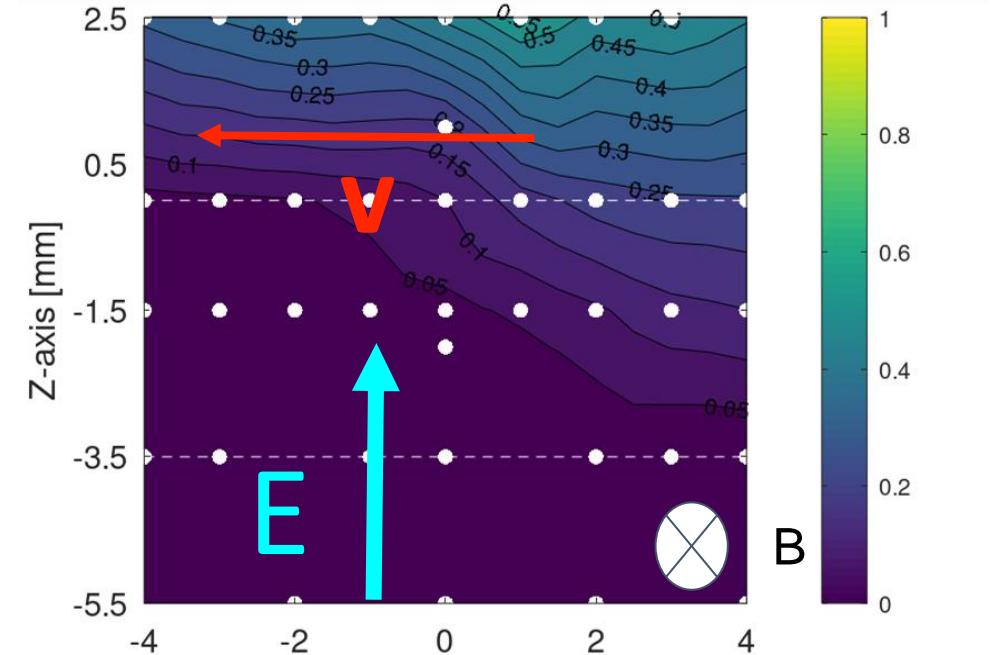
Because in the extraction area we apply magnetic field for electron deflection, the ExB drift is corresponding application of extraction field and the deflection field.

$$r = mv/qB \quad v = (kT/m)^{0.5}$$

With estimated ion temperature 0.01-0.05eV

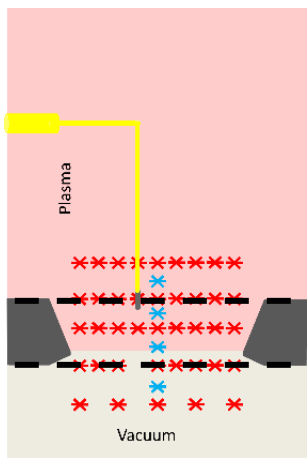
Larmor radius is 0.6-1.5mm

Radius is smaller than plasma drifting length. However, the drift direction of plasma is opposite to right hand rule.



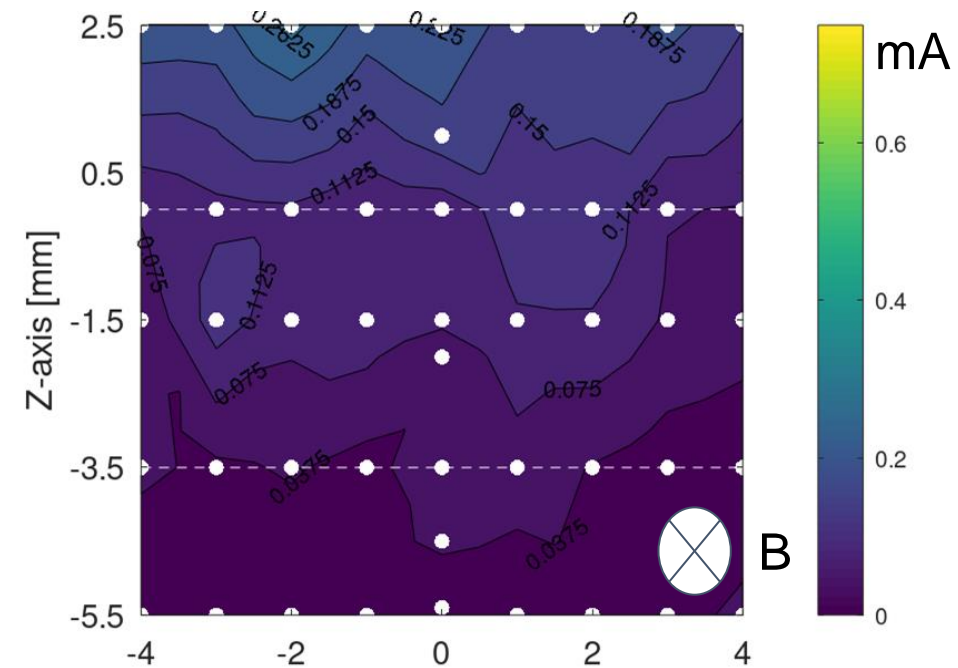
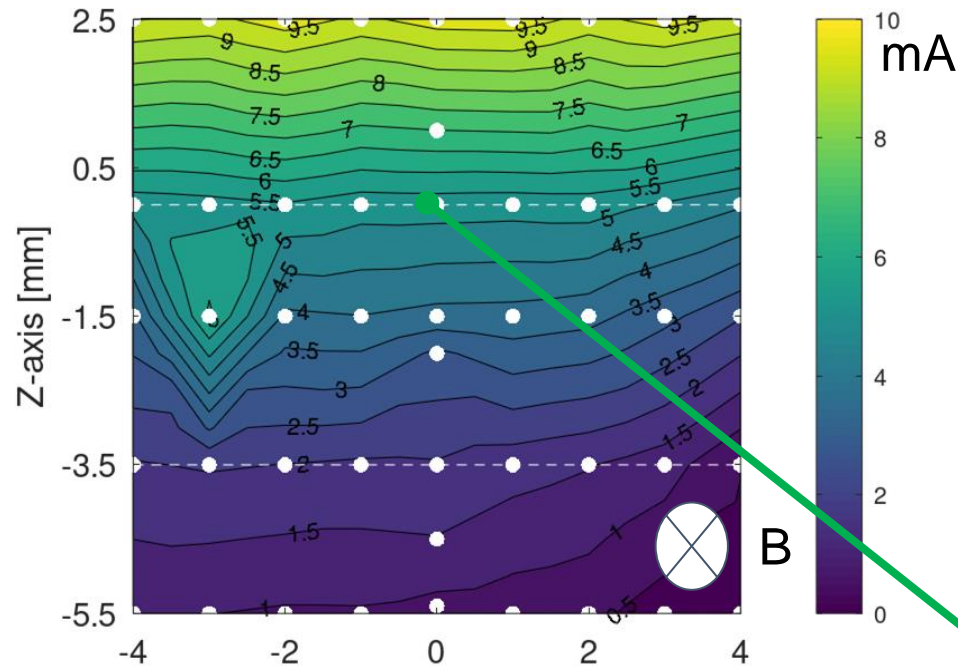
Appendix 2 non-caesiated plot

w/o-Cs $V_{ext}=0$

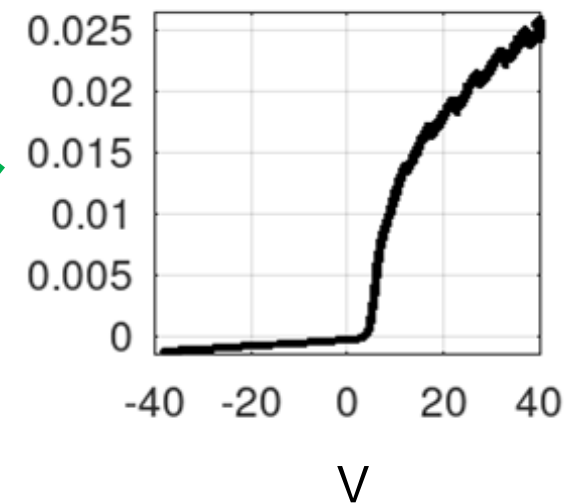


Negatively Charged Saturation Current

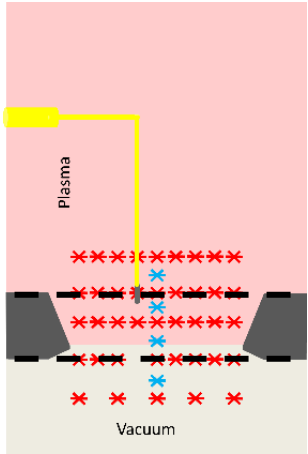
Positively Charged Saturation Current



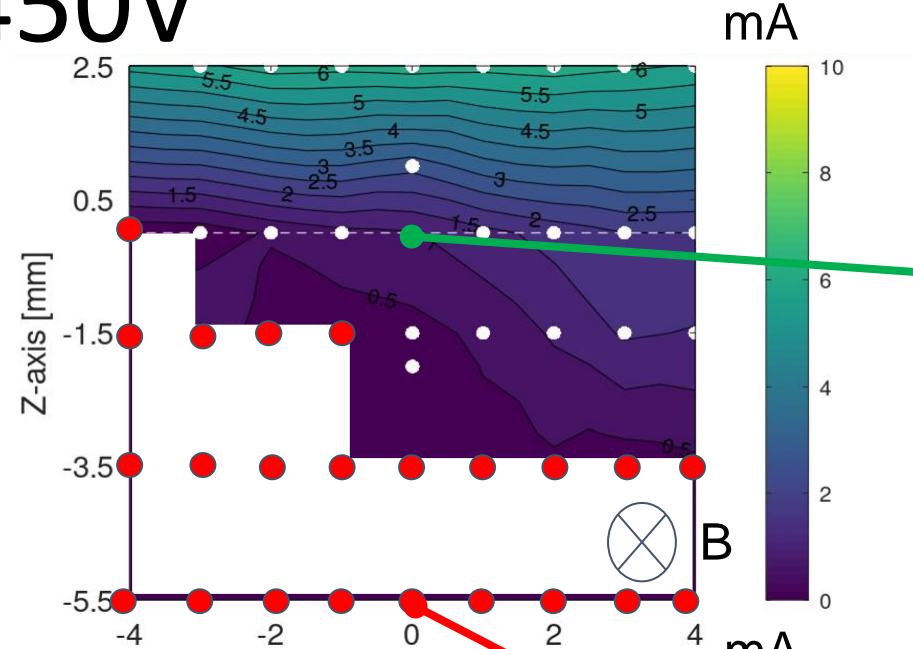
Normal IV curve



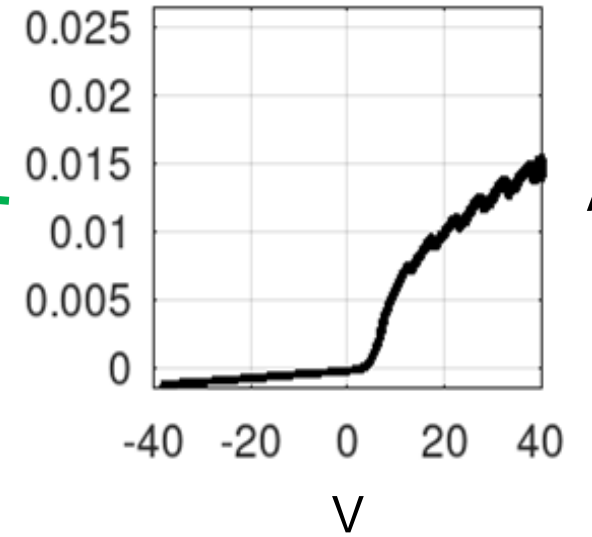
w/o-Cs $V_{ext}=450V$



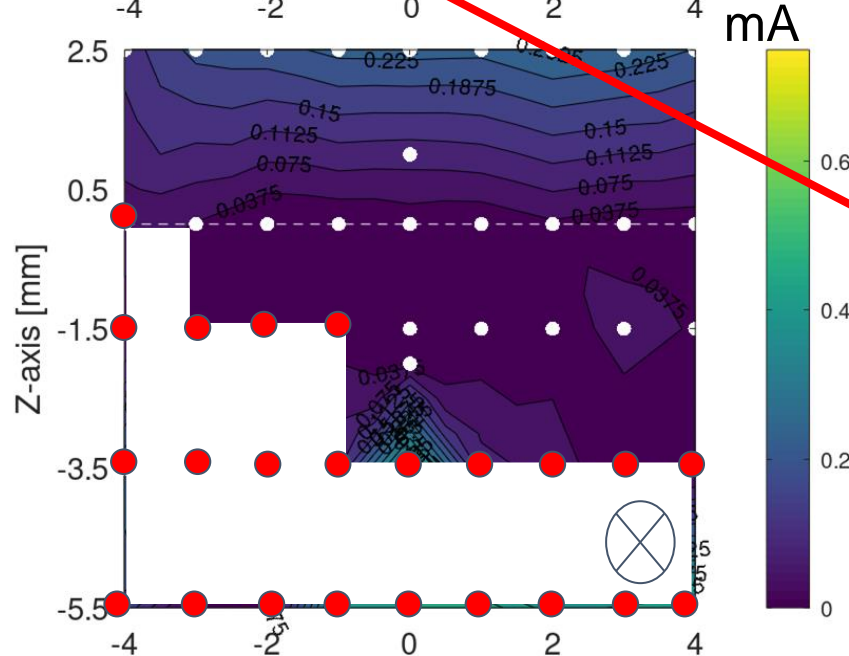
Negatively Charged Saturation Current



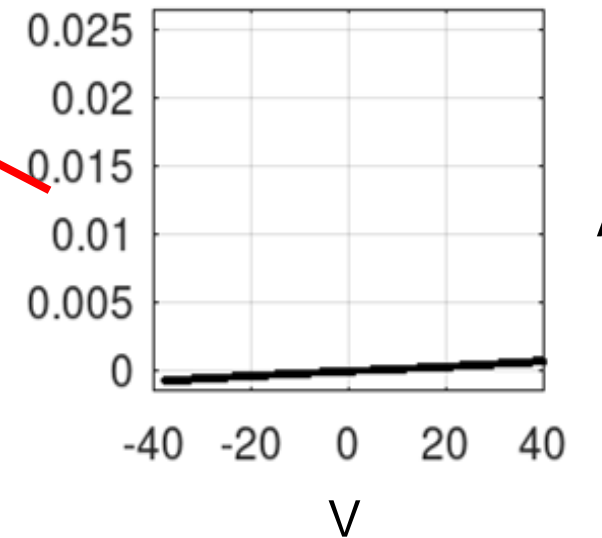
Normal IV curve



Positively Charged Saturation Current



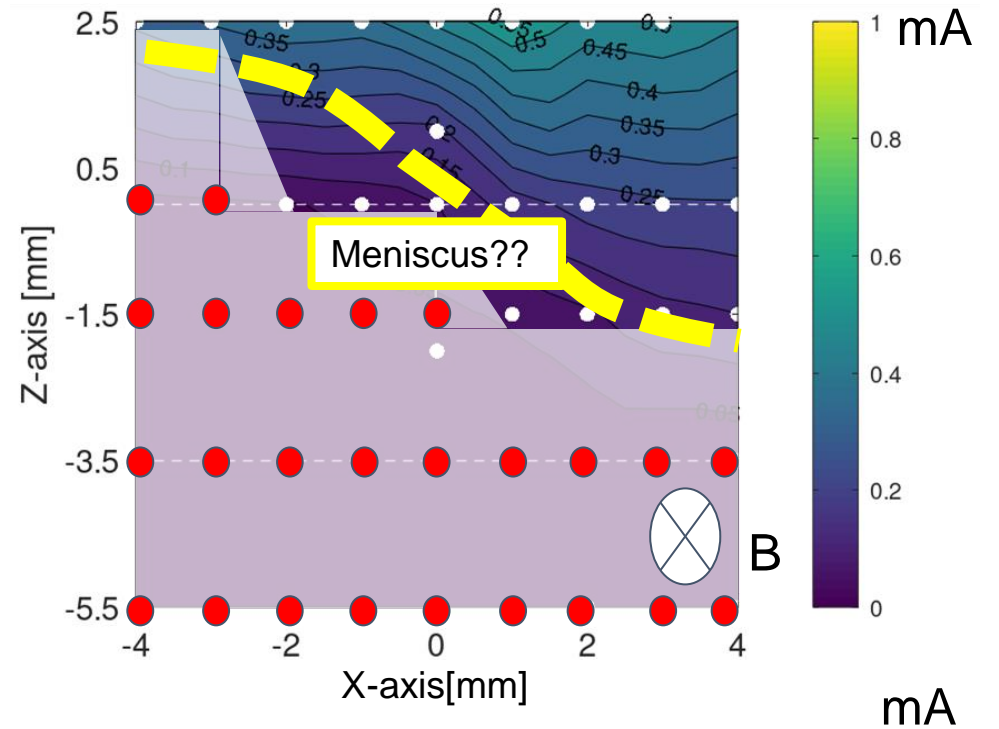
Anomaly IV curve ●



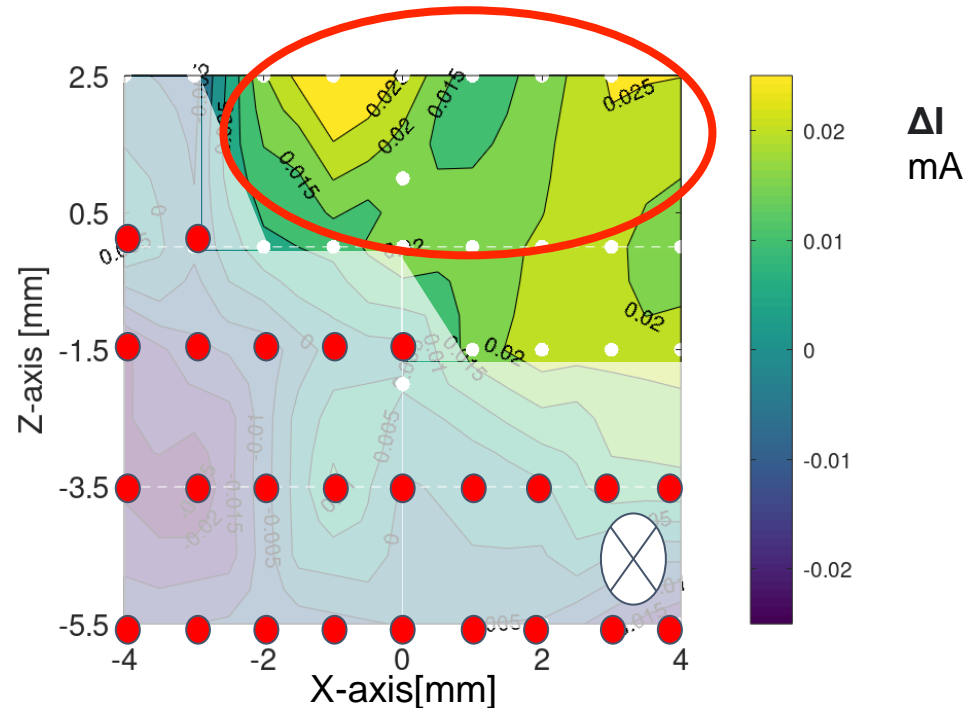
Appendix 3 emphasis

Meniscus Boundary

The boundary of plasma can consider by appears of anomaly I-V curve which is correspond to current contour.

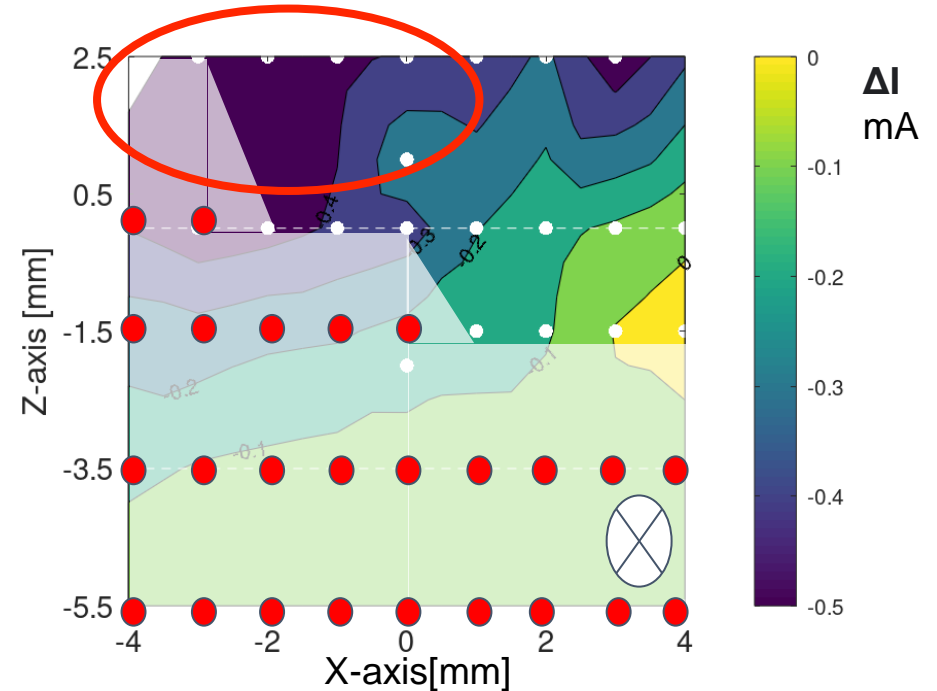


Accumulation of charge particle



The difference of Positively charged saturation current between $V_{ext} = 450V$ and $V_{ext} = 0V$

$$\Delta I = I_{pos_sat_V450} - I_{pos_sat_V0}$$

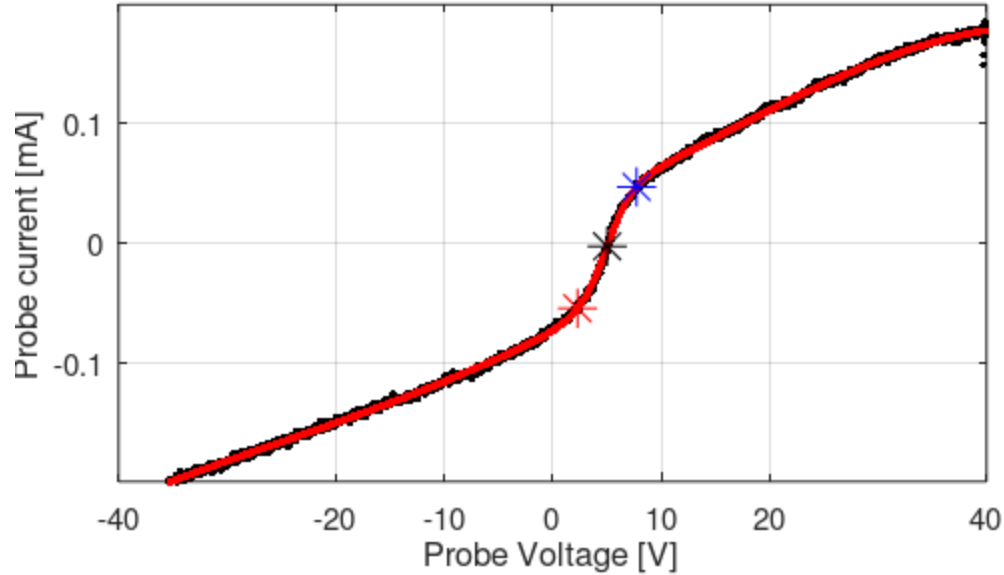


The difference of Negative charged saturation current between $V_{ext} = 450V$ and $V_{ext} = 0V$

$$\Delta I = I_{neg_sat_V450} - I_{neg_sat_V0}$$

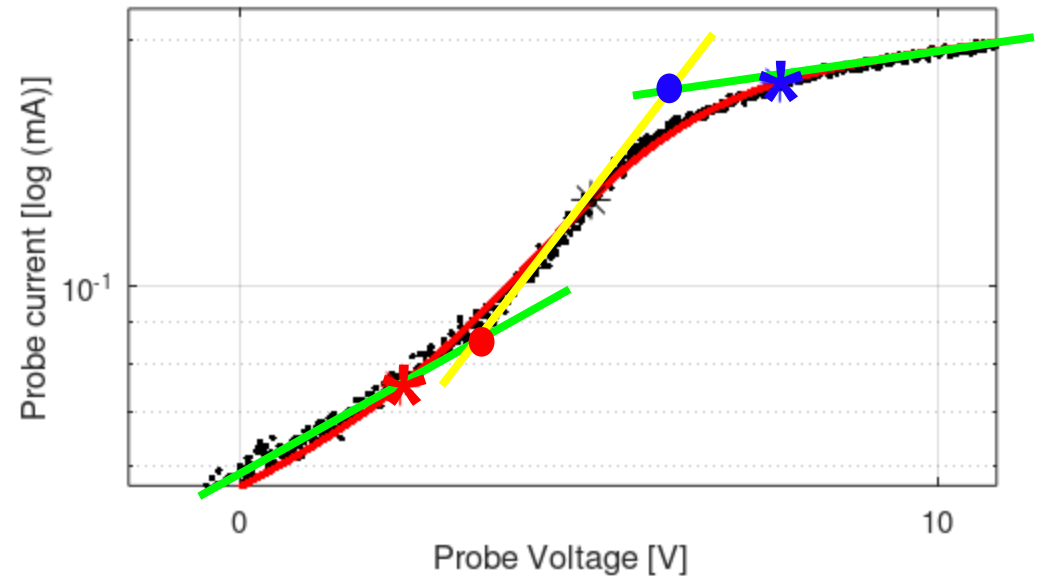
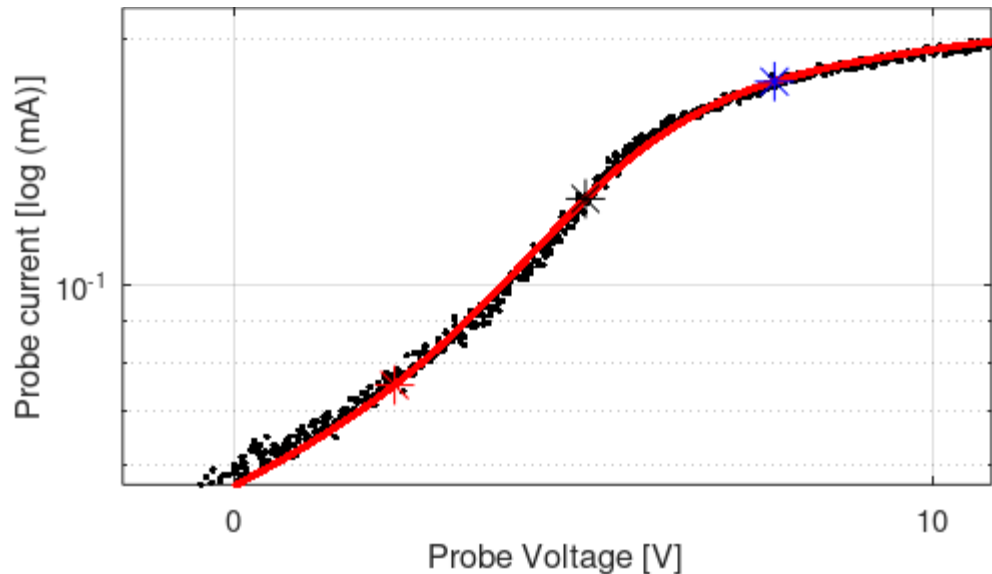
The difference of current shows accumulation of charge particle

Third derivative and tracing method



$$I = (a_0 + a_1x + a_2x^2 + a_2x^3)e^{\tanh(bx)} + c$$
$$x = V_{bias} - V_s$$

Fitting function for tracking retard region and smoothing for third derivative.



Sheath effect

Orbital motion Limit Theory (OML)

$$I = \frac{q_\alpha n_{\alpha 0} A_{sph}}{4} V_{th} + \frac{A_{cyl}}{4} (q_\alpha n_{\alpha 0}) V_{th} \left[\frac{r_s}{r_p} \text{Erf}(\hat{u}_s) + e^{|\hat{\phi}_p|} \text{Erfc}(\sqrt{\hat{u}_s^2 + |\hat{\phi}_p|}) \right]$$

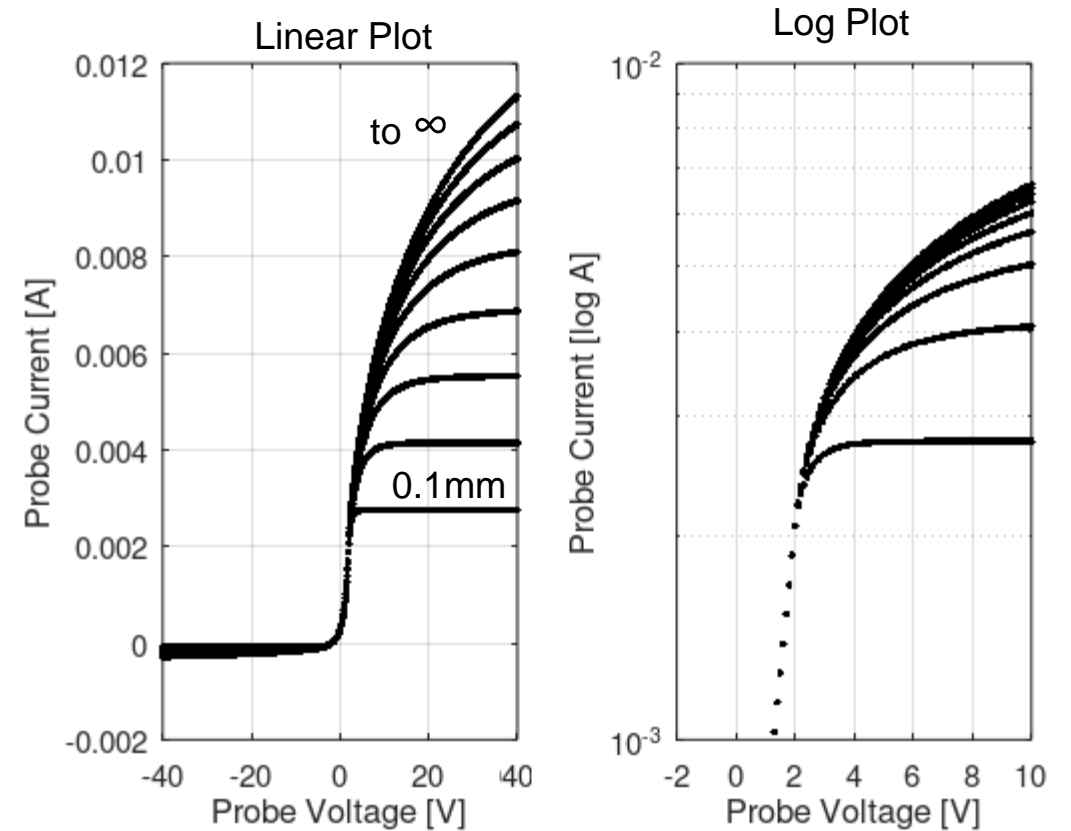
The OML predicted that sheath of plasma effect the increase of current in saturation region. Saturation also distorted under the effect of the sheath.

OML is famous use with square-root approximation when consider sheath is large (10 time of probe radius).

$$I(r_p) = I_{es} \frac{2}{\sqrt{\pi}} \left(1 + \frac{|q_\alpha \phi_p|}{K_B T_\alpha} \right)^{1/2}$$

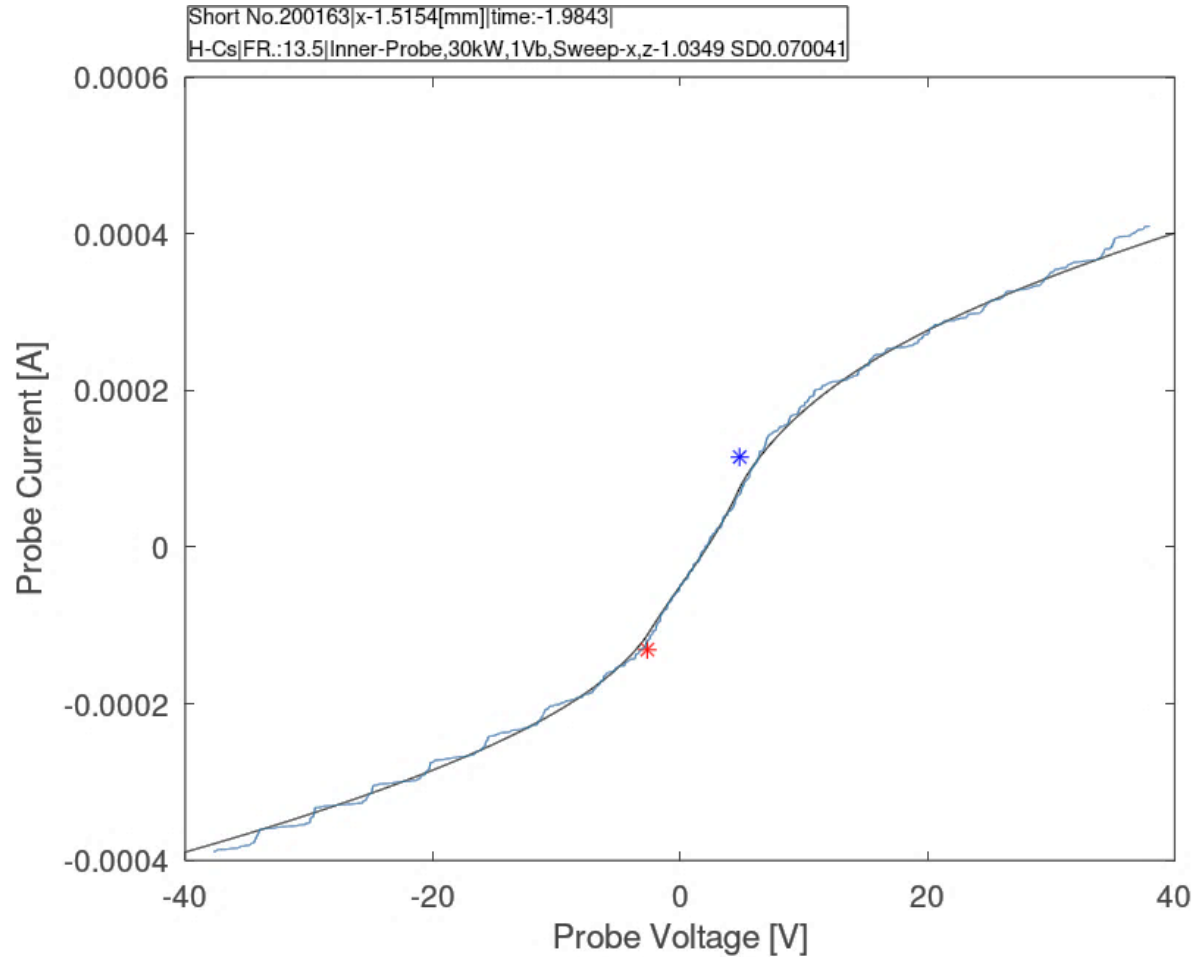
In electronegative plasma, it is possible that the distortion affected to the temperature tracing which is reach to 5eV in our measurement.

OML Theory Plot

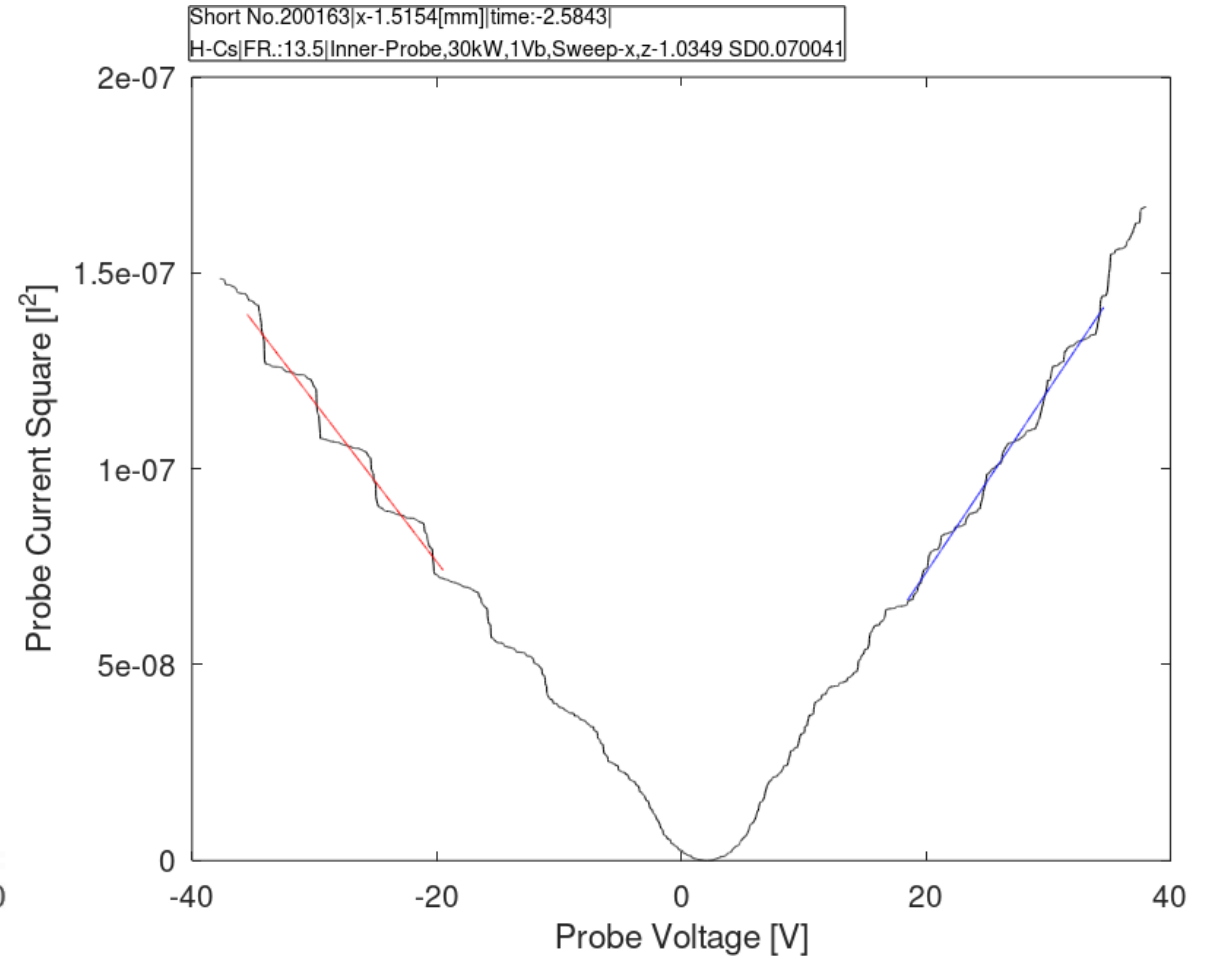


Small radius and short length probe

Linear Plot



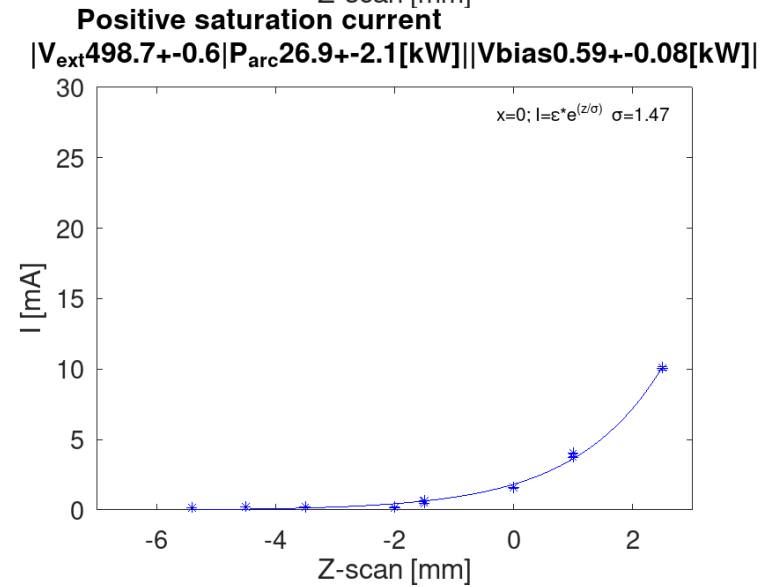
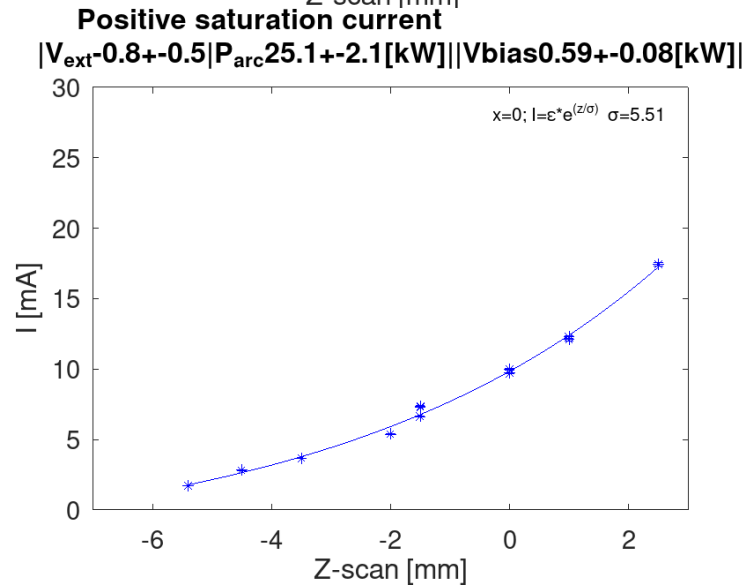
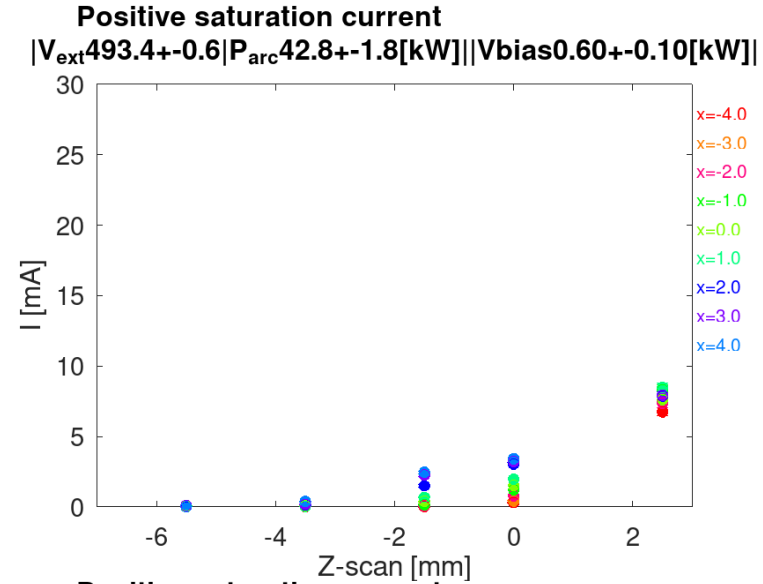
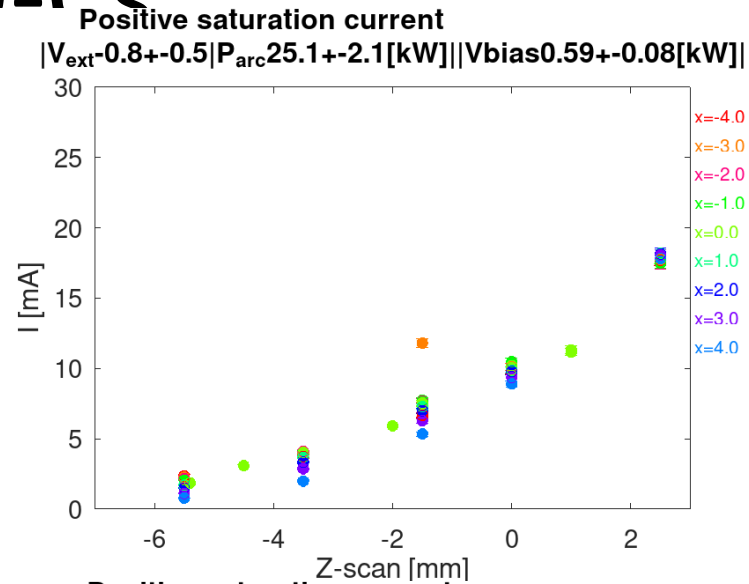
I-square Plot



Appendix 4 Meniscus and shielding properties

Electron plasma Meniscus Boundary

W/O- r_s

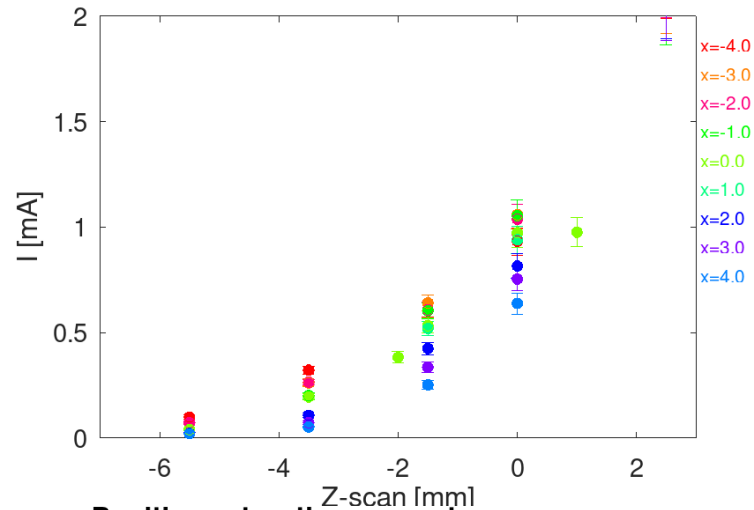


Electron plasma Meniscus Boundary

W-Cs

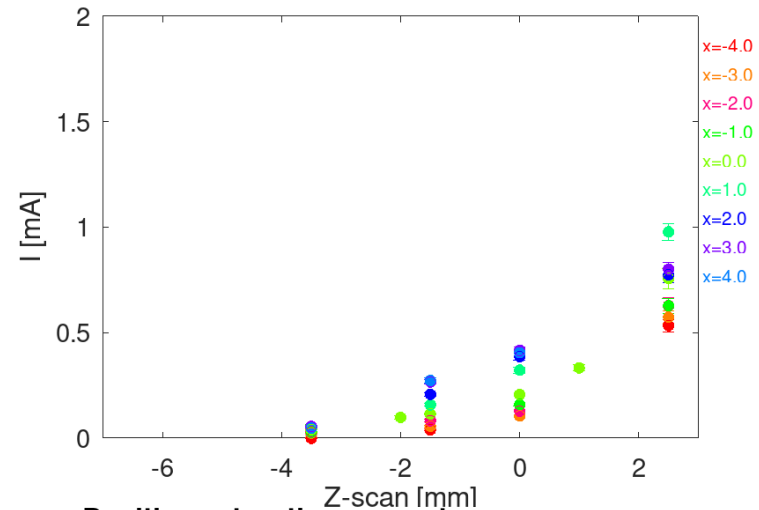
Positive saturation current

$|V_{ext} 0.2 \pm 0.5 | P_{arc} 24.5 \pm 2.1 [kW] | | V_{bias} 0.61 \pm 0.09 [kW] |$



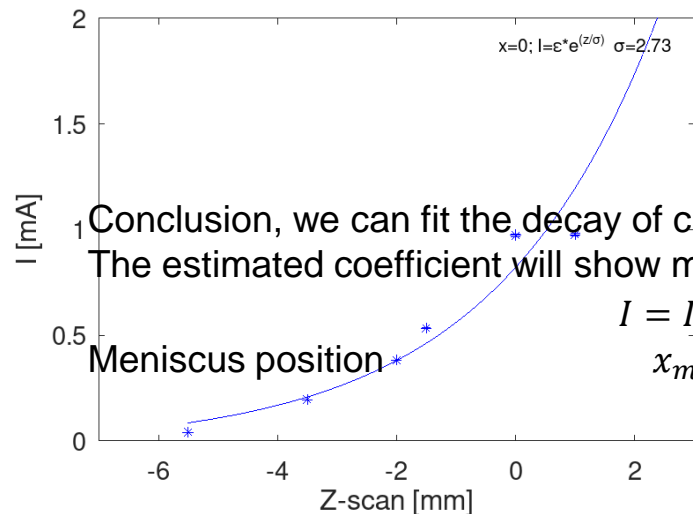
Positive saturation current

$|V_{ext} 462.8 \pm 6.5 | P_{arc} 25.4 \pm 2.1 [kW] | | V_{bias} 0.60 \pm 0.09 [kW] |$



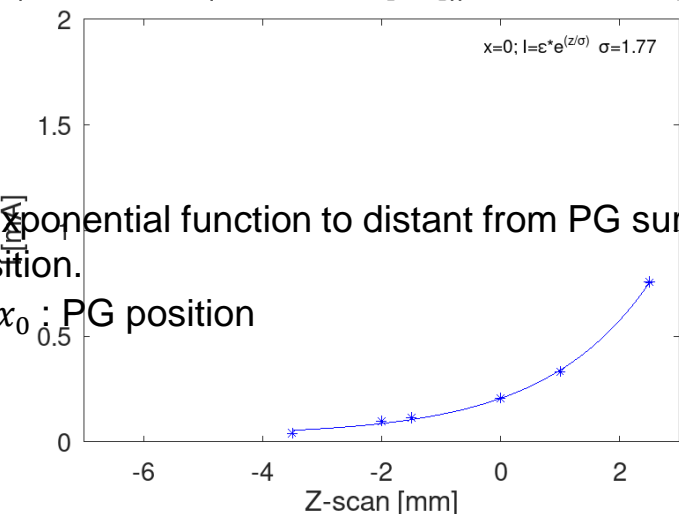
Positive saturation current

$|V_{ext} 0.2 \pm 0.5 | P_{arc} 24.5 \pm 2.1 [kW] | | V_{bias} 0.61 \pm 0.09 [kW] |$



Positive saturation current

$|V_{ext} 462.8 \pm 6.5 | P_{arc} 25.4 \pm 2.1 [kW] | | V_{bias} 0.60 \pm 0.09 [kW] |$



Conclusion, we can fit the decay of current with exponential function to distant from PG surface. The estimated coefficient will show meniscus position.

$$I = I_0 e^{(x-x_0)/\lambda}; \quad x_0: \text{PG position}$$

$$x_m = \lambda [m]$$

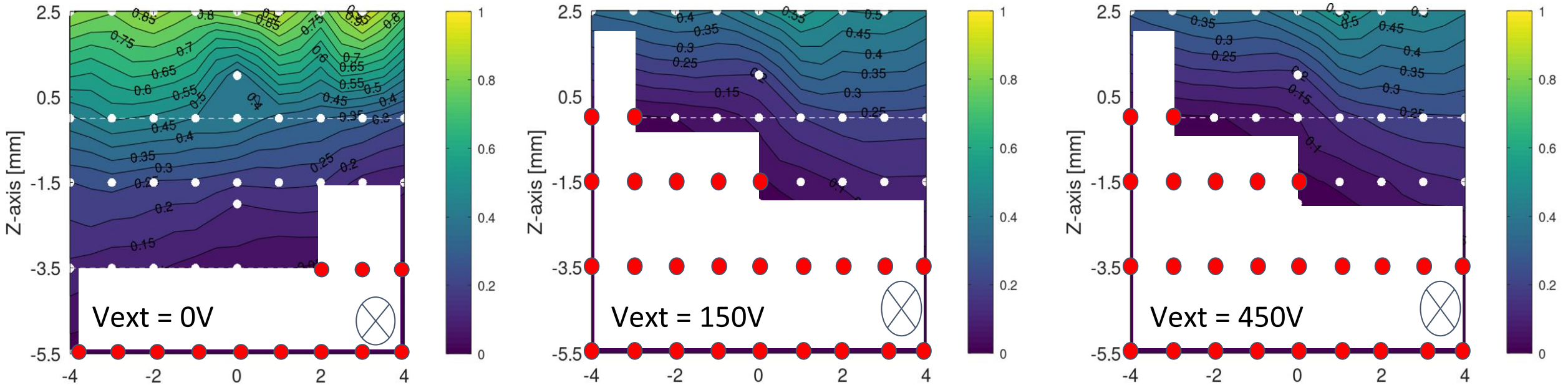
Meniscus position

Appendix 5 Parc or Vext Dependence

w/-Cs

Negatively Saturation current Vext dependence

Parc = 25kW w/-Cs

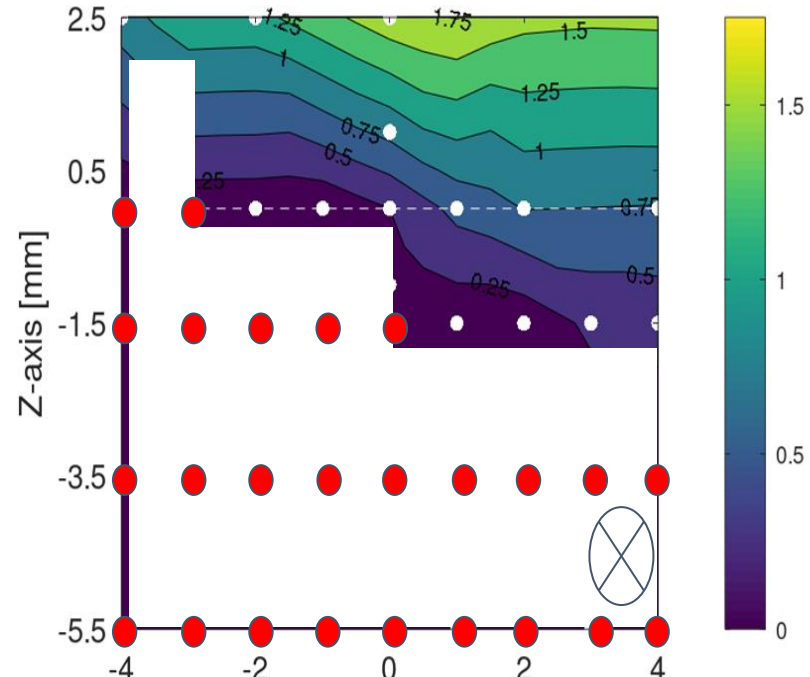
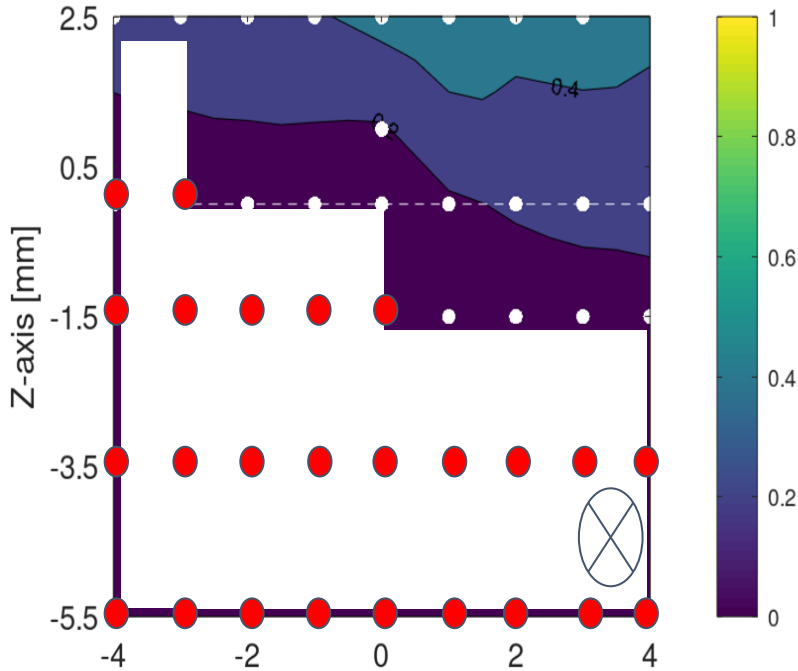


Electric field effect



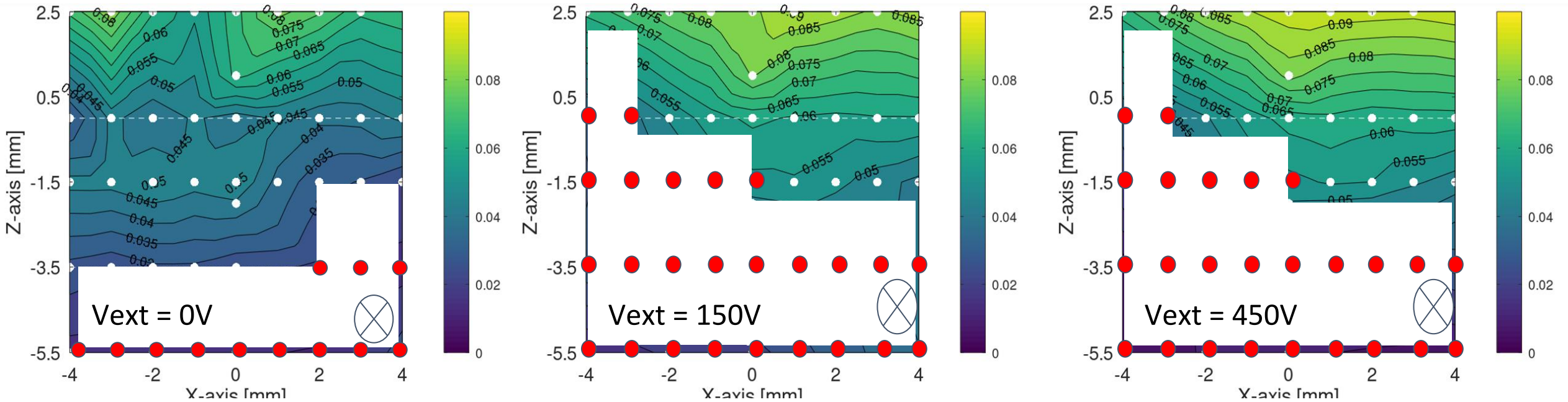
Negatively charged Saturation current Arc Power dependence

$V_{ext} = 450V$ w/-Cs



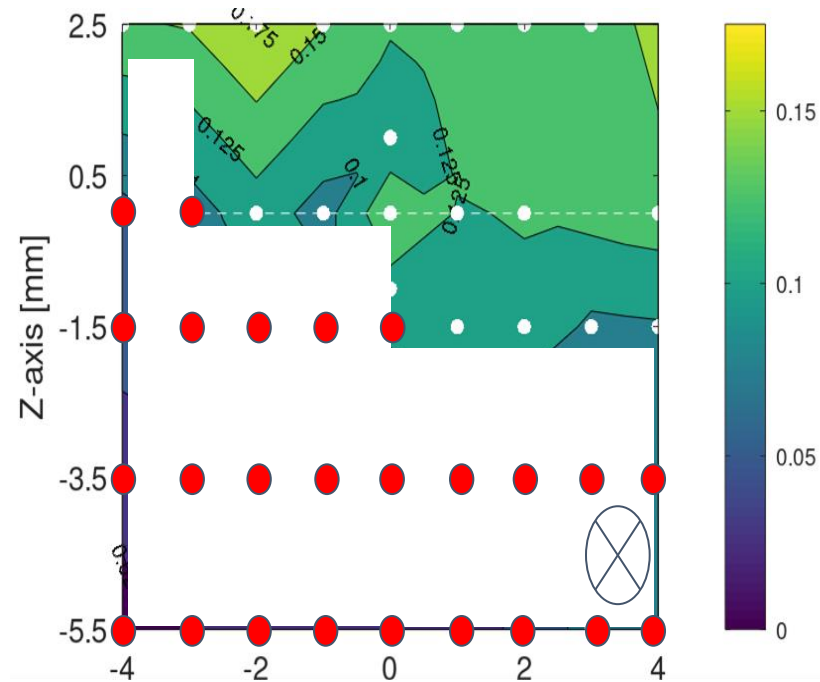
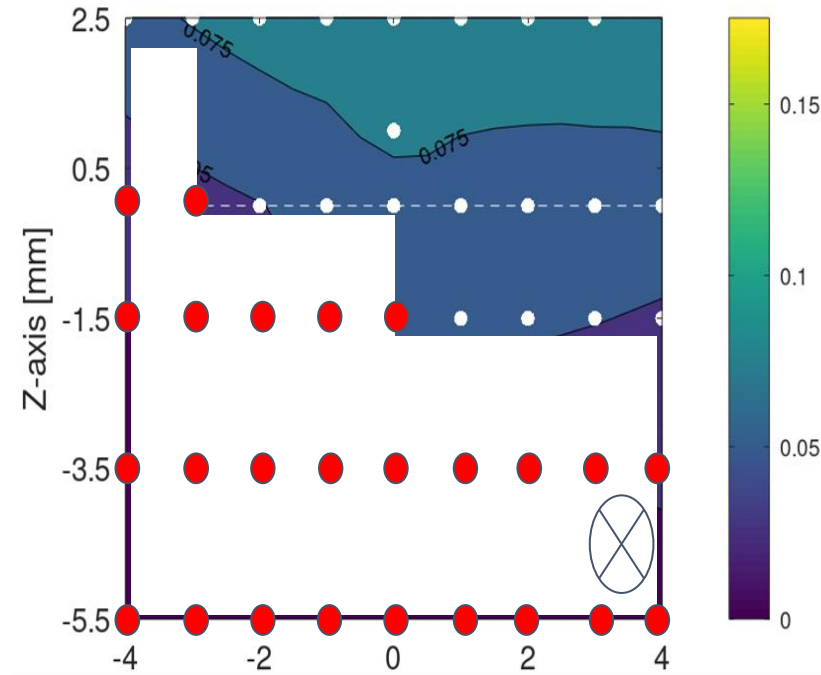
Positively Charged Saturation current Vext dependence

Parc = 25kW w/-Cs



Positively saturation current Arc power dependence

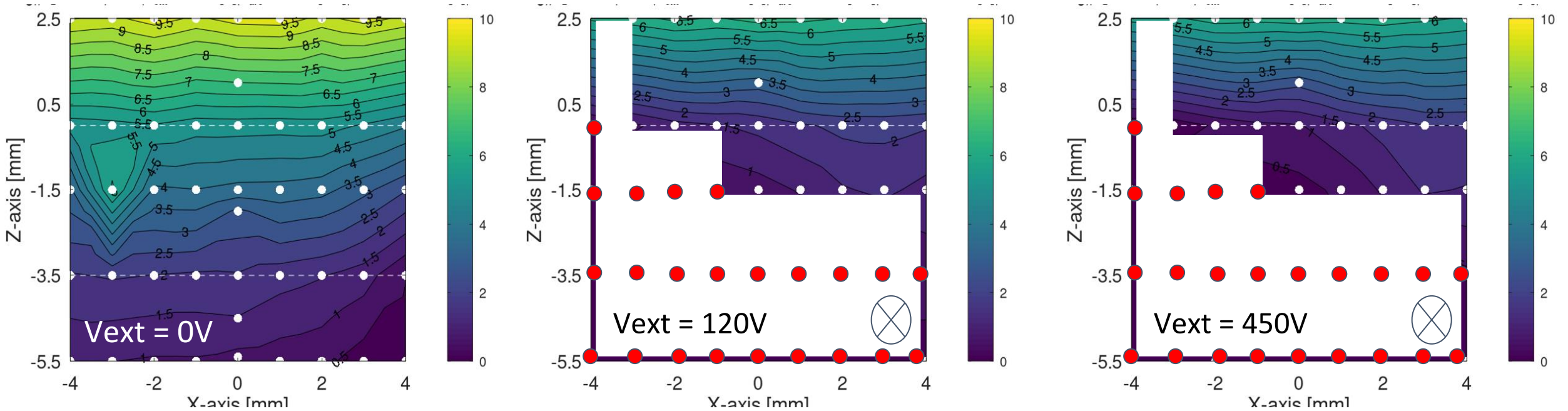
$V_{ext} = 450V$ w/-Cs



w/o-Cs

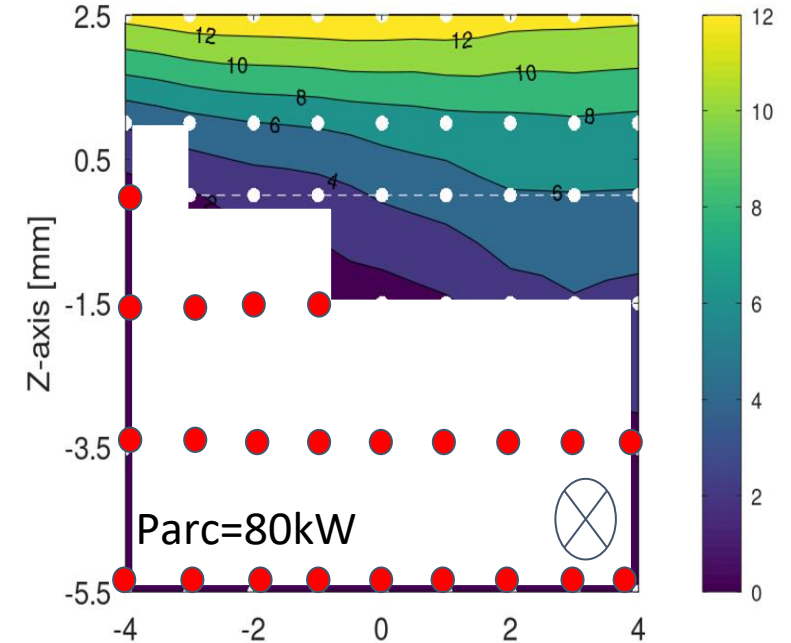
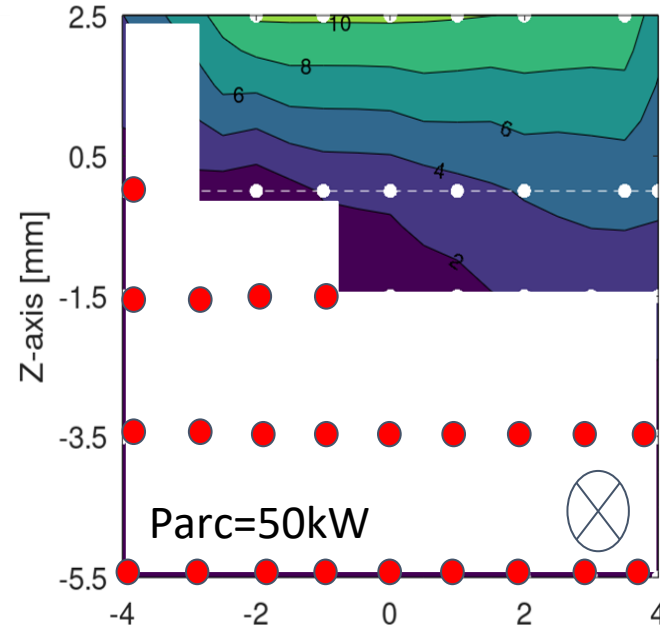
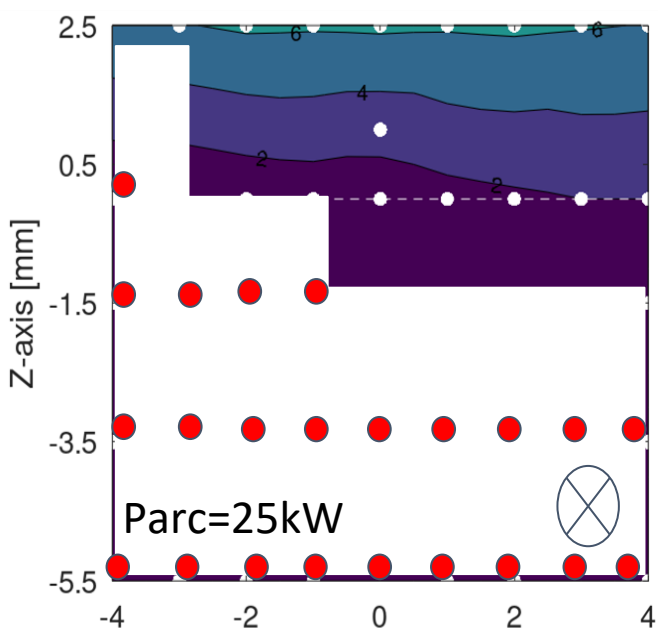
Negatively Charged Saturation current Vext dependence

Parc = 25kW w/o-Cs



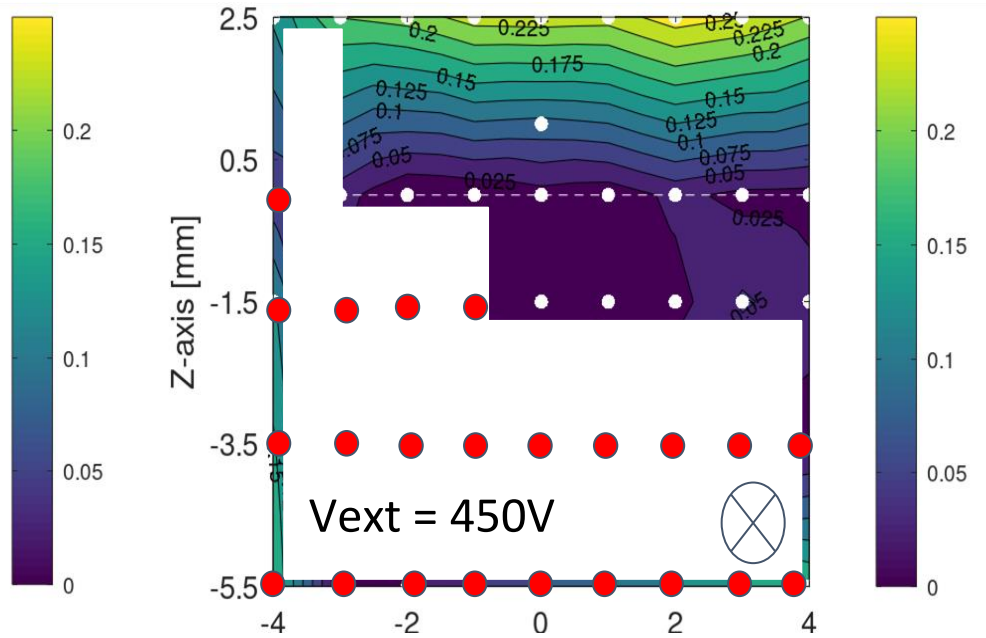
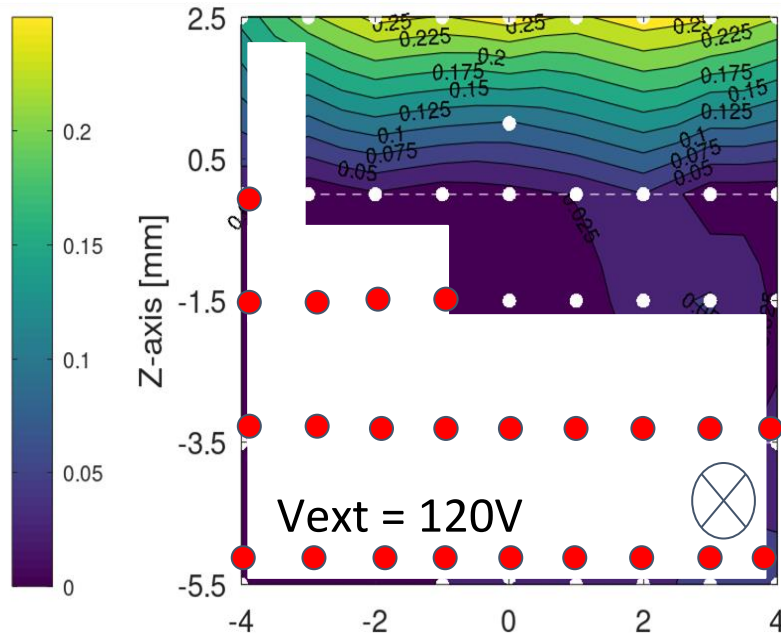
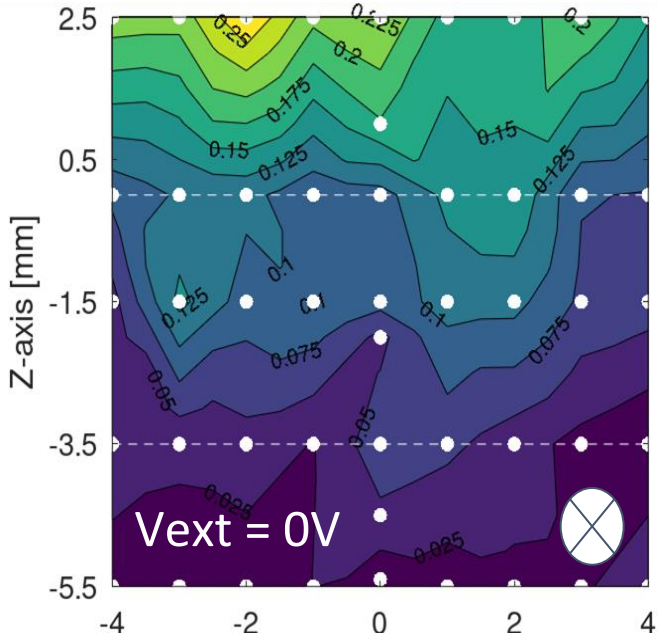
Negatively Charged Saturation current Arc power dependence

$V_{ext} = 450V$ w/o-Cs



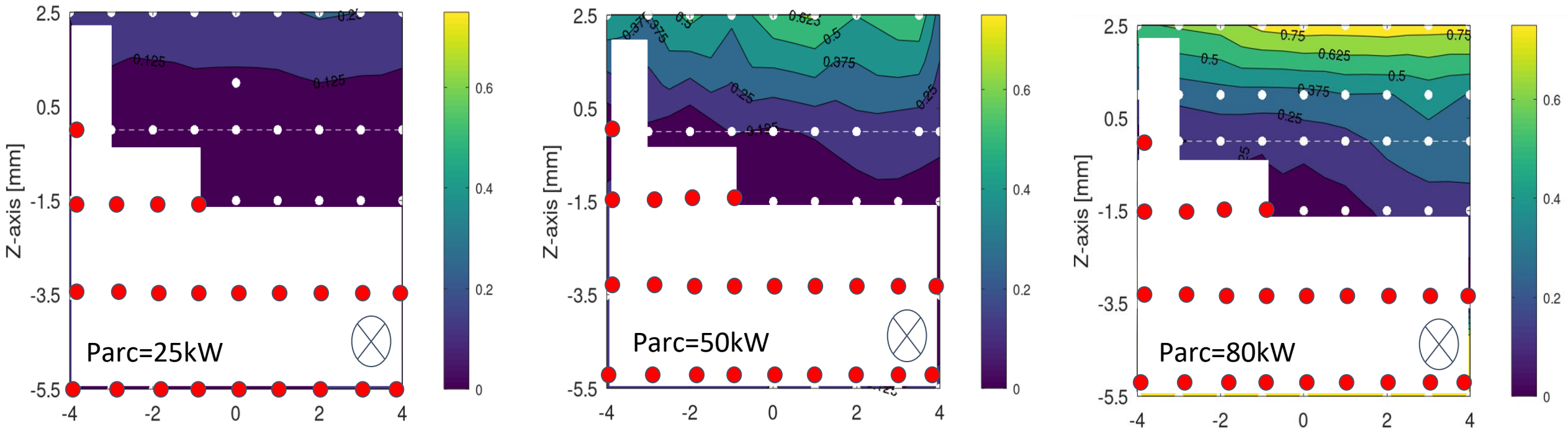
Positively charge saturation current V_{ext} dependence

Parc = 25kW w/o-Cs



Positively charged saturation current V_{ext} dependence

$V_{ext} = 450V$ w/o-Cs



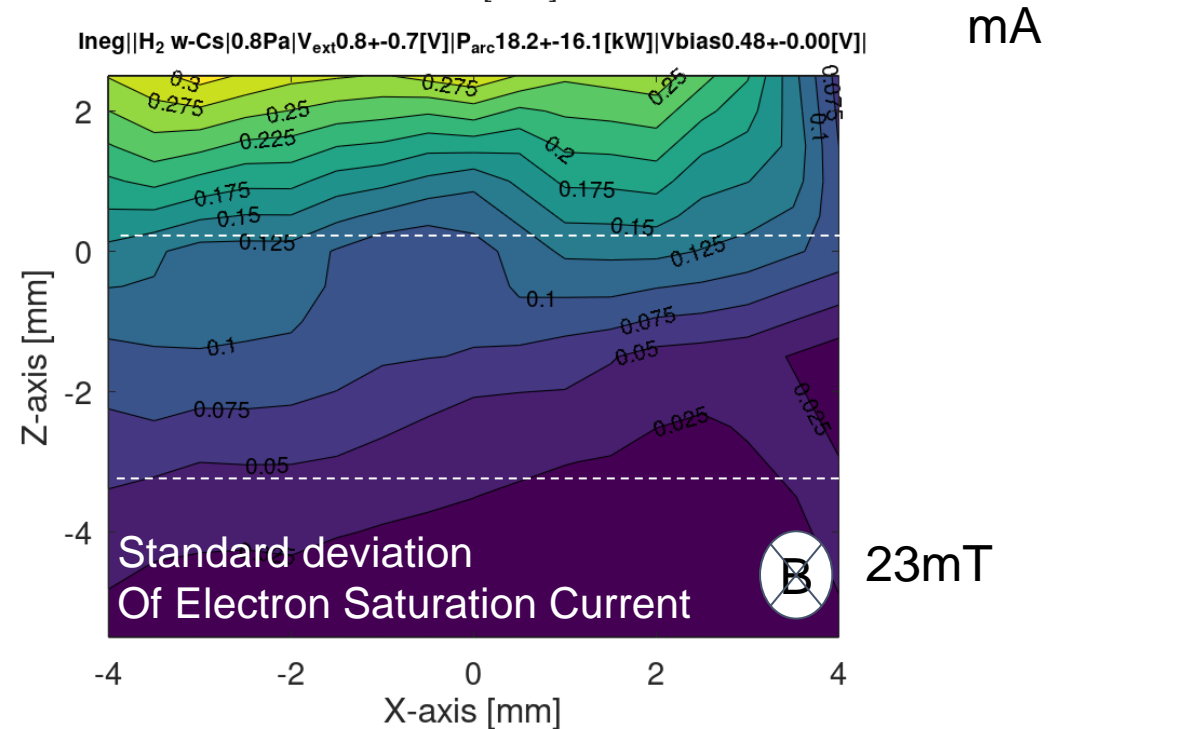
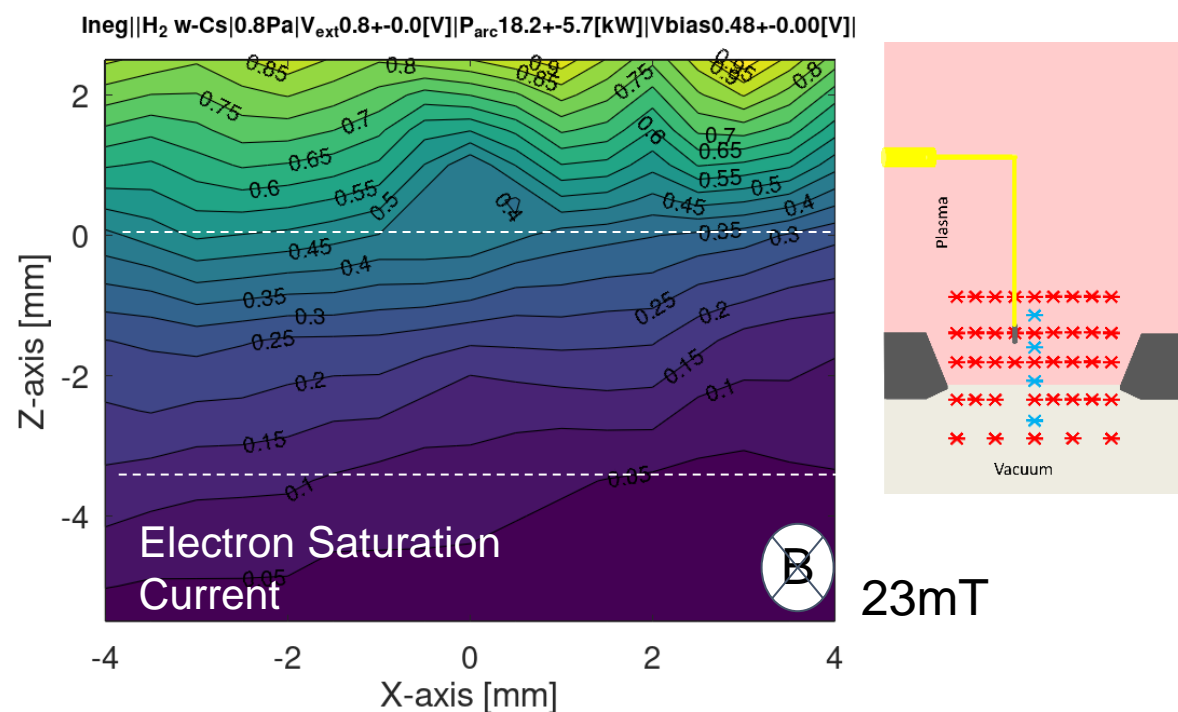
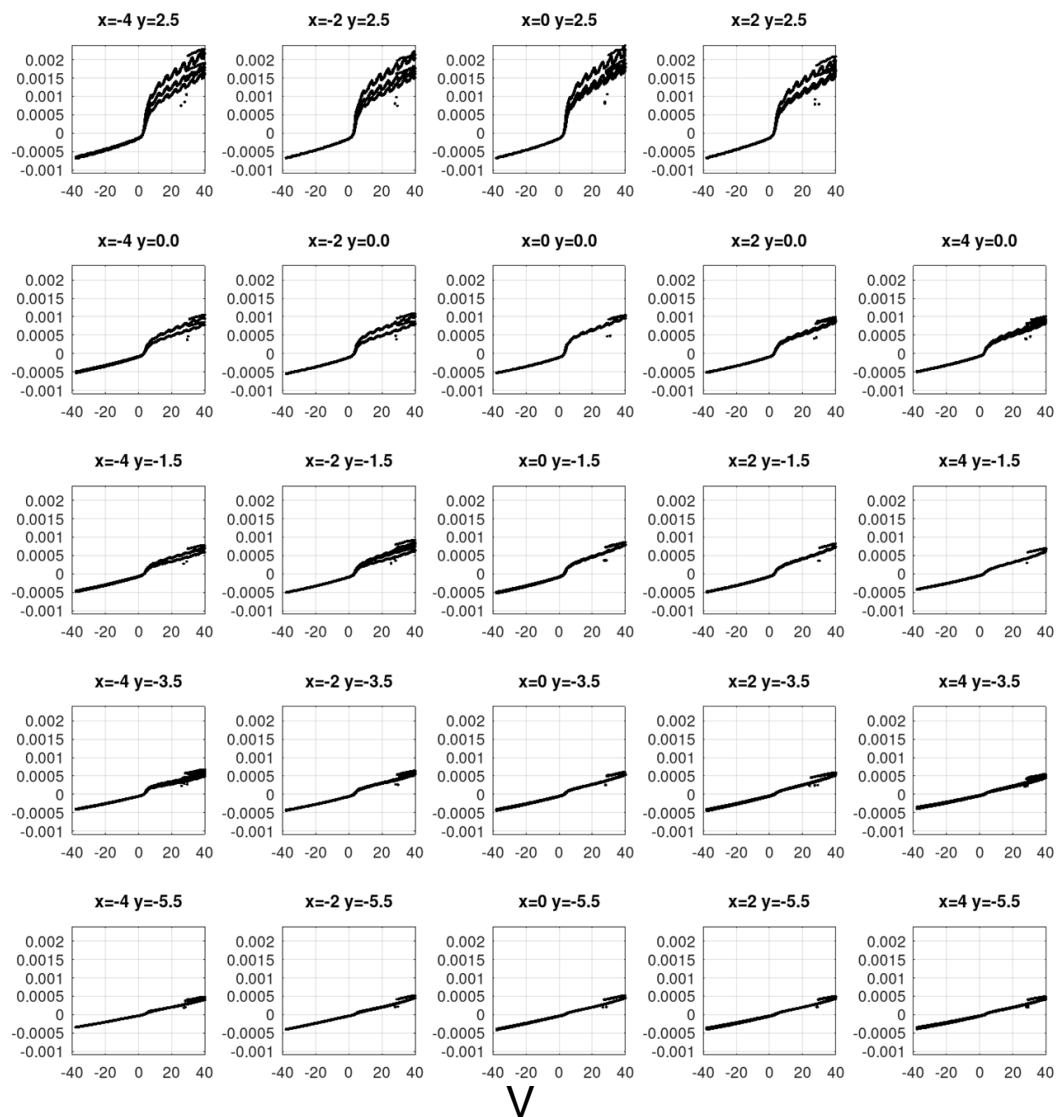
Beam width perveance plot

Appendix 4 Each point curve

w-Cs

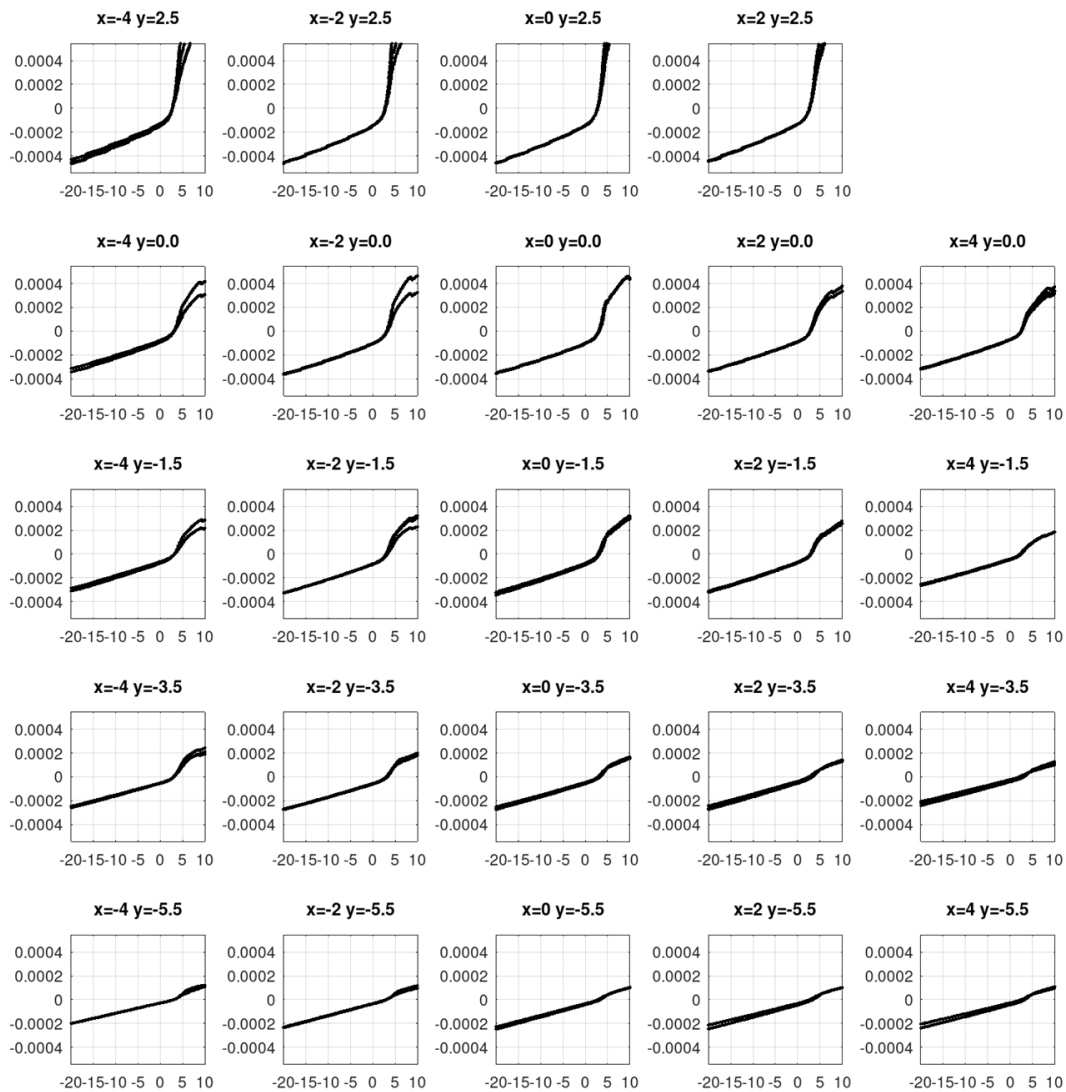
w-Cs $V_{ext}=0$

Time average IVcurve| $V_{ext}3.0+-0.7[V]$ | $P_{arc}19.2+-1.0[kW]$ | $V_{bias}0.5+-0.0[V]$ | $CRD0.1+-0.2[10^{17}m^{-3}]$



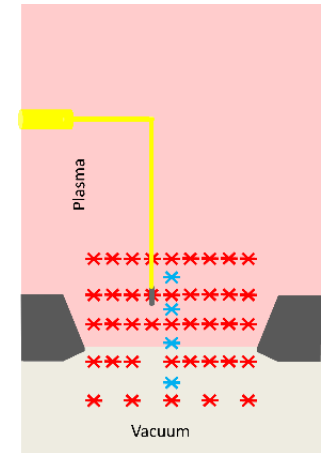
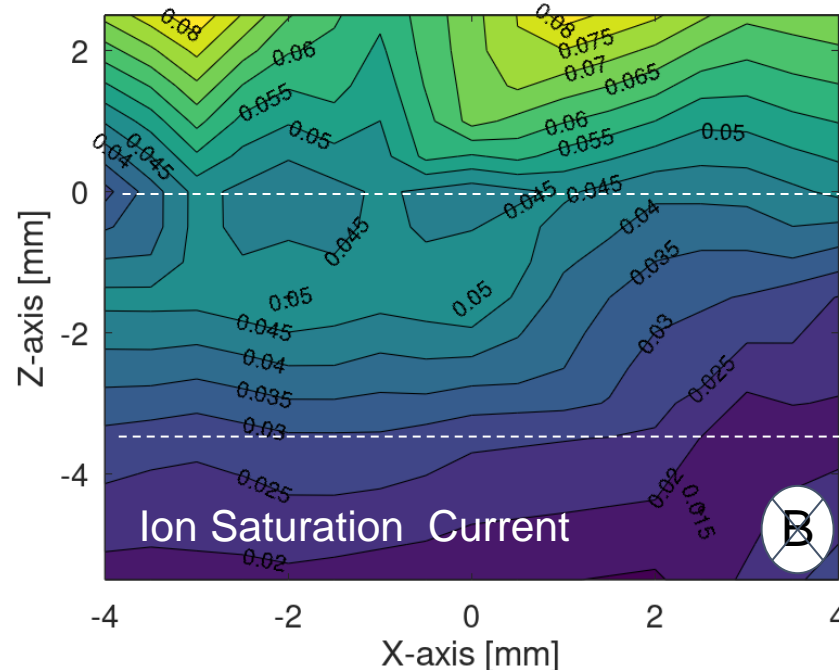
w-Cs V_{ext}=0

Time average I_V curve |V_{ext}3.0+-0.7[V]|P_{arc}19.2+-1.0[kW]|V_{bias}0.5+-0.0[V]|CRD0.1+-0.2[10¹⁷m⁻³]



V

I_{pos}|H₂ w-Cs|0.8Pa|V_{ext}0.8+-0.0[V]|P_{arc}18.2+-5.7[kW]|V_{bias}0.48+-0.00[V]

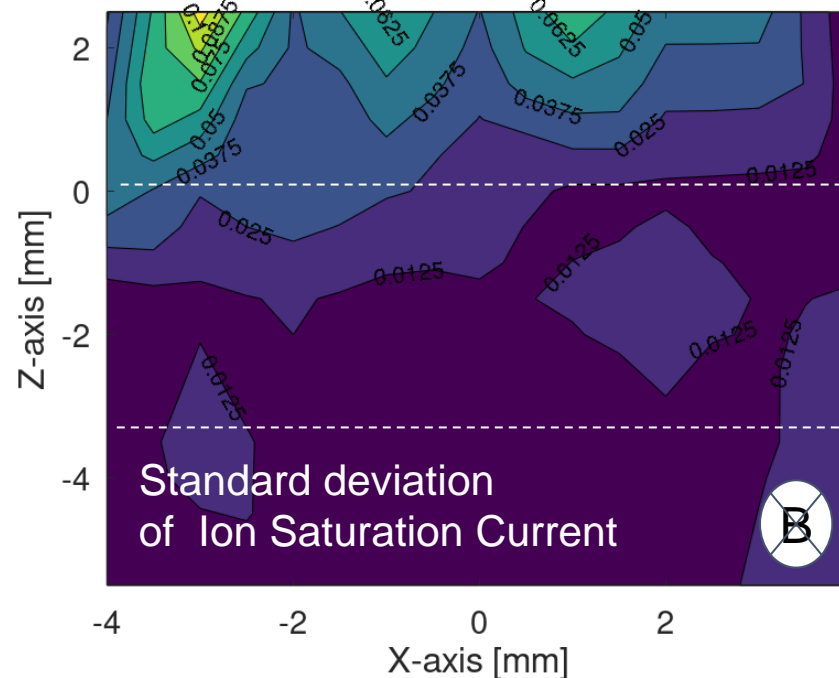


23mT

A

I_{pos}|H₂ w-Cs|0.8Pa|V_{ext}0.8+-0.7[V]|P_{arc}18.2+-16.1[kW]|V_{bias}0.48+-0.00[V]

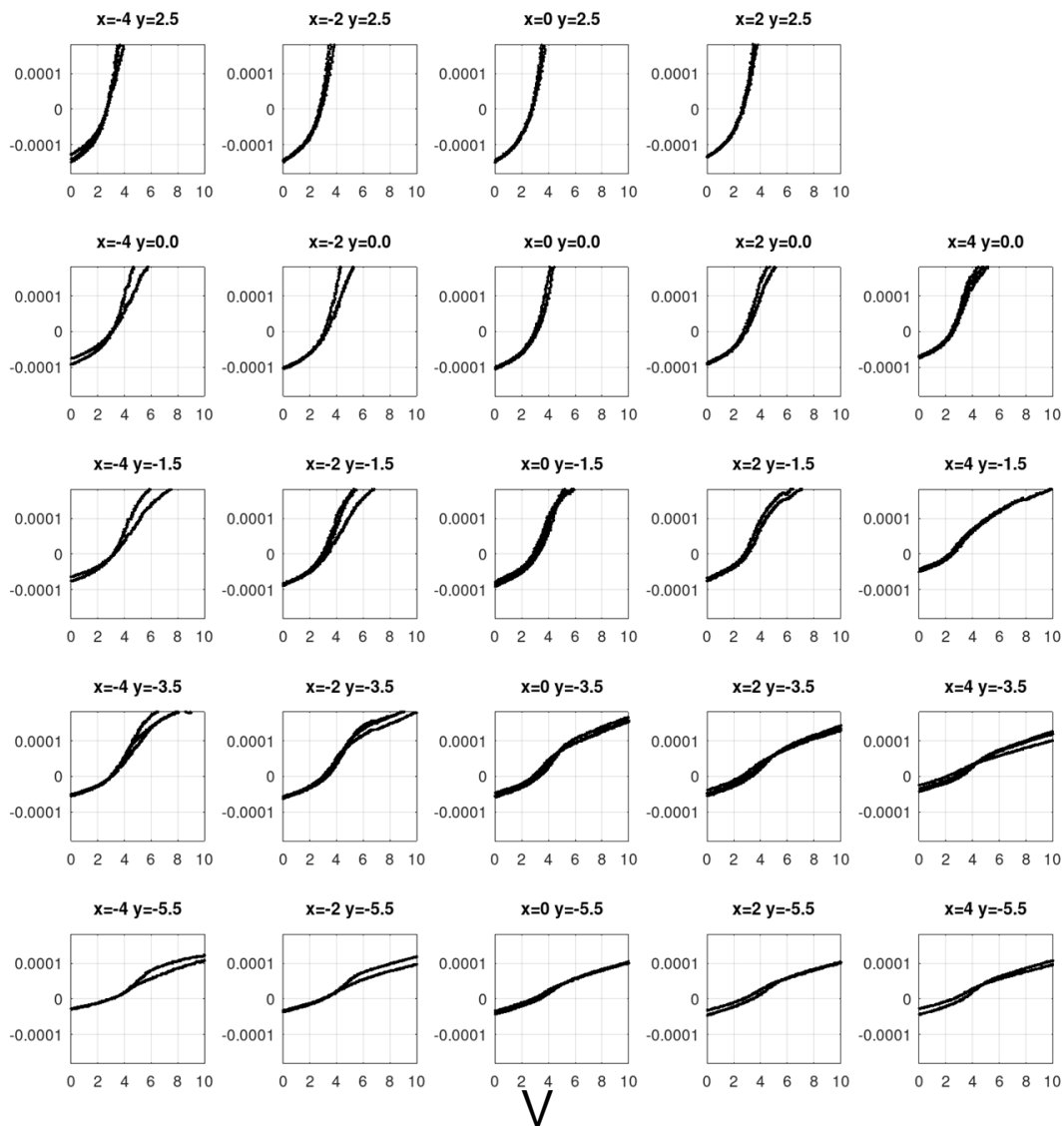
mA



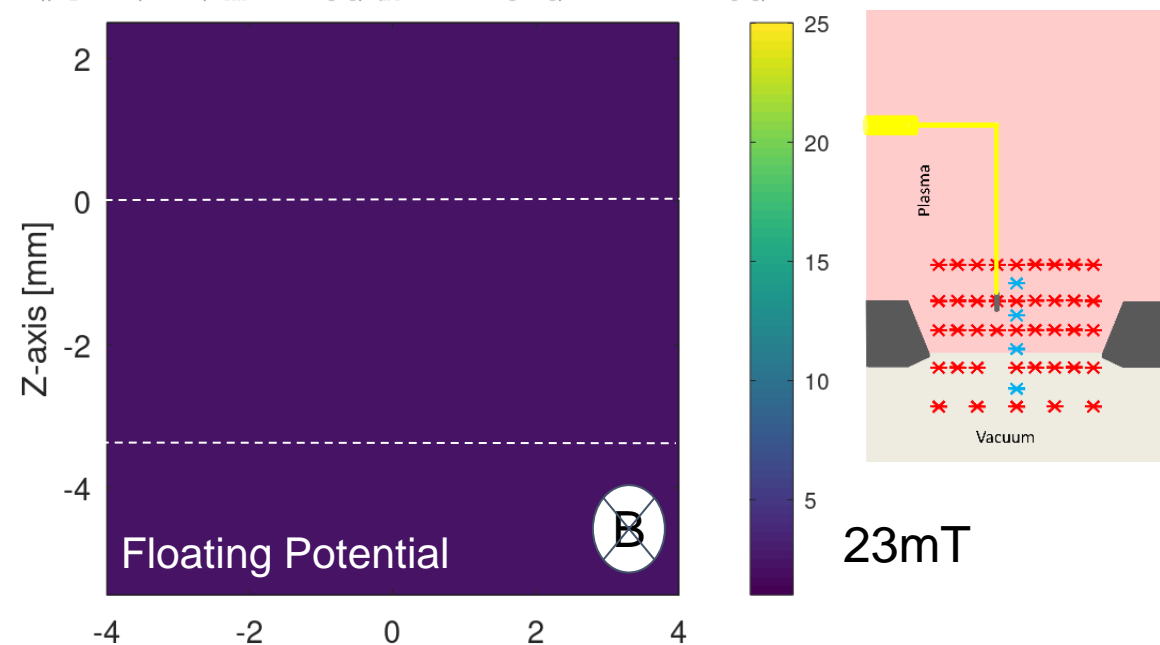
23mT

w-Cs $V_{ext}=0V$

Time average IVcurve| $V_{ext}3.0+-0.7[V]$ | $P_{arc}19.2+-1.0[kW]$ | $V_{bias}0.5+-0.0[V]$ | $CRD0.1+-0.2[10^{17}m^{-3}]$

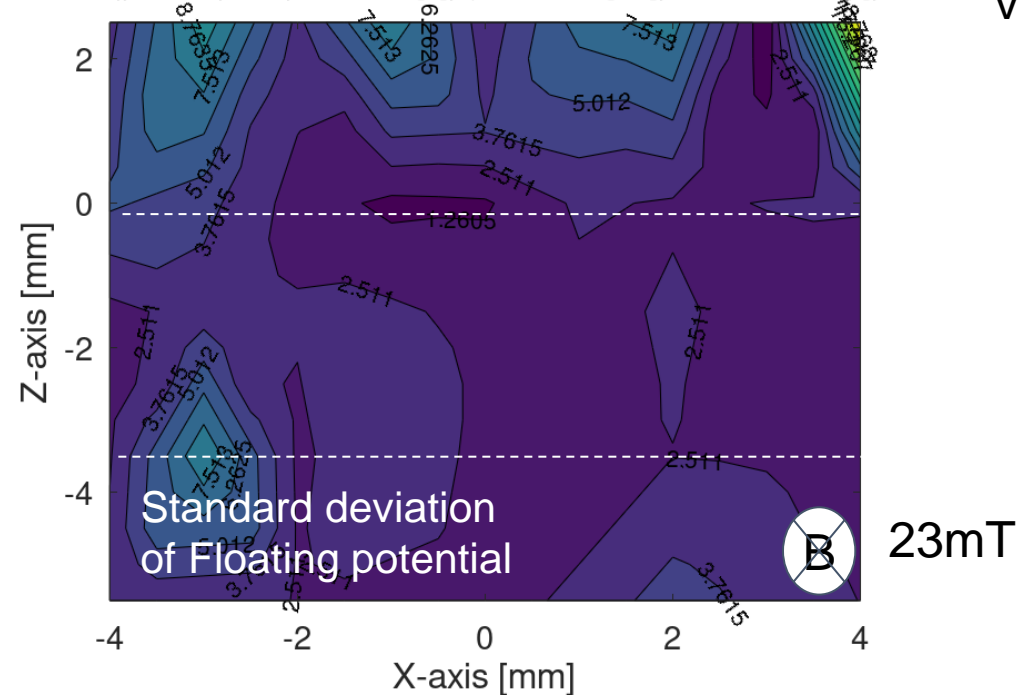


$V_f||H_2$ w-Cs|0.8Pa| $V_{ext}0.8+-0.7[V]$ | $P_{arc}18.2+-16.1[kW]$ | $V_{bias}0.48+-0.00[V]$



A

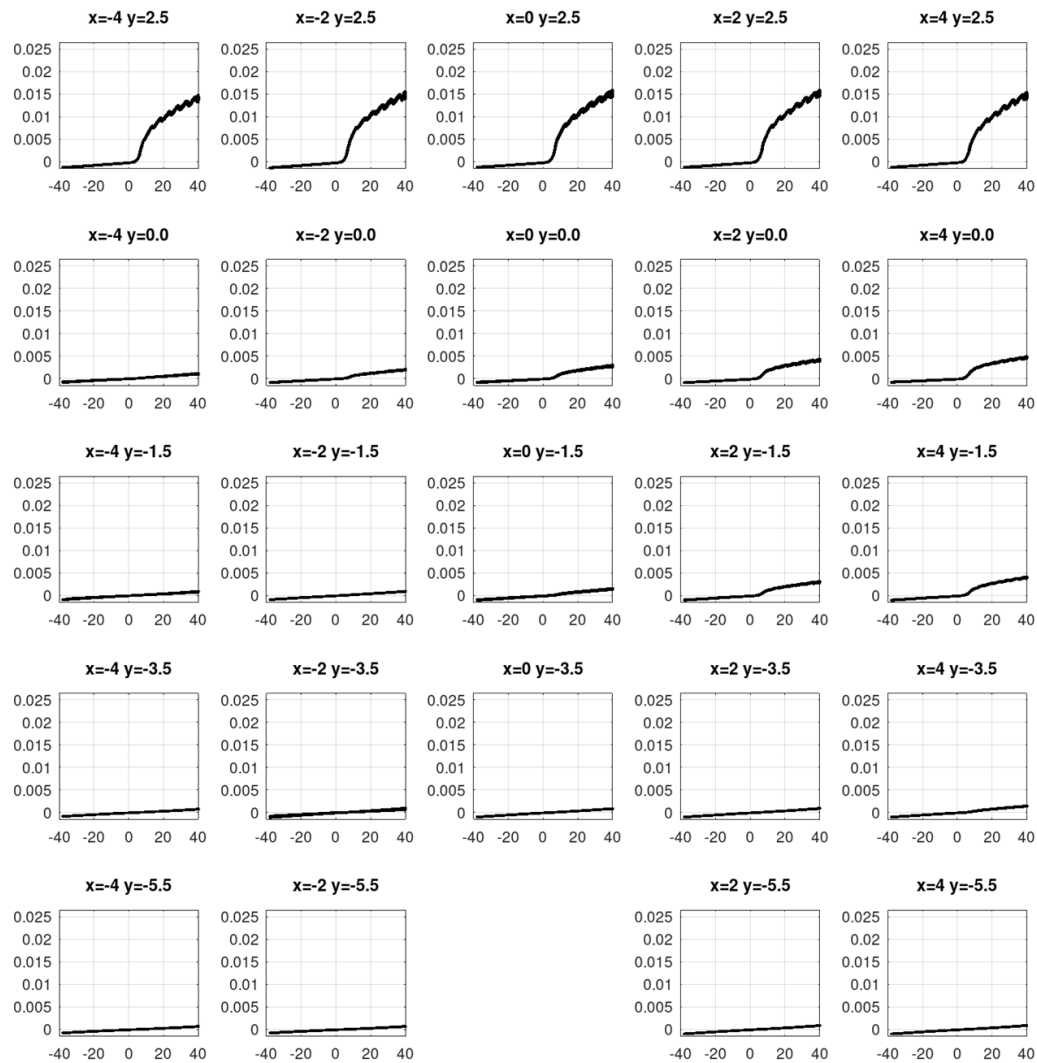
$V_f||H_2$ w-Cs|0.8Pa| $V_{ext}0.8+-0.7[V]$ | $P_{arc}18.2+-16.1[kW]$ | $V_{bias}0.48+-0.00[V]$



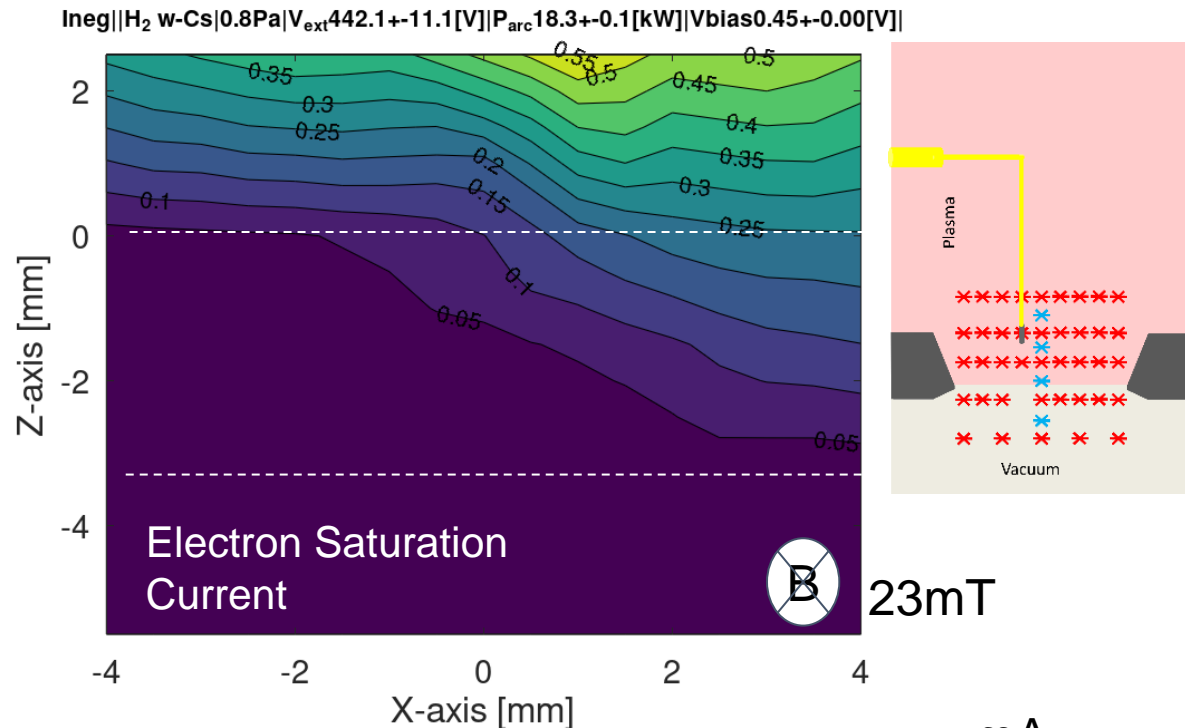
V

w-Cs $V_{ext}=450V$

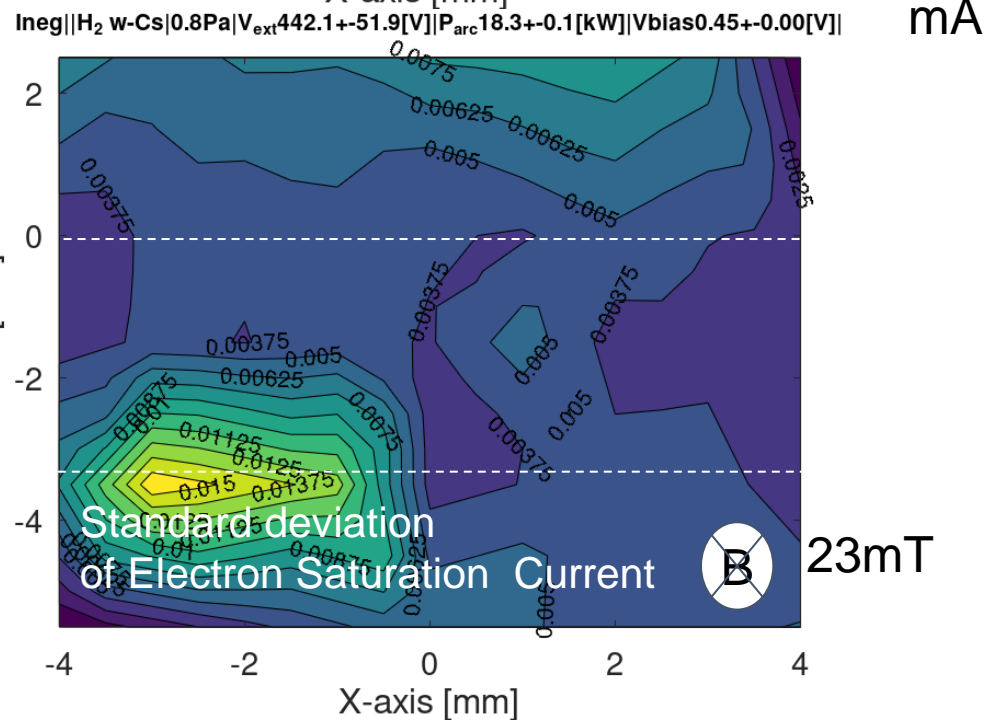
Time average IVcurve $|V_{ext}496.6+-1.8[V]|P_{arc}12.7+-0.8[kW]|V_{bias}0.5+-0.0[V]|CRD0.1+-0.1[10^{17}m^{-3}]$



V

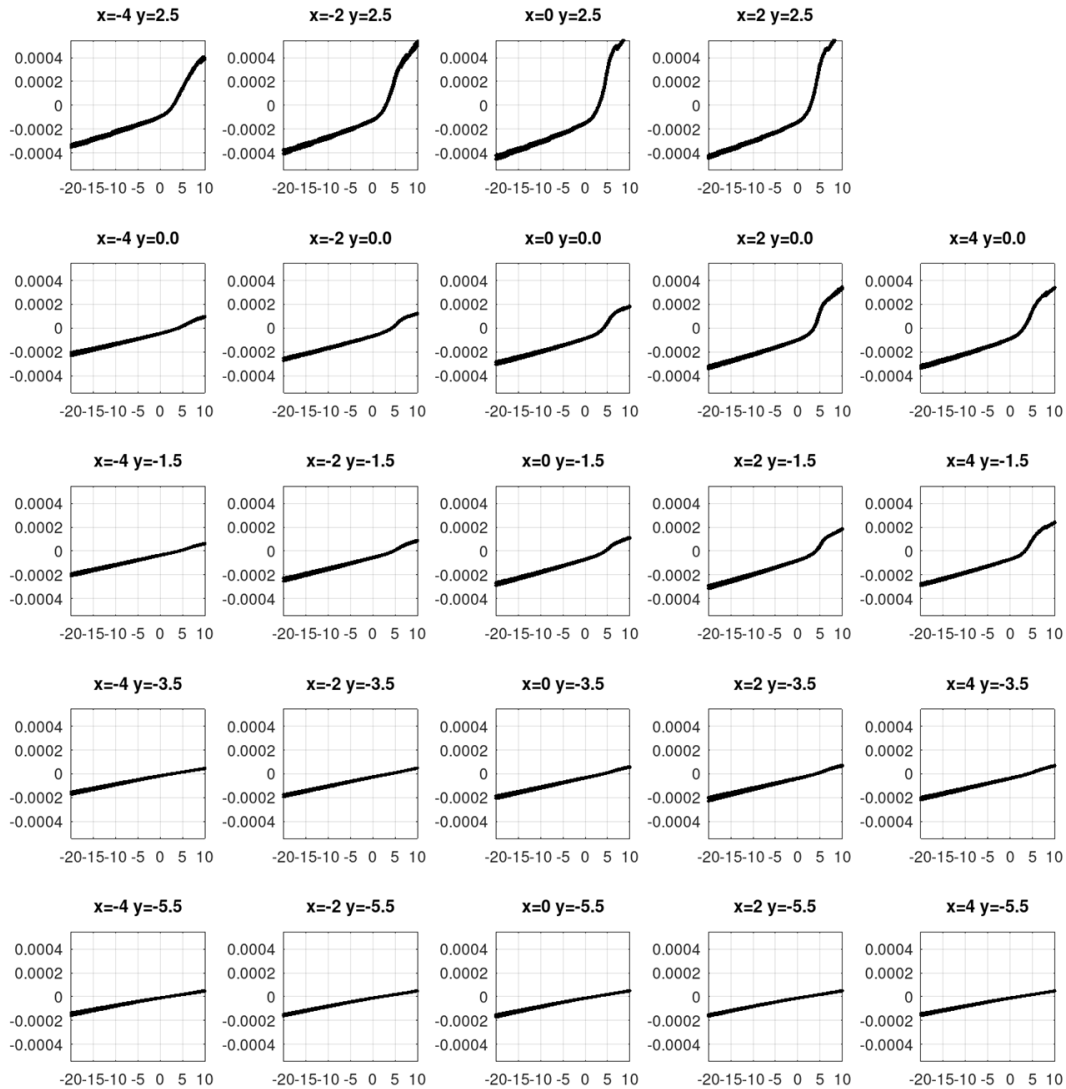


A



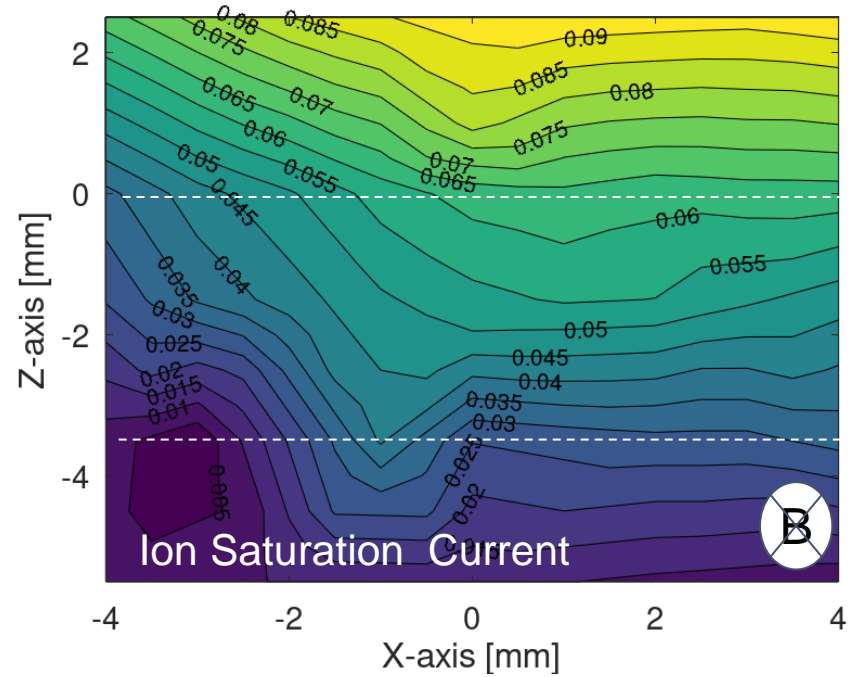
w-Cs $V_{ext}=450V$

Time average I_V curve $|V_{ext}463.5 \pm 4.6[V]|P_{arc}19.2 \pm 1.0[kW]|V_{bias}0.5 \pm 0.0[V]|CRD0.1 \pm 0.2[10^{17}m^{-3}]$



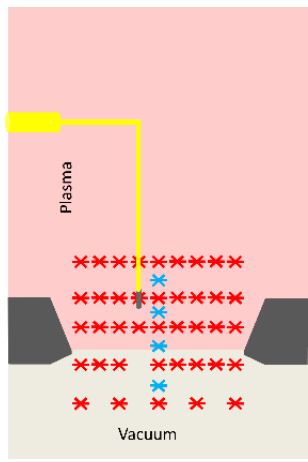
V

$I_{pos}|H_2$ w-Cs|0.8Pa| $V_{ext}442.1 \pm 11.1[V]|P_{arc}18.3 \pm 0.1[kW]|V_{bias}0.45 \pm 0.00[V]$



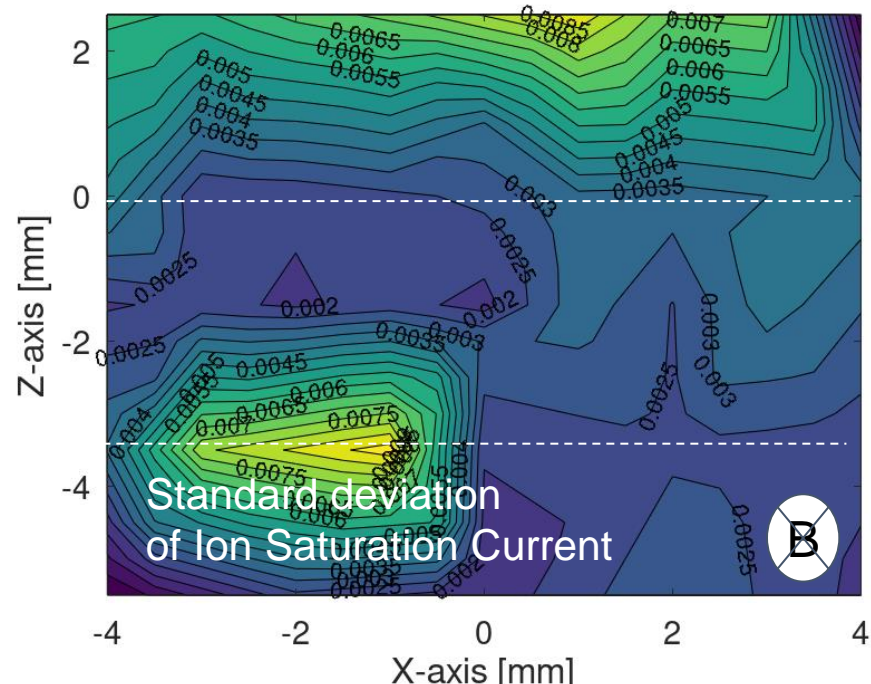
Ion Saturation Current

23mT



A

$I_{pos}|H_2$ w-Cs|0.8Pa| $V_{ext}442.1 \pm 51.9[V]|P_{arc}18.3 \pm 0.1[kW]|V_{bias}0.45 \pm 0.00[V]$



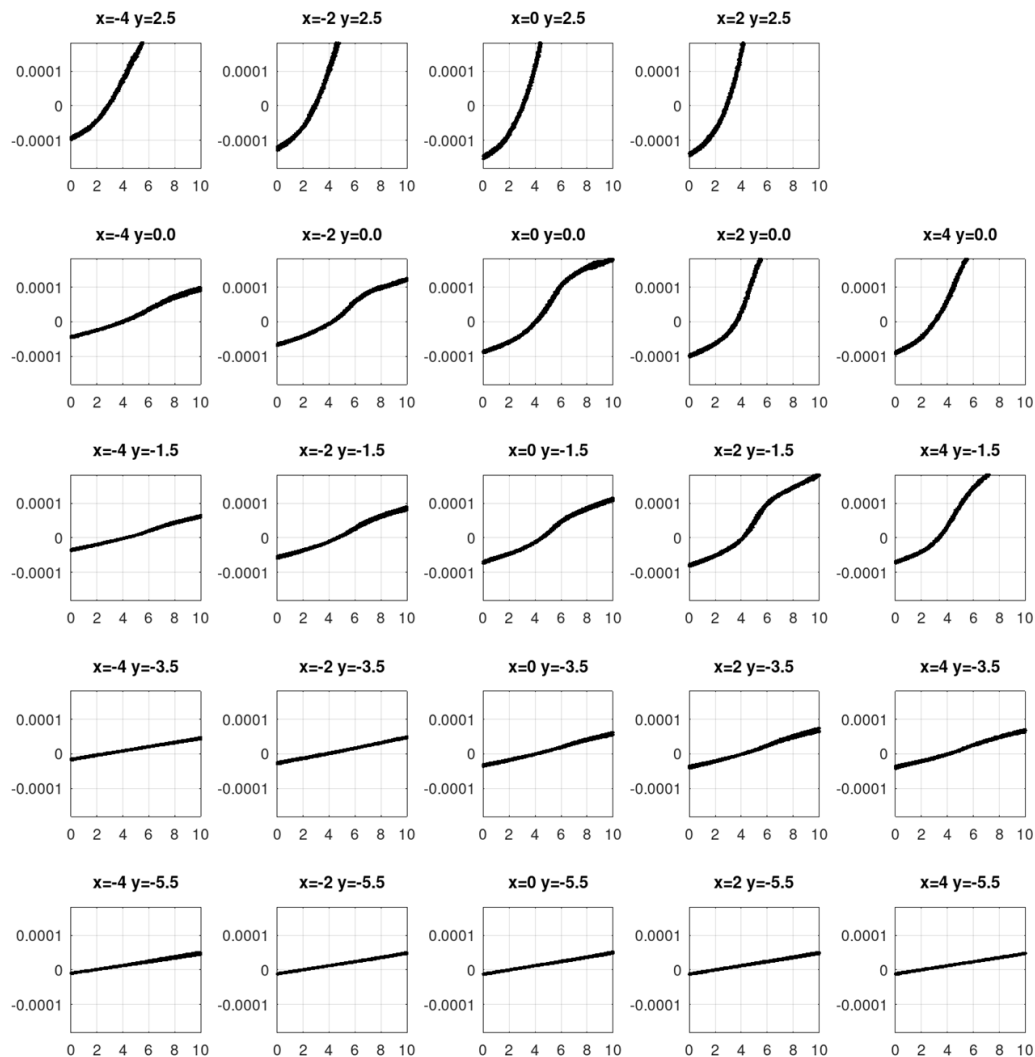
Standard deviation of Ion Saturation Current

23mT

mA

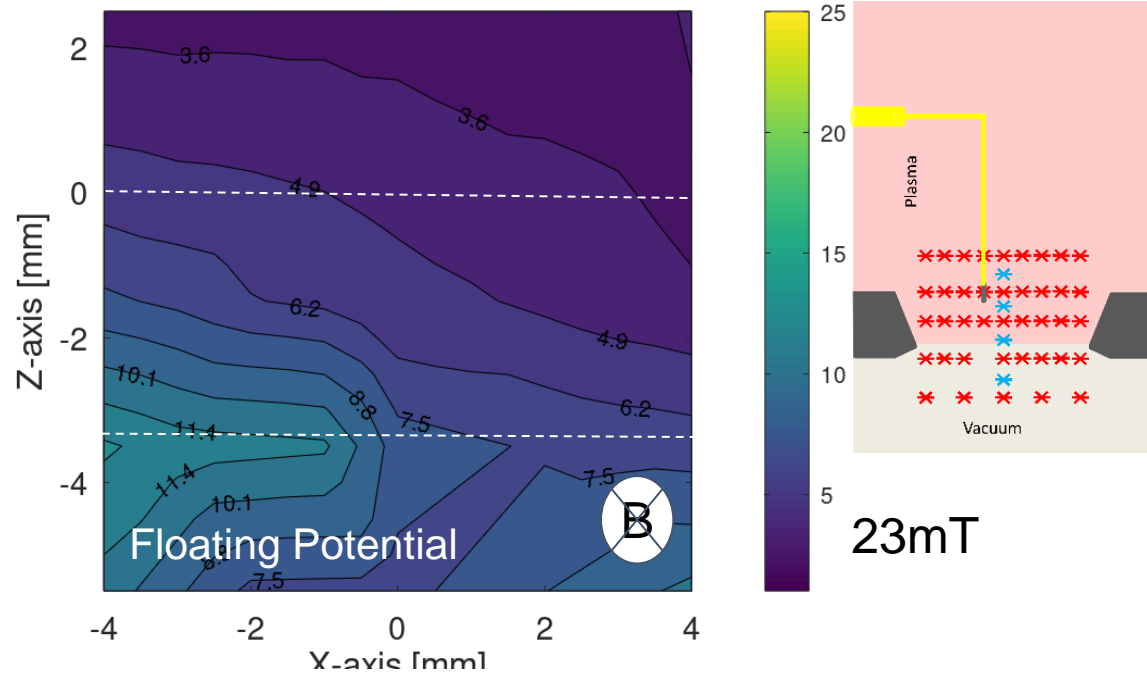
w-Cs $V_{ext}=450V$

Time average IVcurve [$V_{ext}463.5 \pm 4.6[V]$] [$P_{arc}19.2 \pm 1.0[kW]$] [$V_{bias}0.5 \pm 0.0[V]$] [$CRD0.1 \pm 0.2[10^{17}m^{-3}]$]



V

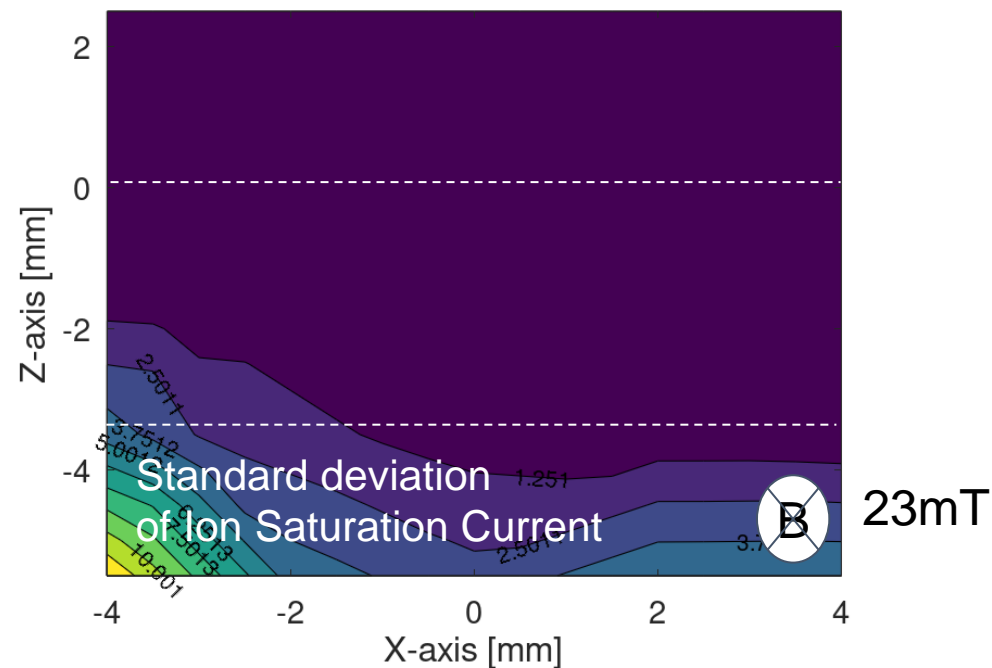
Vf[|H₂ w-Cs|0.8Pa|V_{ext}442.1+51.9[V]|P_{arc}18.3+0.1[kW]|V_{bias}0.45+0.00[V]]



A

Vf[|H₂ w-Cs|0.8Pa|V_{ext}442.1+51.9[V]|P_{arc}18.3+0.1[kW]|V_{bias}0.45+0.00[V]]

V

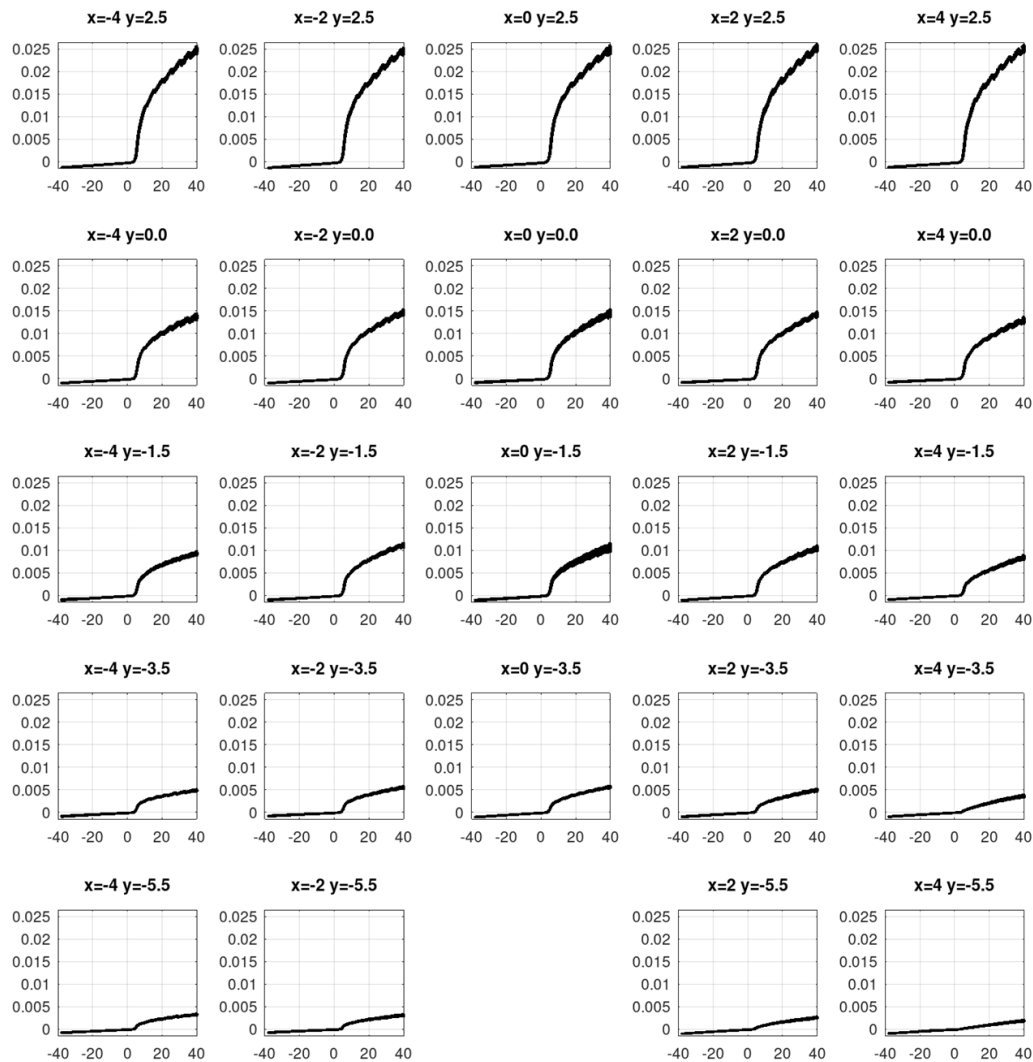


23mT

w/o-Cs

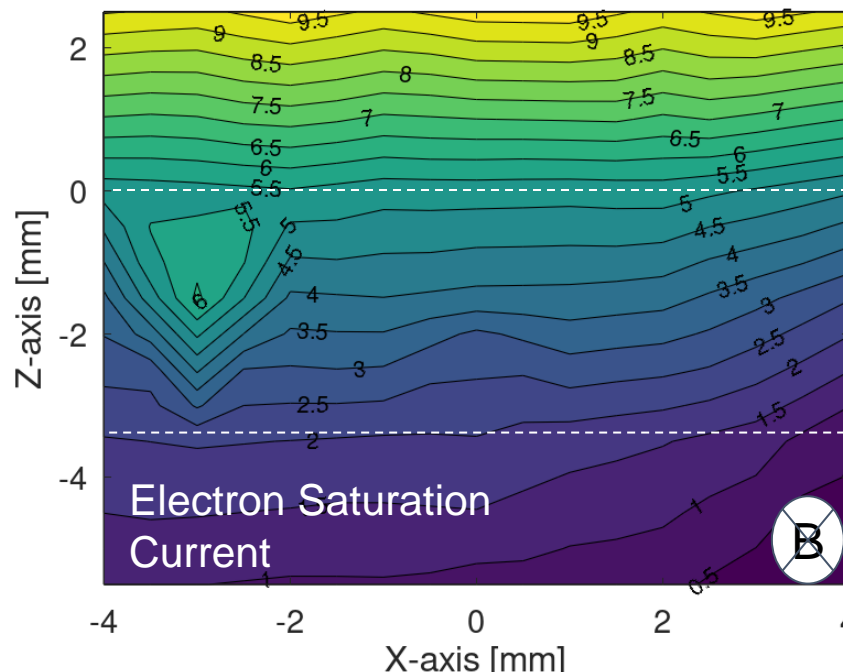
w/o-Cs $V_{ext}=0$

Time average IVcurve $|V_{ext}-0.7+-1.0[V]| |P_{arc} 12.7+-0.8[kW]| |V_{bias} 0.5+-0.0[V]| |CRD 0.1+-0.1[10^{17}m^{-3}]|$

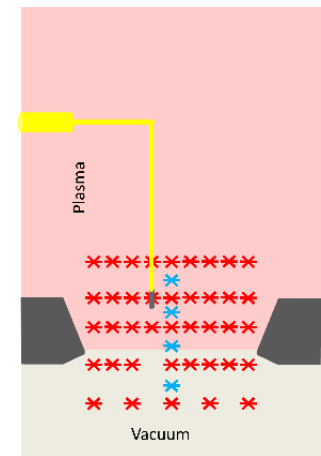


V

$|n_{eg}| |H_2 \text{ w/o-CS}| |0.8Pa| |V_{ext}-0.7+-0.4[V]| |P_{arc} 12.7+-0.0[kW]| |V_{bias} 0.47+-0.00[V]|$



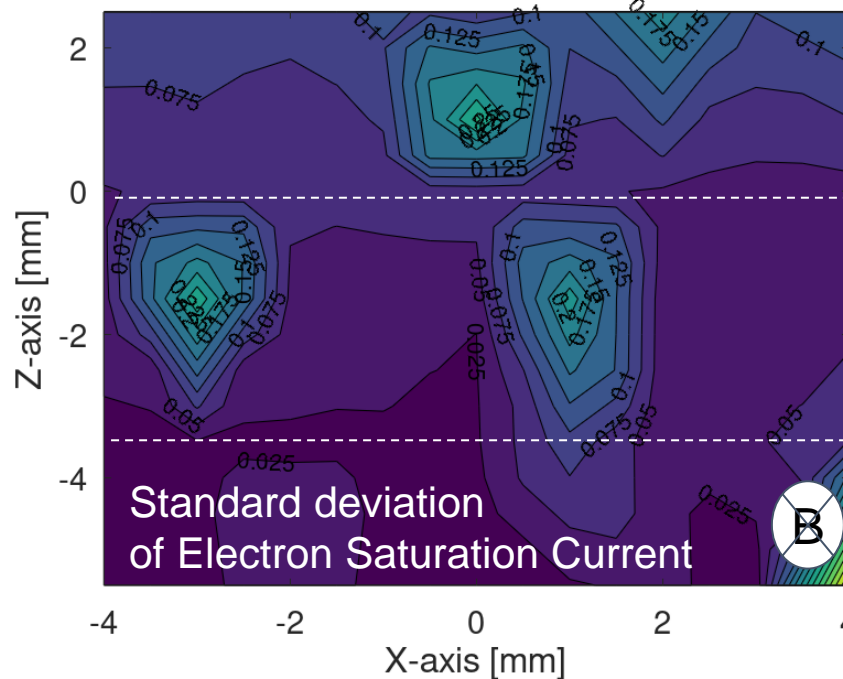
23mT



A

$|n_{eg}| |H_2 \text{ w/o-CS}| |0.8Pa| |V_{ext}-0.7+-0.5[V]| |P_{arc} 12.7+-0.0[kW]| |V_{bias} 0.47+-0.00[V]|$

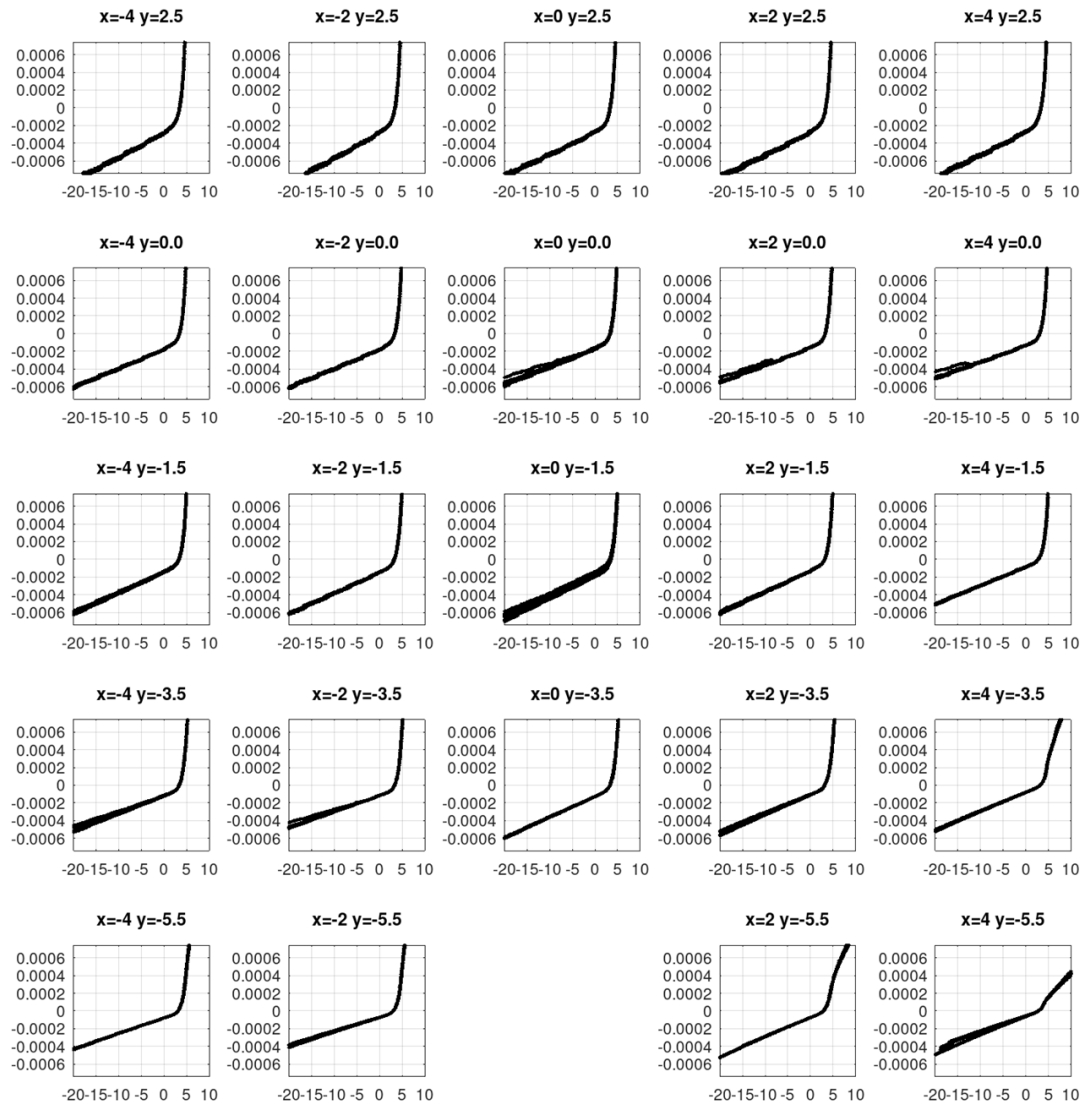
mA



23mT

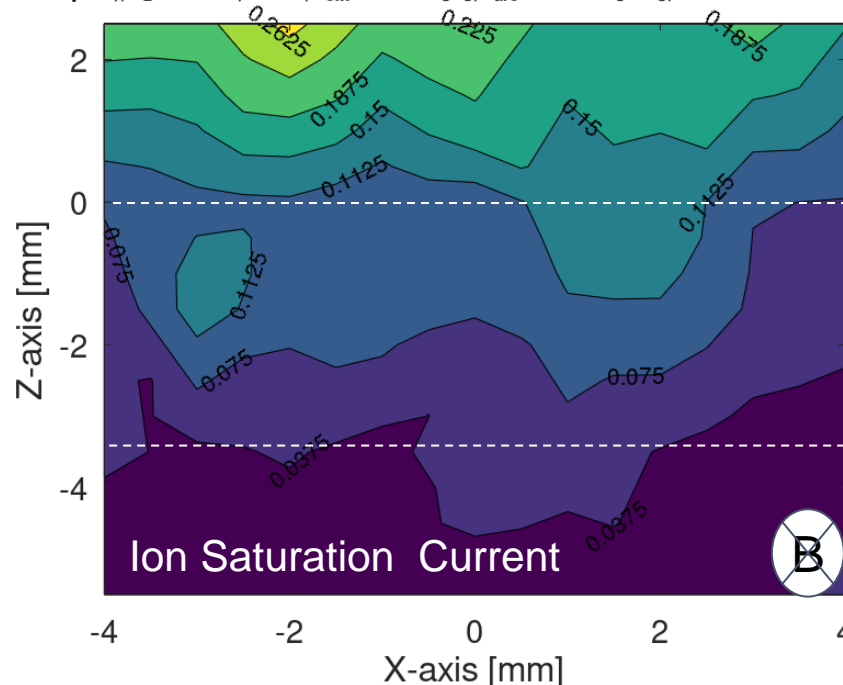
w/o-Cs $V_{ext}=0$

Time average IVcurve $|V_{ext}-0.7+-1.0[V]|P_{arc}12.7+-0.8[kW]|V_{bias}0.5+-0.0[V]|CRD0.1+-0.1[10^{17}m^{-3}]$



V

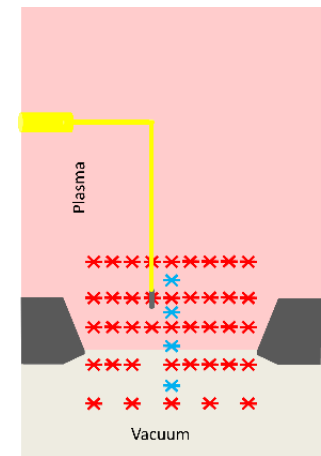
$I_{ps} || H_2$ w/o-Cs $|0.8Pa|V_{ext}-0.7+-0.5[V]|P_{arc}12.7+-0.0[kW]|V_{bias}0.47+-0.00[V]$



Ion Saturation Current

B

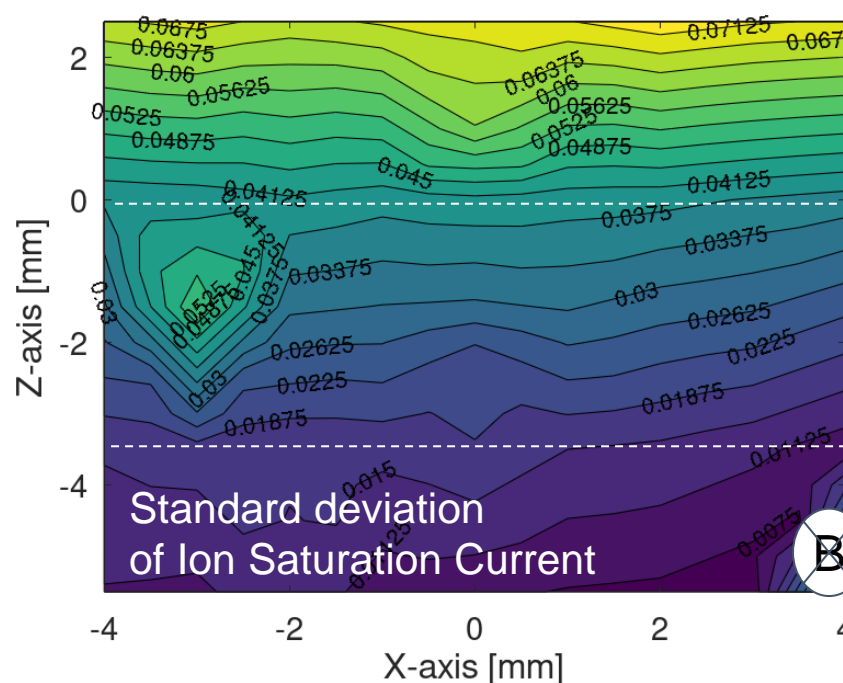
23mT



A

$I_{ps} || H_2$ w/o-Cs $|0.8Pa|V_{ext}-0.7+-0.5[V]|P_{arc}12.7+-0.0[kW]|V_{bias}0.47+-0.00[V]$

mA



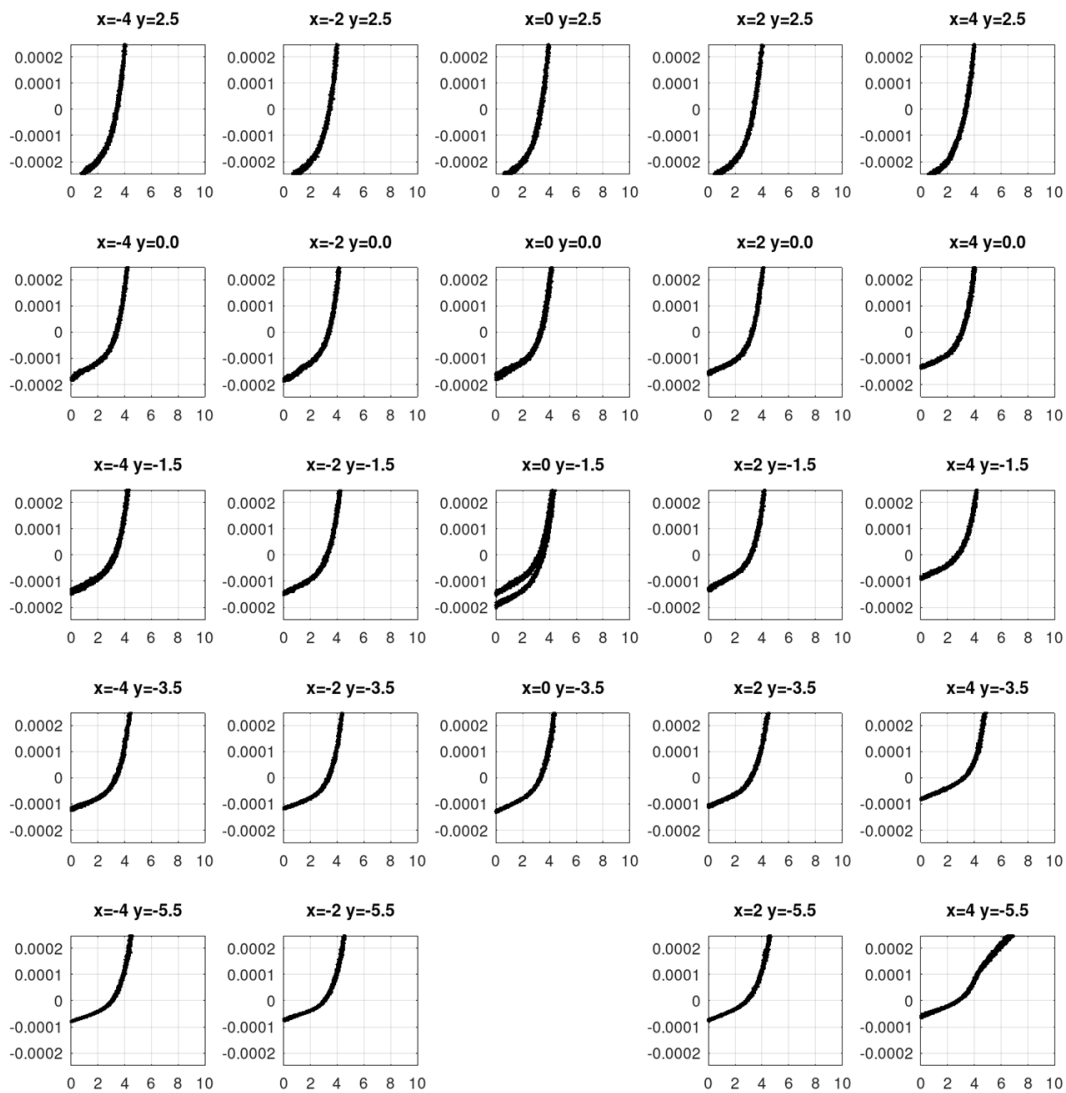
Standard deviation of Ion Saturation Current

B

23mT

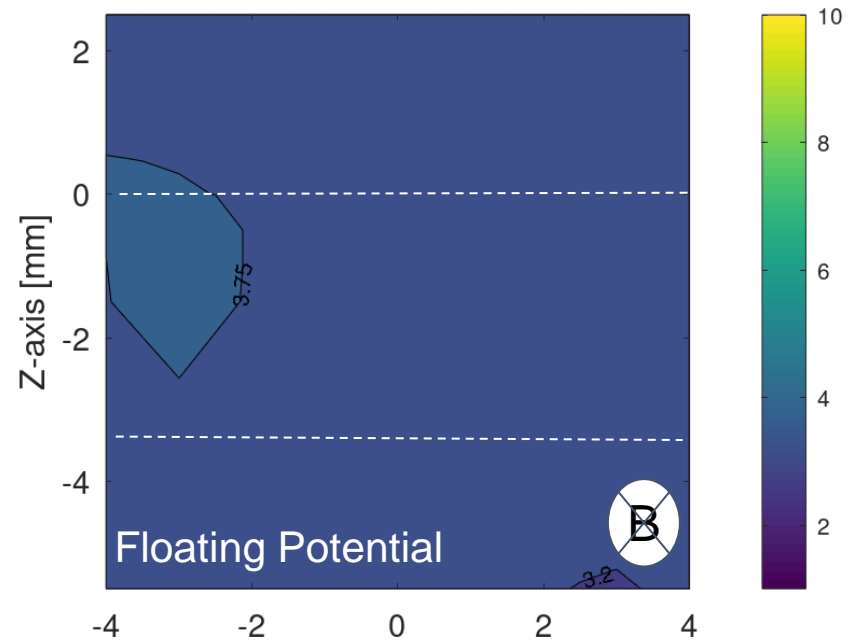
w/o-Cs $V_{ext}=0V$

Time average IVcurve| $V_{ext}=0.7\pm 1.0[V]$ | $P_{arc}=12.7\pm 0.8[kW]$ | $V_{bias}=0.5\pm 0.0[V]$ | $CRD=0.1\pm 0.1[10^{17}m^{-3}]$

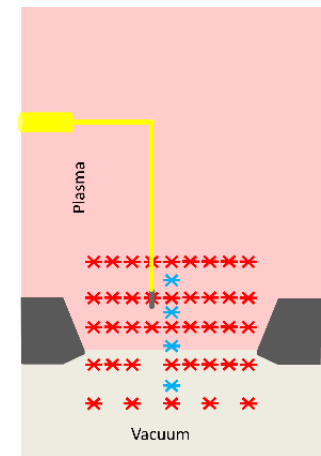


V

$V_f || H_2$ w/o-CS|0.8Pa| $V_{ext}=0.7\pm 0.5[V]$ | $P_{arc}=12.7\pm 0.0[kW]$ | $V_{bias}=0.47\pm 0.00[V]$

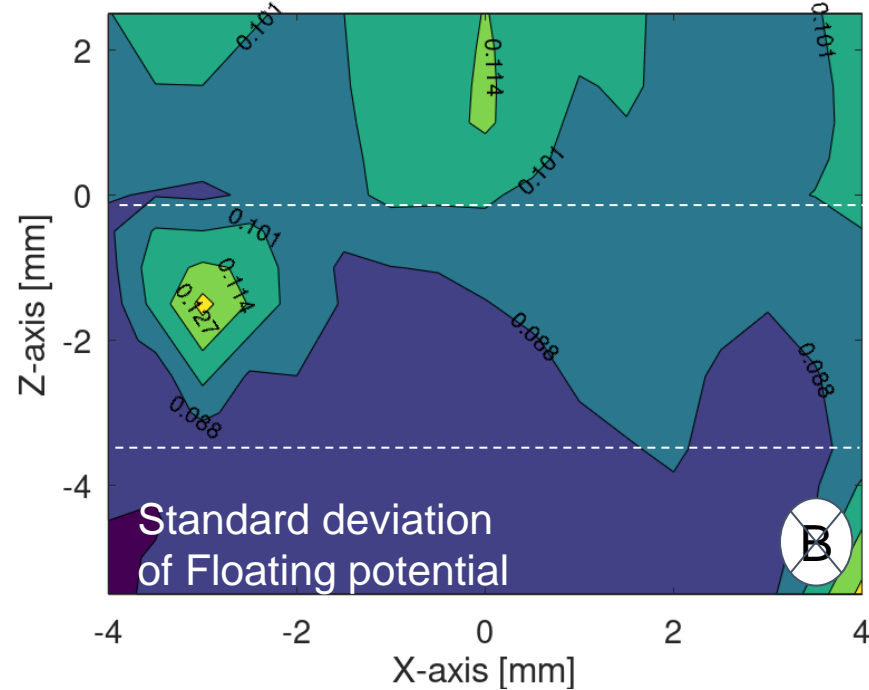


23mT



A

$V_f || H_2$ w/o-CS|0.8Pa| $V_{ext}=0.7\pm 0.5[V]$ | $P_{arc}=12.7\pm 0.0[kW]$ | $V_{bias}=0.47\pm 0.00[V]$

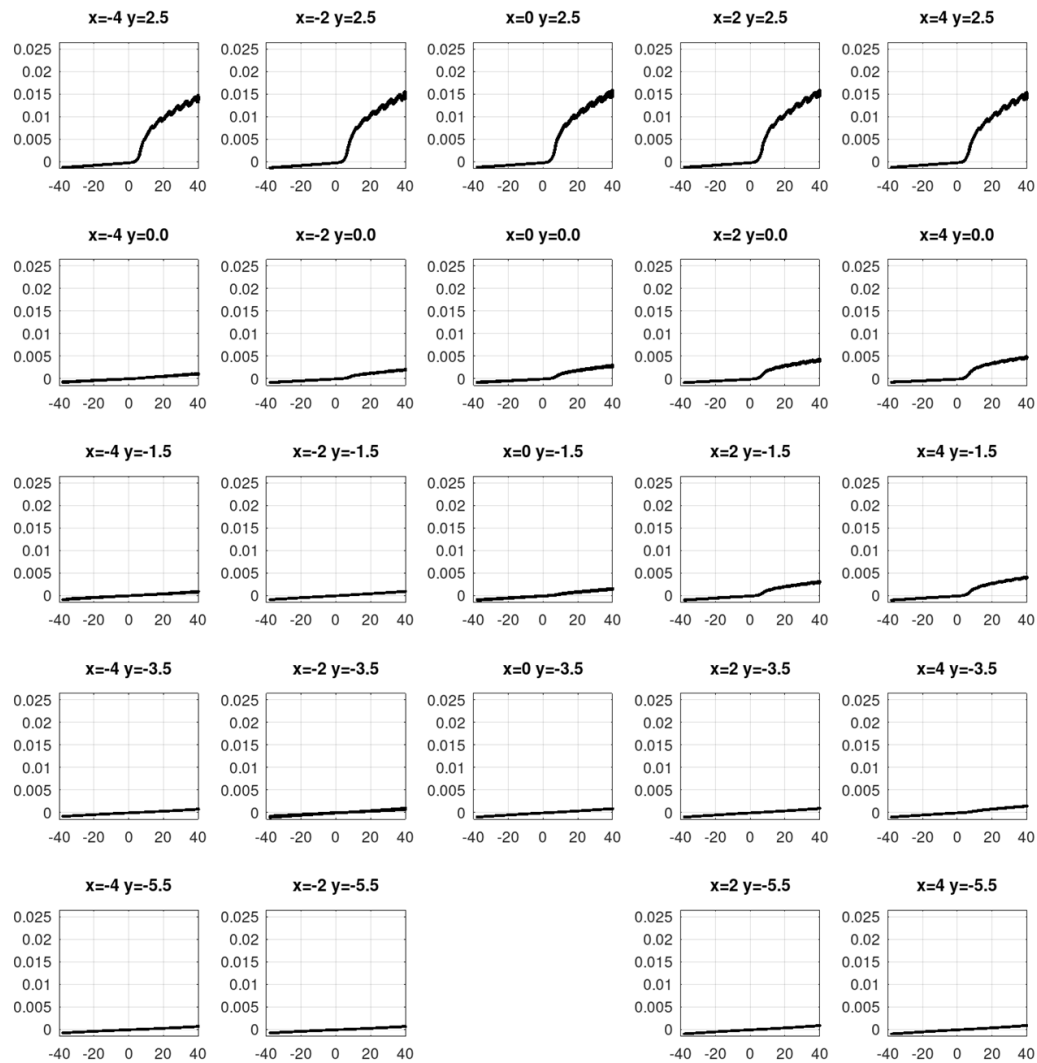


23mT

V

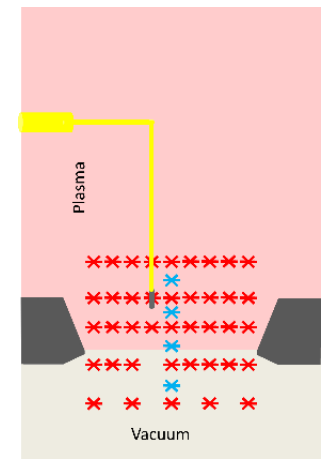
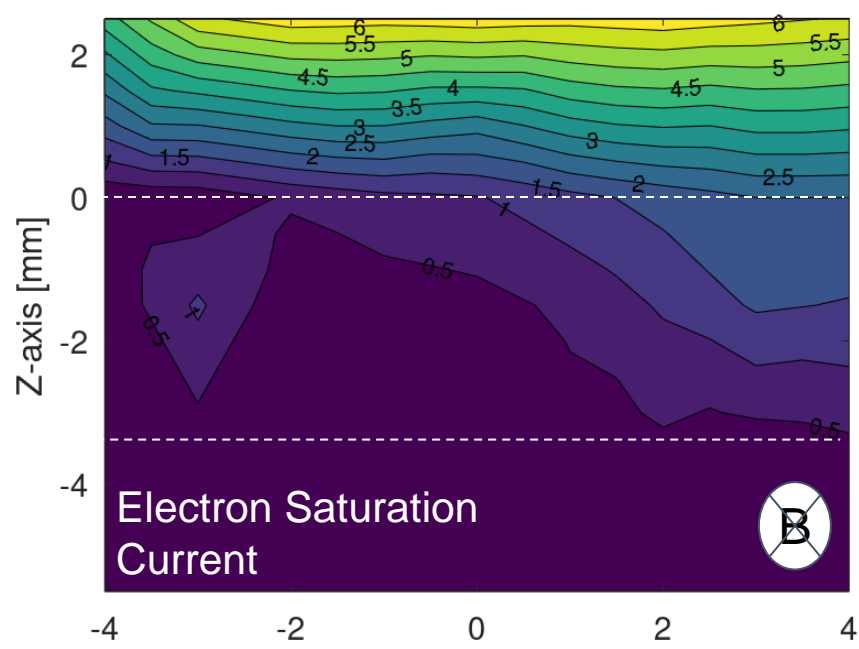
w/o-Cs $V_{ext}=450V$

Time average IVcurve $|V_{ext}496.6+-1.8[V]|P_{arc}12.7+-0.8[kW]|V_{bias}0.5+-0.0[V]|CRD0.1+-0.1[10^{17}m^{-3}]$



V

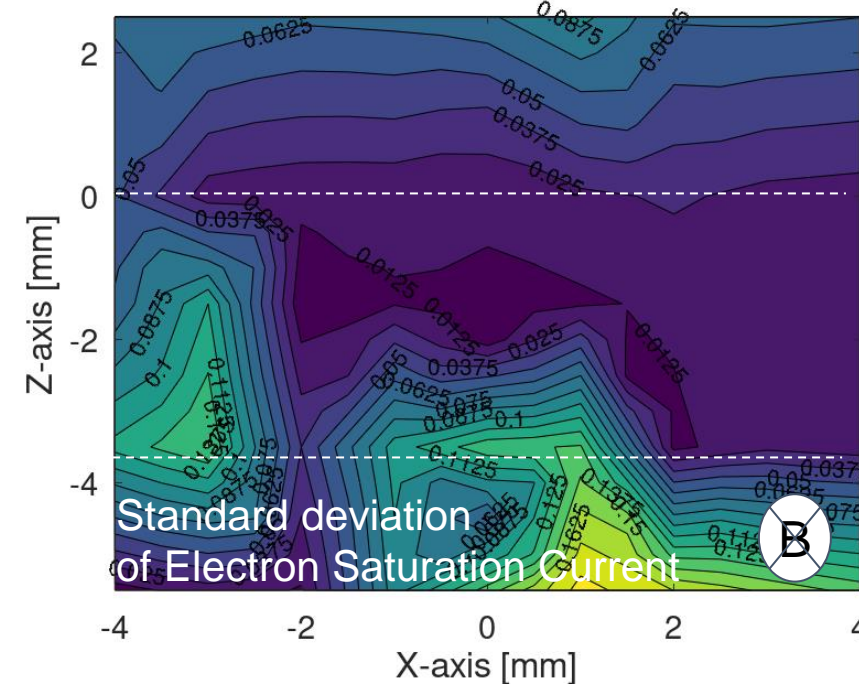
$I_{neg}[H_2 \text{ w/o-CS}|0.8Pa|V_{ext}469.5+-3.9[V]|P_{arc}12.0+-0.0[kW]|V_{bias}0.44+-0.00[V]]$



23mT

A

$I_{neg}[H_2 \text{ w/o-CS}|0.8Pa|V_{ext}469.5+-17.8[V]|P_{arc}12.0+-0.0[kW]|V_{bias}0.44+-0.00[V]]$

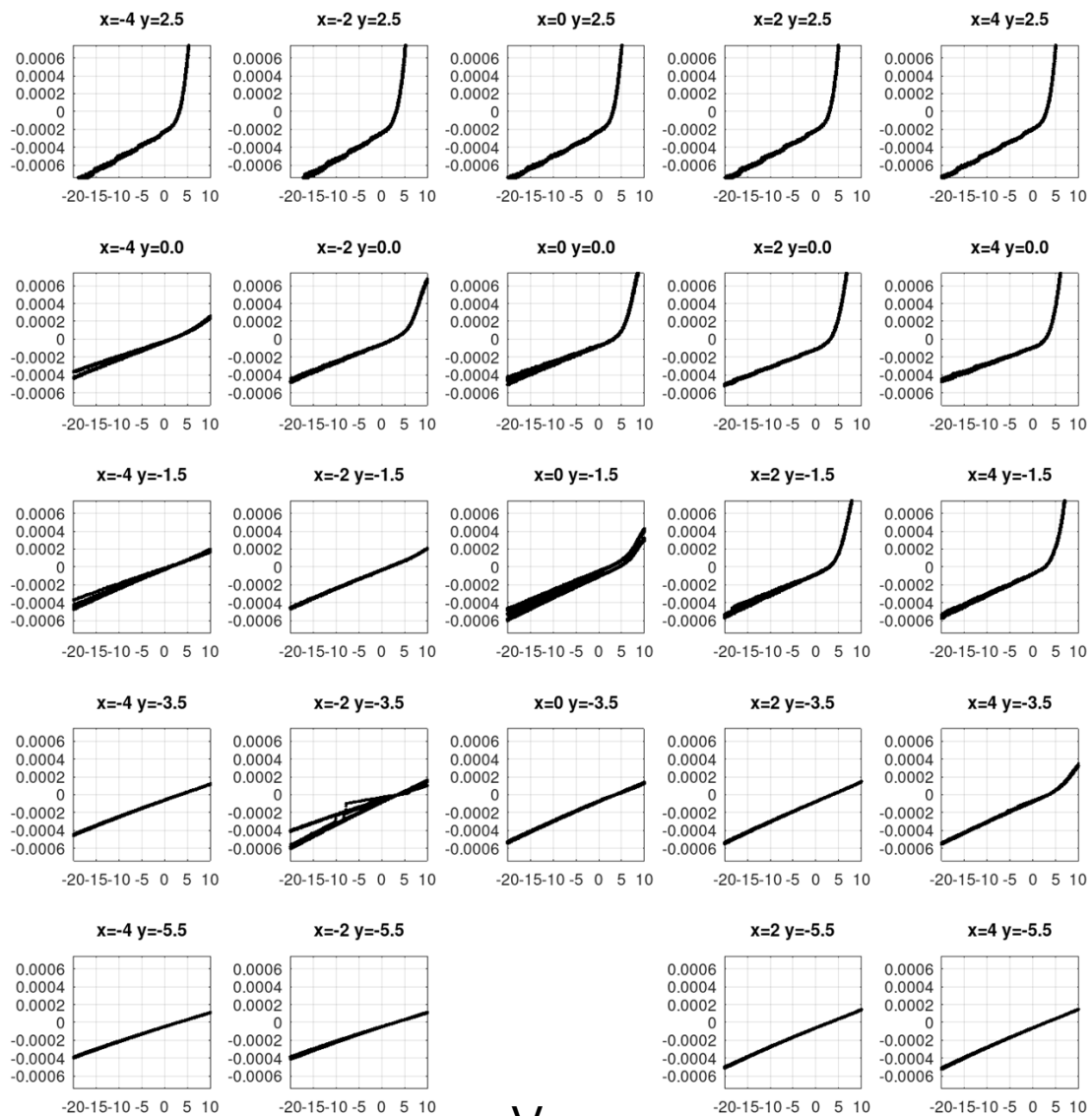


mA

23mT

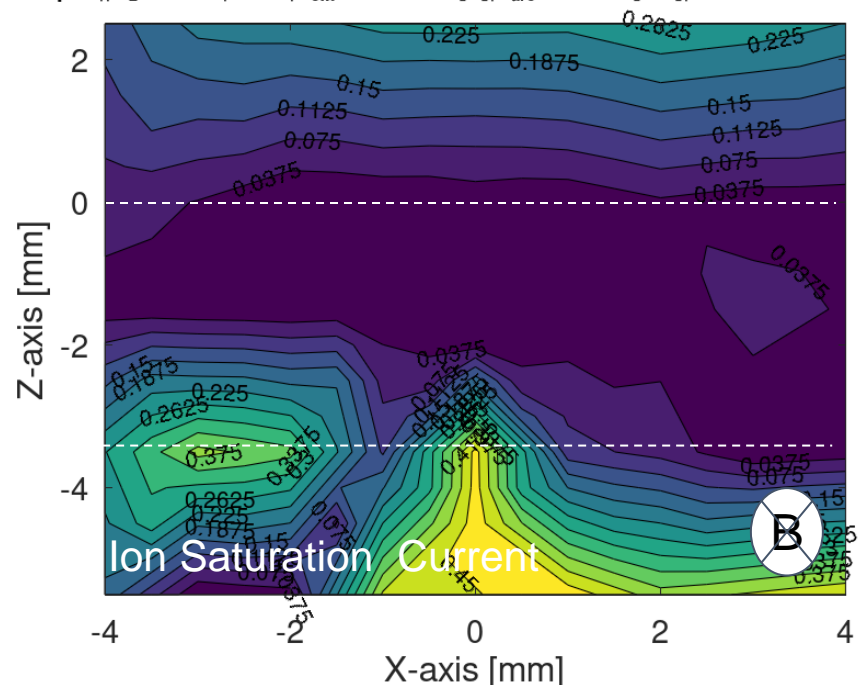
w/o-Cs $V_{ext}=450V$

Time average IVcurve| $V_{ext}496.6\pm 1.8[V]$ | $P_{arc}12.7\pm 0.8[kW]$ | $V_{bias}0.5\pm 0.0[V]$ | $CRD0.1\pm 0.1[10^{17}m^{-3}]$



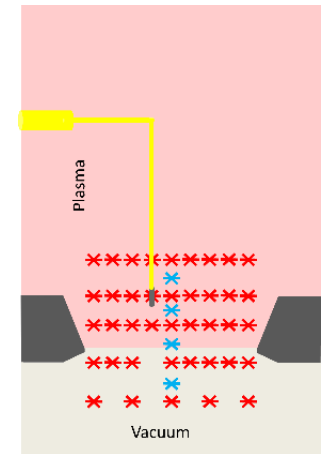
V

$I_{pos}|H_2\ w/o-Cs|0.8Pa|V_{ext}469.5\pm 17.8[V]|P_{arc}12.0\pm 0.0[kW]|V_{bias}0.44\pm 0.00[V]$



Ion Saturation Current

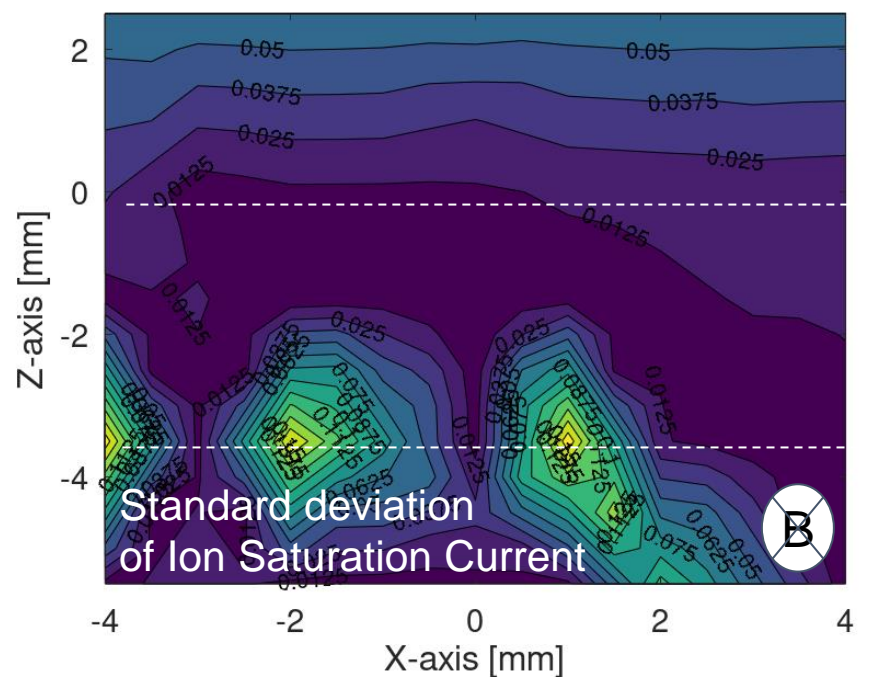
23mT



A

$I_{pos}|H_2\ w/o-Cs|0.8Pa|V_{ext}469.5\pm 17.8[V]|P_{arc}12.0\pm 0.0[kW]|V_{bias}0.44\pm 0.00[V]$

mA

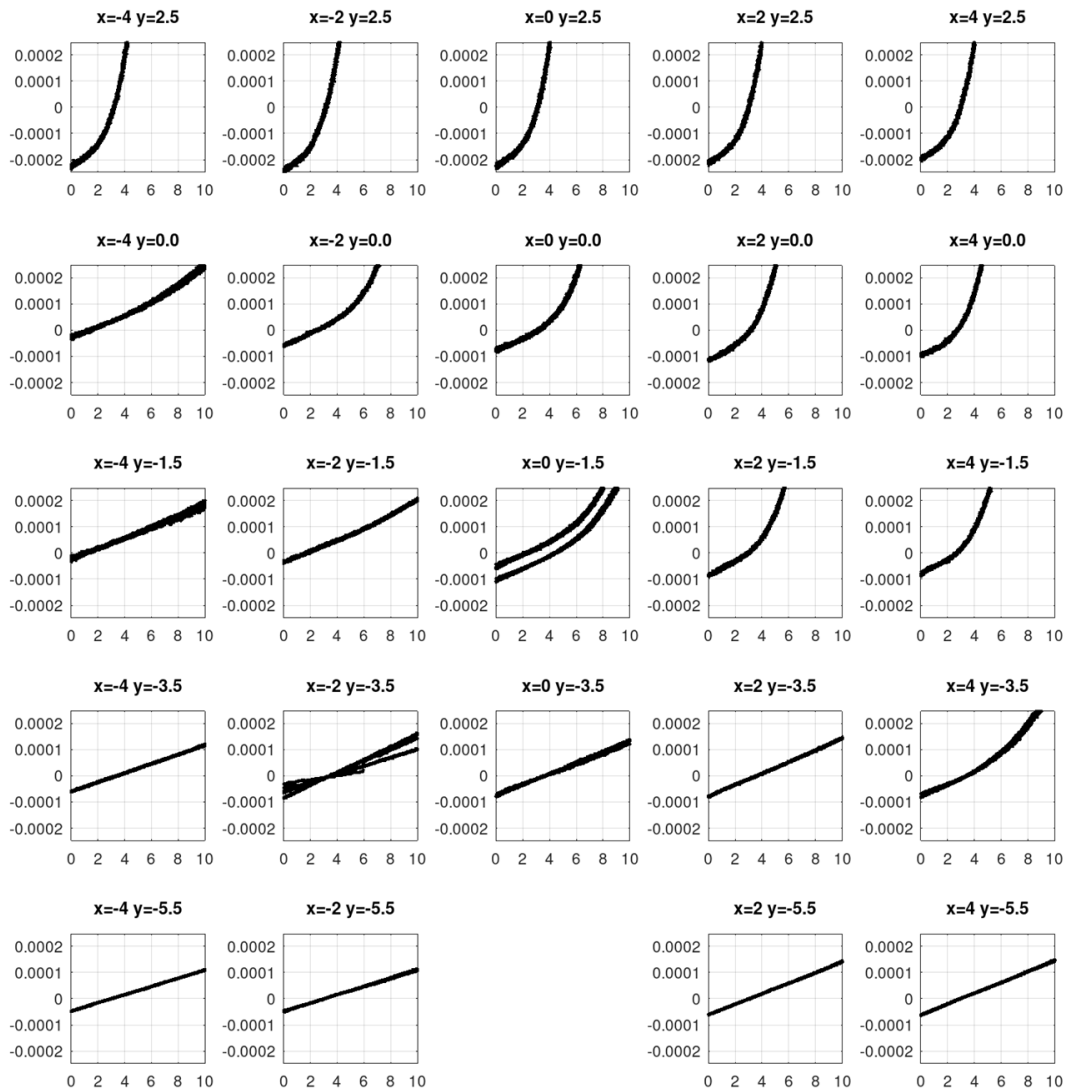


Standard deviation of Ion Saturation Current

23mT

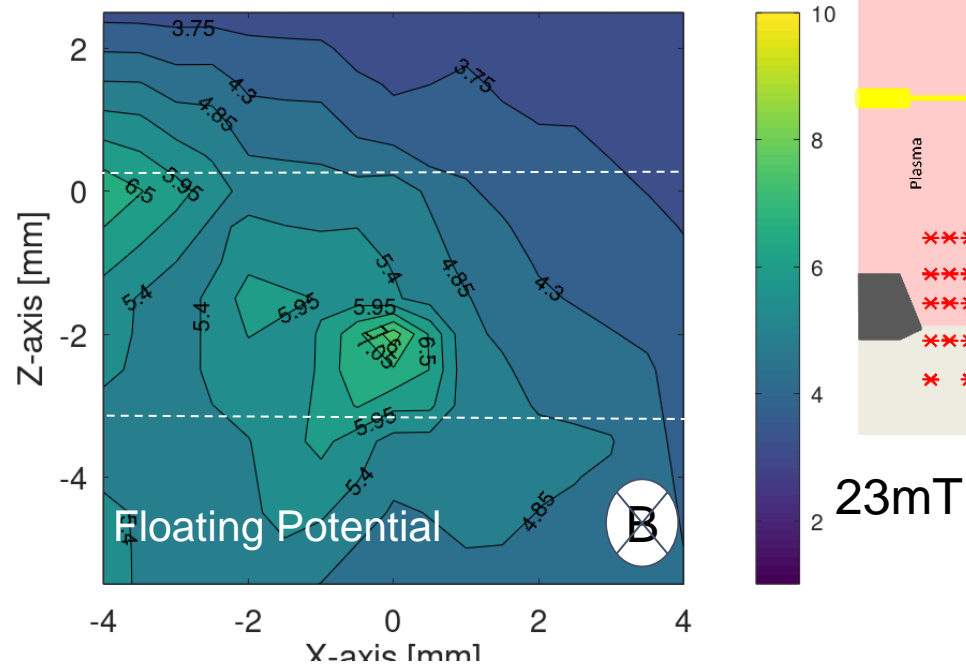
w/o-Cs $V_{ext}=450V$

Time average IVcurve $|V_{ext}496.6\pm 1.8[V]|P_{arc}12.7\pm 0.8[kW]|V_{bias}0.5\pm 0.0[V]|CRD0.1\pm 0.1[10^{17}m^{-3}]$



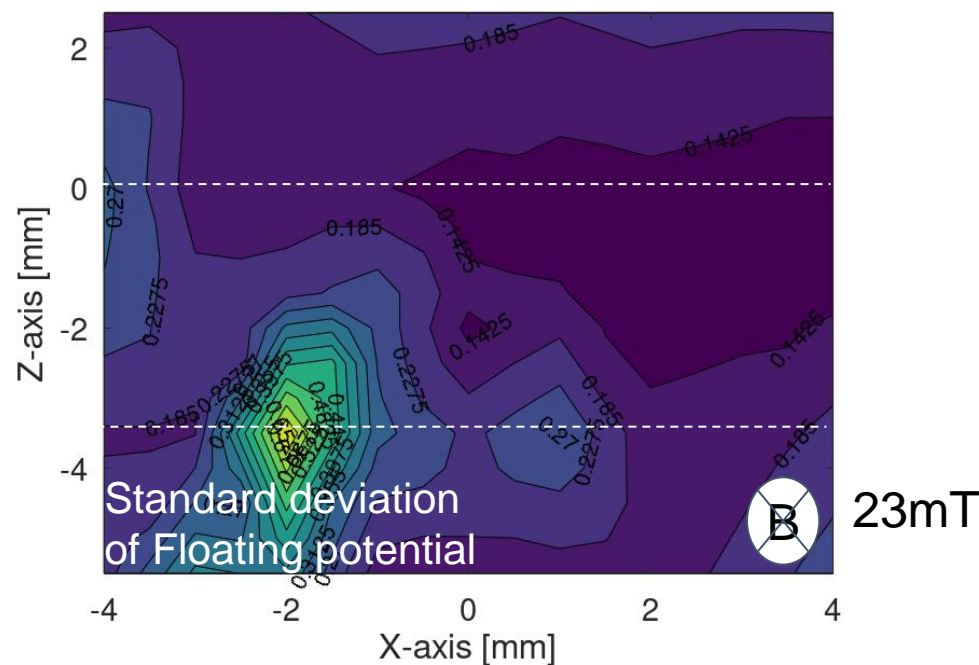
V

$V_f||H_2$ w/o-CS|0.8Pa| $V_{ext}469.5\pm 17.8[V]|P_{arc}12.0\pm 0.0[kW]|V_{bias}0.44\pm 0.00[V]$



A

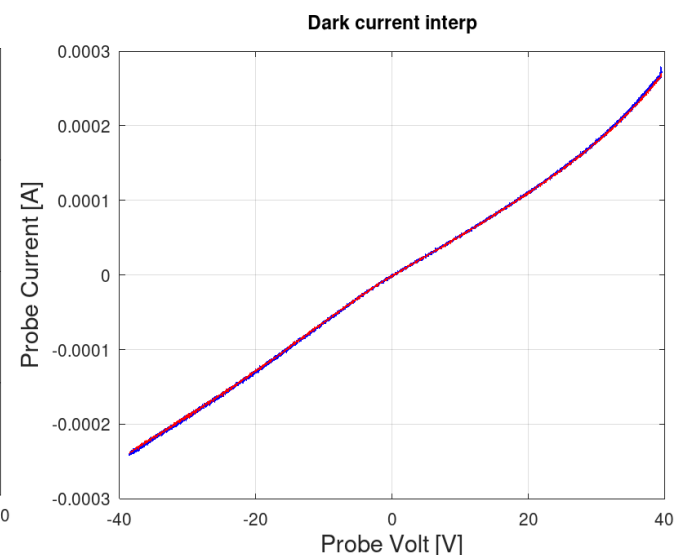
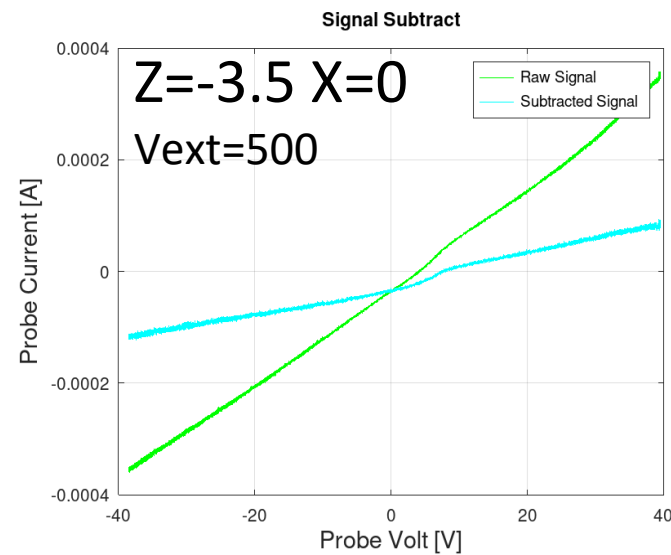
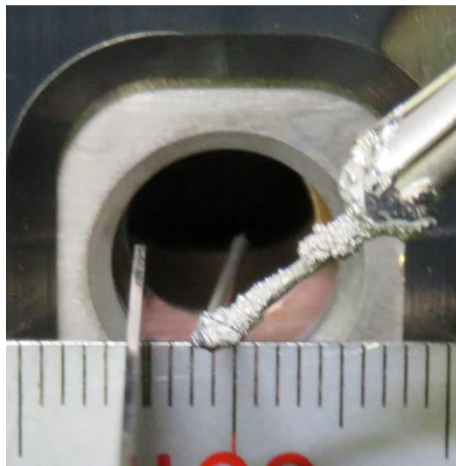
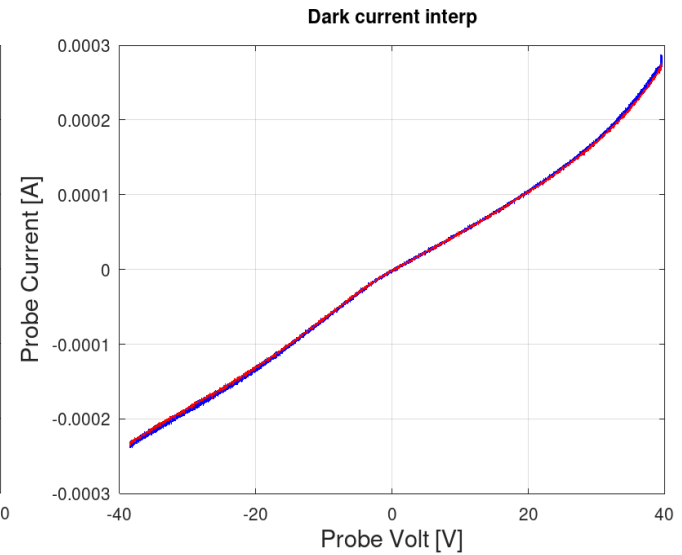
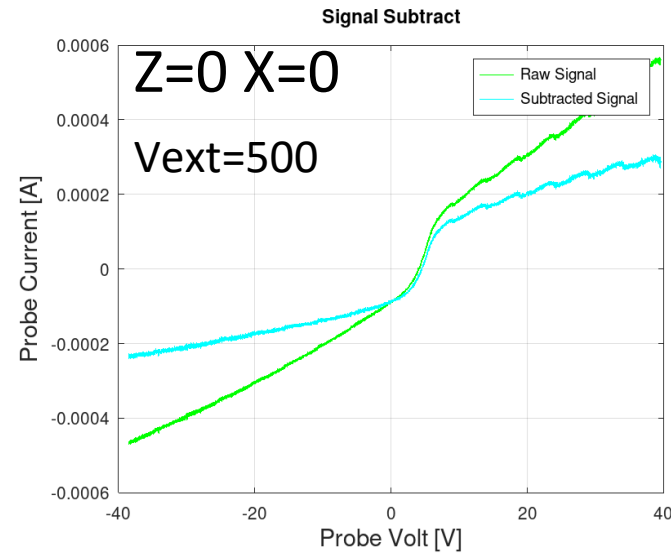
$V_f||H_2$ w/o-CS|0.8Pa| $V_{ext}469.5\pm 17.8[V]|P_{arc}12.0\pm 0.0[kW]|V_{bias}0.44\pm 0.00[V]$



Appendix 5 Leak Current

Dark current effect

W-Cs



Backup

Ion Source Condition

Negative ion source at NBI-Test Stand

- Ion Source : filament-arc type
- Input discharge power: 50kW
- Plasma density: $2 \times 10^{17} \text{ m}^{-3}$
- Puffing gas H₂ :0.8 Pa
- with and without Cs seeding

- Accelerator Grid: PG, EG, and GG
- Bias voltage 0.4V
- Extraction voltage 0,150,250,300,500V

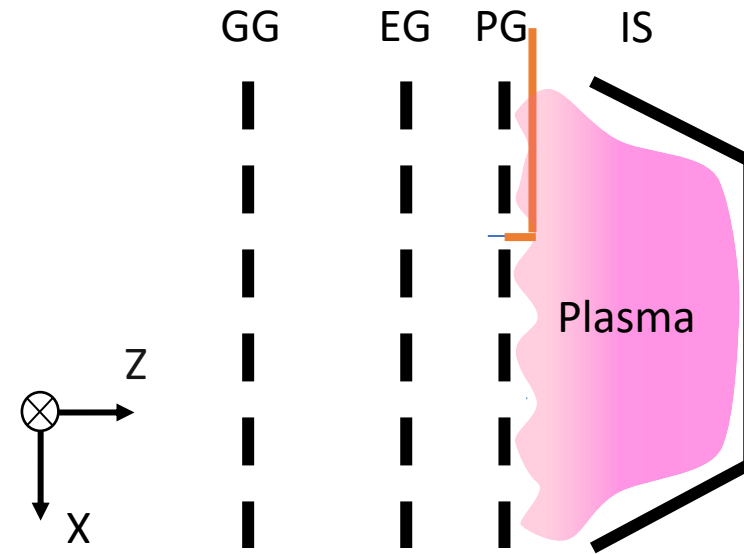
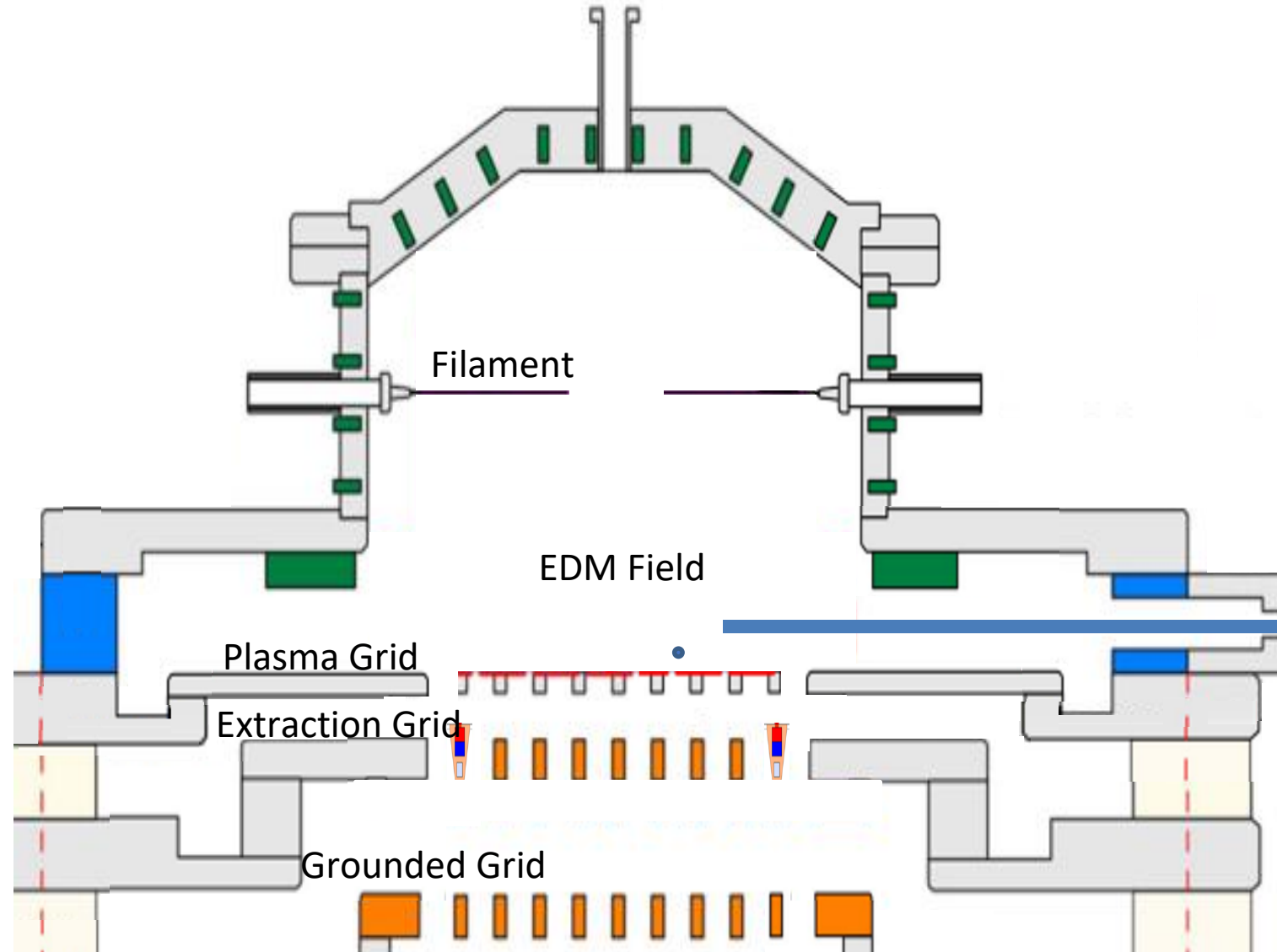
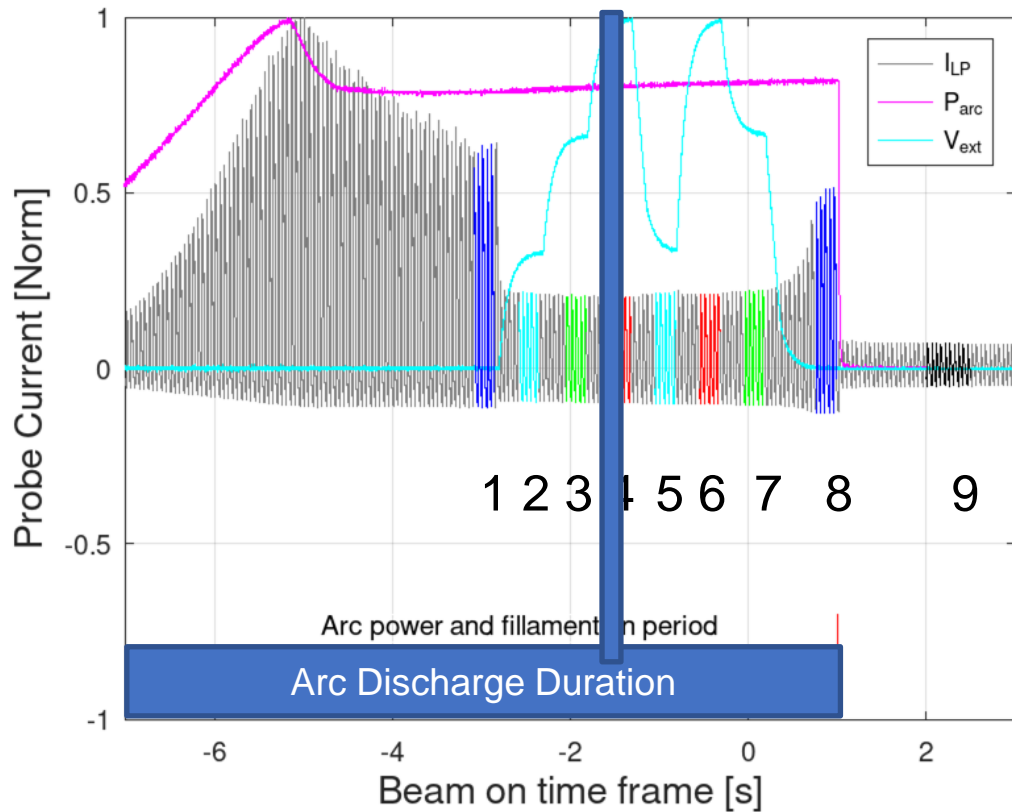


Fig. 4. Diagram of the ion source setup.

Experiment setup

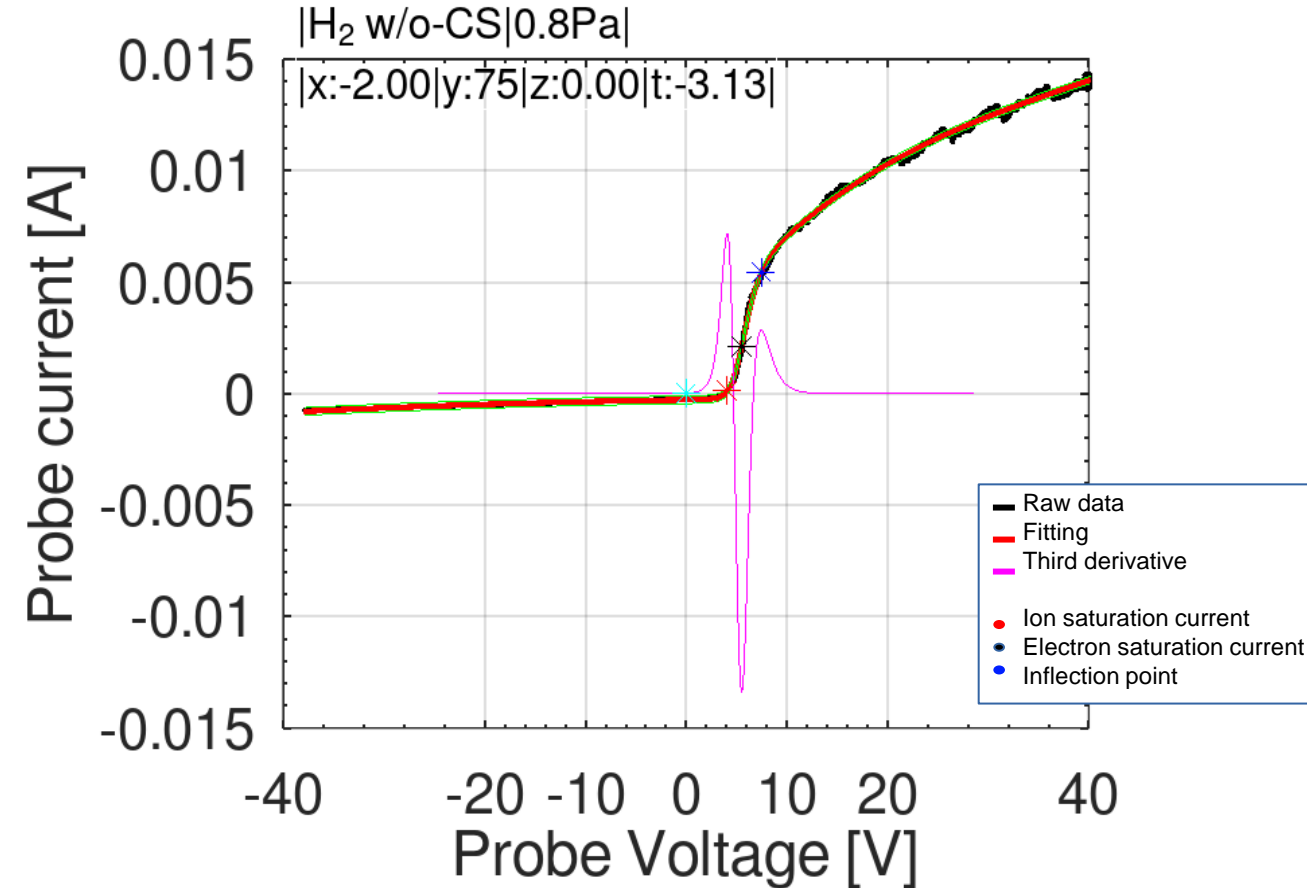


Typical discharge waveform and Langmuir probe signal

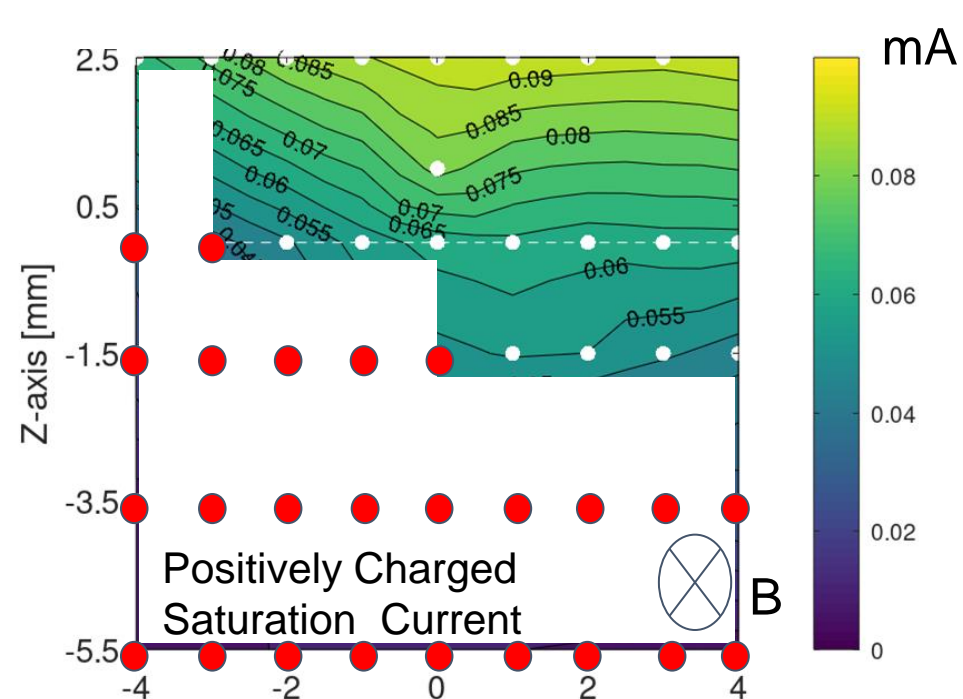
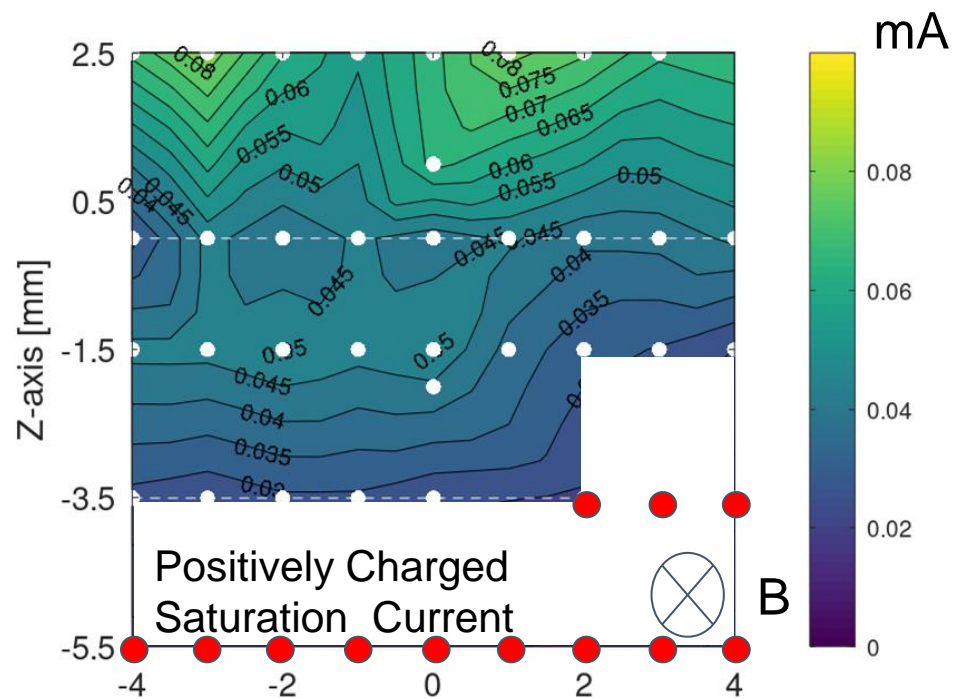
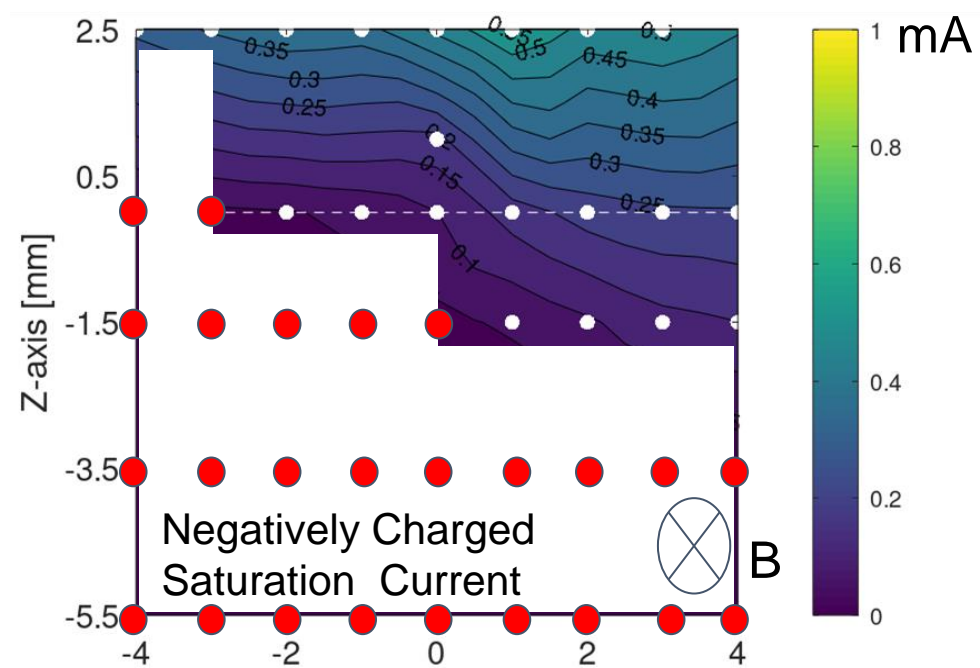
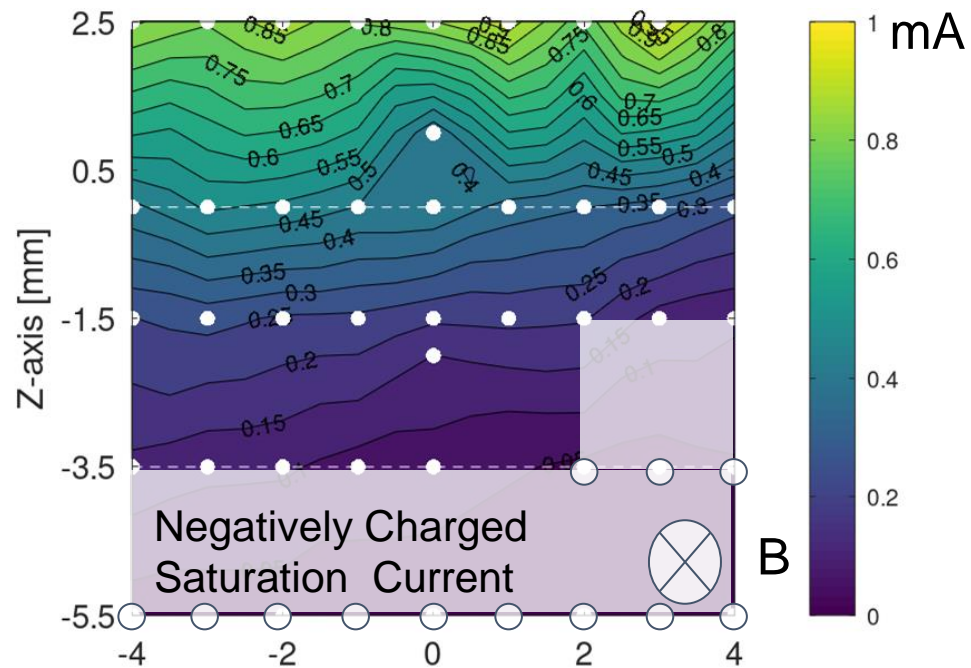


Probe bias is sweeping for diagnostic through out the time of discharge.

The color change on the probe current and number indicate group of sample we take for each V_{ext} level.



Each I-V curve sample are fitted by specific curve. The function will track voltage position of the retard region. Third derivative is calculated from the fitted function. The positive peak of third derivative on lower value and higher probe bias voltage is use as saturation voltage for electron saturation current and location of ion saturation current.



Previous Experiment

Appendix 1 Result comparison

Comparison between Langmuir probe and beam trajectory method

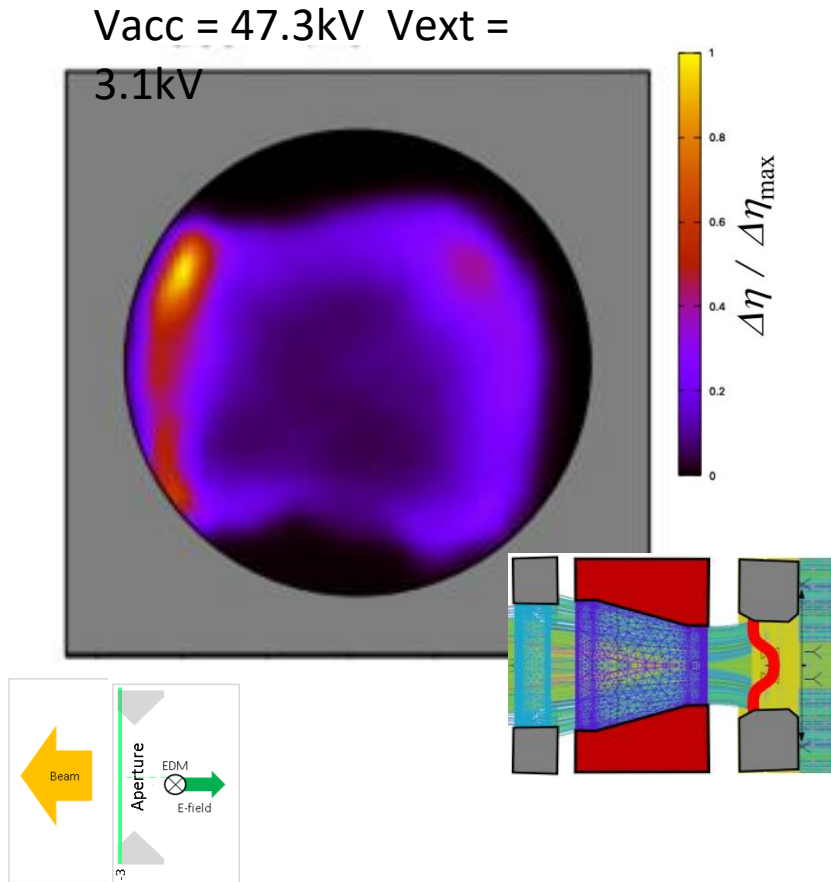


Fig. 16. Flux intensity from fixed perveance
From backward trajectory calculation.

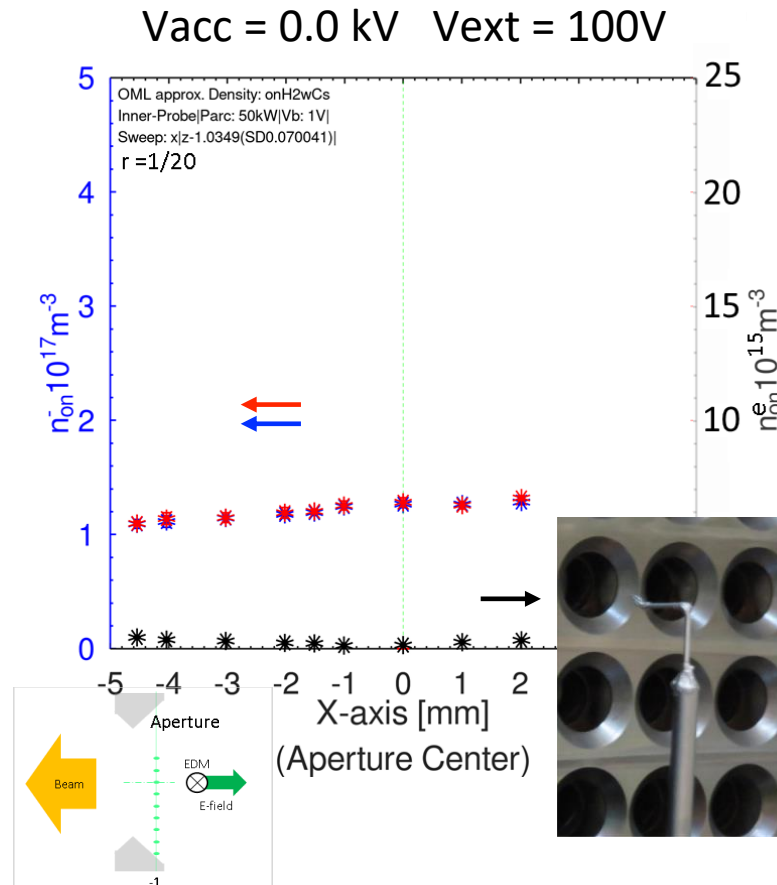


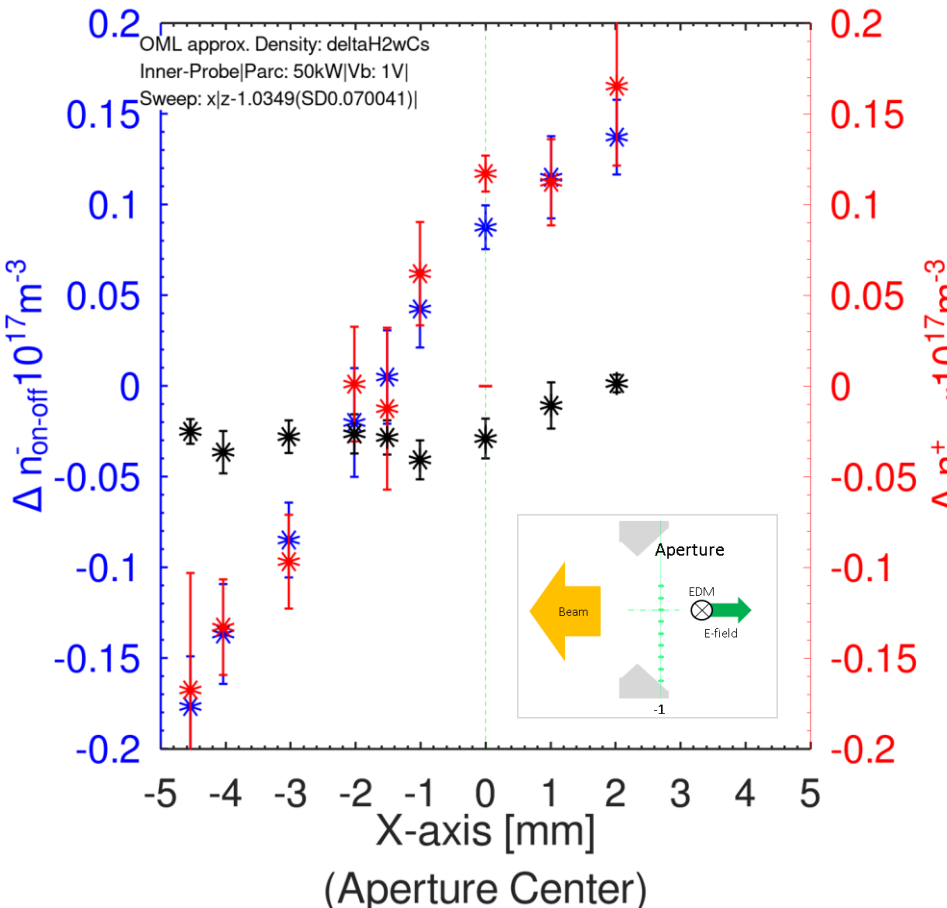
Fig. 17. Langmuir probe scan with applying
extraction potential.

Figure 16 shows intensity of
negative ion flux.

Figure 17 shows density profile of
the plasma.

Extraction Effect

Parc = 50kW



The differences of density before and after beam extraction are shown in figure 15 where the scale is calculated by the following equation ;

$$\Delta n^+ = n^+_{on} - n^+_{off},$$

$$\Delta n^- = n^-_{on} - n^-_{off}.$$



Fig. 15, Hydrogen plasma with cesium saturation current difference between EG 0V and EG 110V plot.

Extraction effect on Density profile

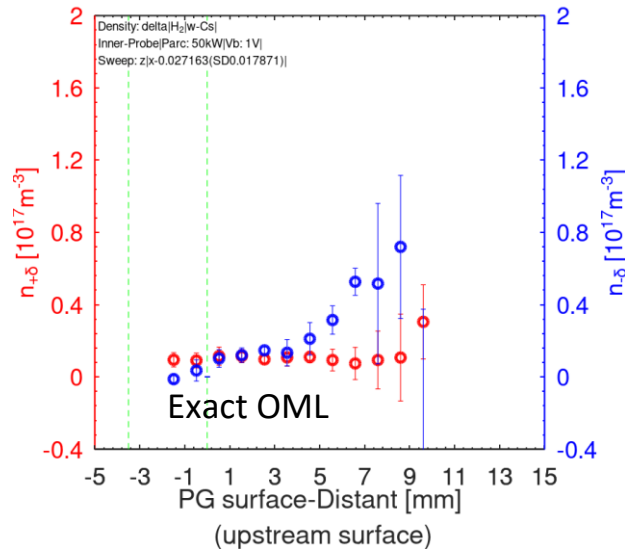


Fig.16. evaluation without electron separation.

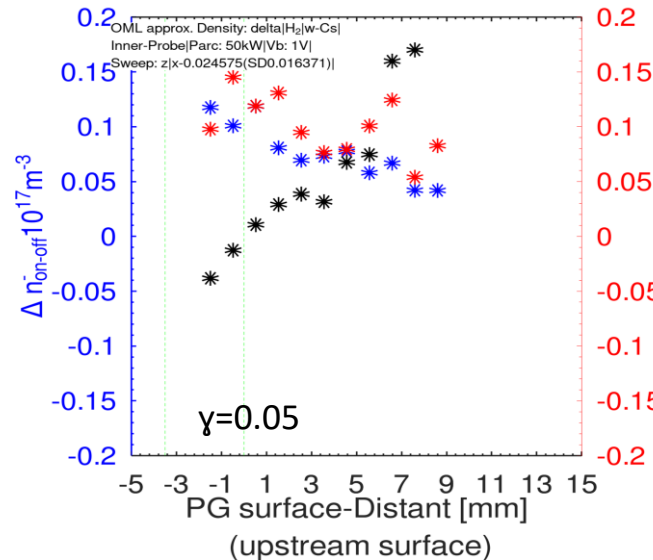


Fig.17. evaluation with electron separation.

The profile shows increasing of density near to PG while electron is reduced when extraction potential is applied.

Still, with small value of “ γ ”, I_{∞}^+ current seem solely depend on I_0^-

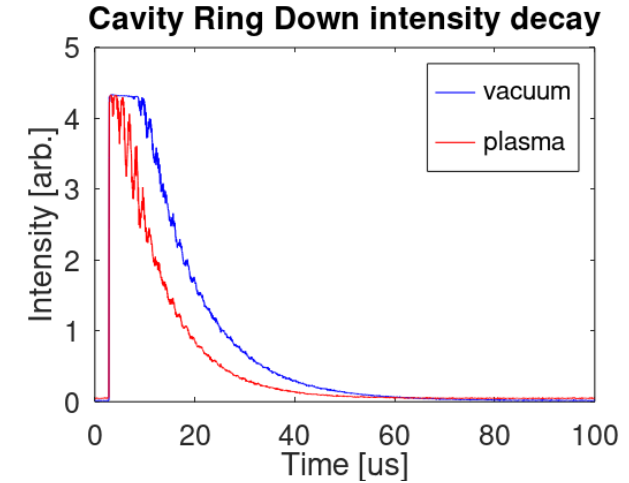
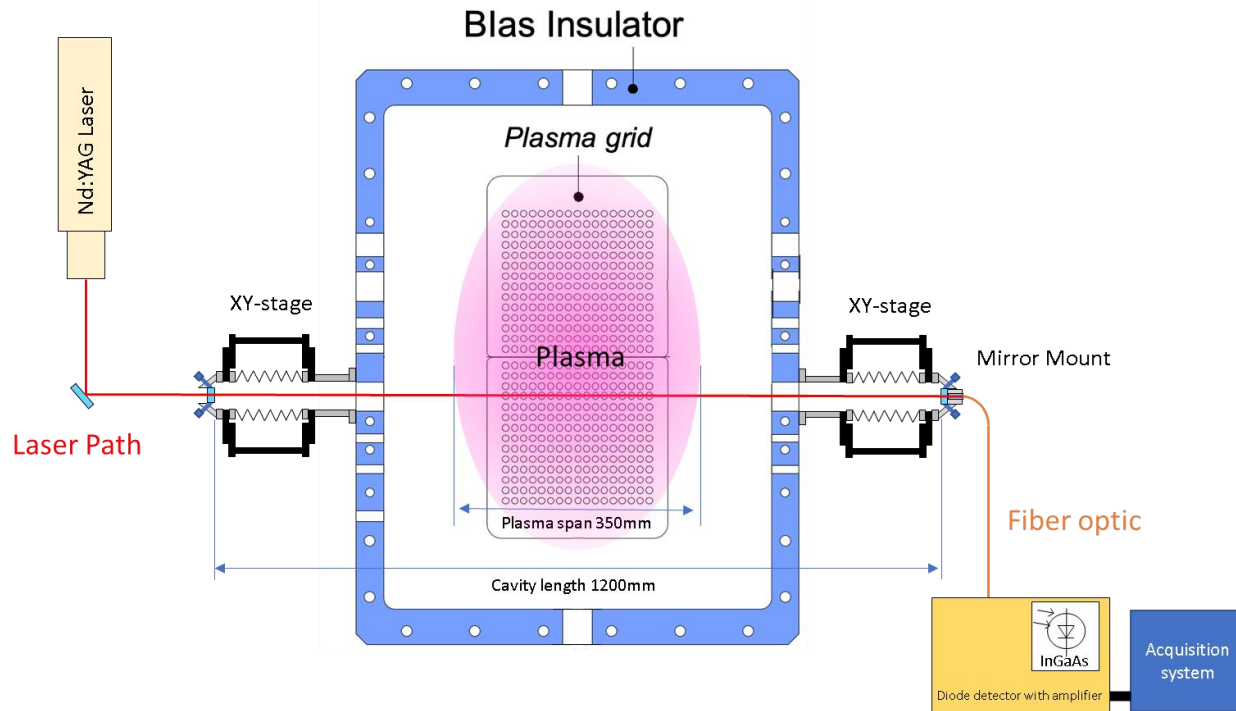
$$I_{neg} = \frac{I_0^- + \gamma I_0^+}{\gamma - 1}$$

Then the reduction of negative ion might be distorted when compare between figure 16 and 17.

However, distinguish between electron and negative ion is clearly importance to evaluate the plasma distribution profile.

Appendix 2 Cavity ring down measurement

Cavity ring down measurement



$$n = \left(\frac{1}{\tau_0} - \frac{1}{\tau} \right) \frac{d}{cL\sigma}$$

Cavity ring down is a line average diagnostic system. Laser absorption when pulse inject into plasma is the theory of measurement. A pair of high reflection mirror is use in the system to increase laser beam traveling time in the plasma. In each reflection, intensity of the laser decrease and intentional leak of laser from mirror led to measurement of laser intensity. With the comparison between vacuum and plasma decay time constant of laser intensity, line average negative ion density can be calculated. The calculation is the develop form of Lambert-Beer equation.

Appendix 4 Extraction Physics

Focusing effect of Meniscus

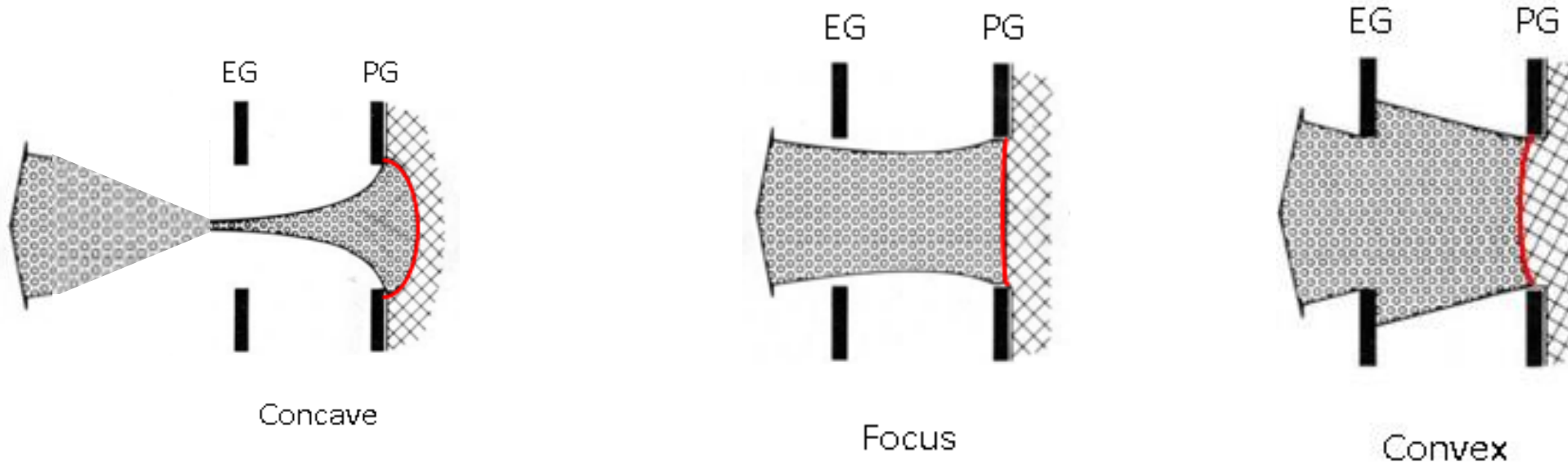


Fig. 3, Meniscus focusing effect

Tarvainen, Olli. (2021). STUDIES OF ELECTRON CYCLOTRON RESONANCE ION SOURCE PLASMA PHYSICS.

- Focusing effect of the meniscus shape appear in to three case.
- First concave, when extraction field is too high, the extracted negative ion are over perveance.
- Second focused, the optimal perveance is obtain and match to the next stage of acceleration
- Third convex, when plasma pressure is too high, the extracted negative are under perveance

Extraction Physics of positive ion source

“The positive ion flow region downstream from the plasma meniscus is automatically adjusted to the state that the distance between the meniscus and the electrode, the potential distribution, the flow pattern etc. are all described approximately valid by the space-charge-limited flow regime. Thus, in a plasma source, the shape and position of the ion-emissive surface are always automatically adjusting so that the ion flow is simultaneously emission limited by the plasma and the space-charge limited by the extraction voltage.”

Kyoung-Jae Chung, Department of Nuclear Engineering, Seoul National University

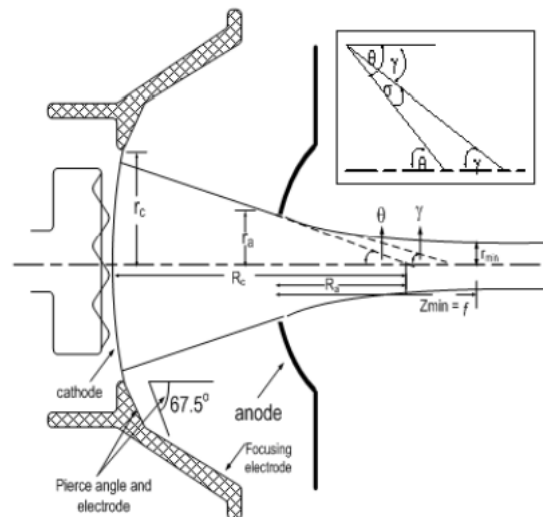
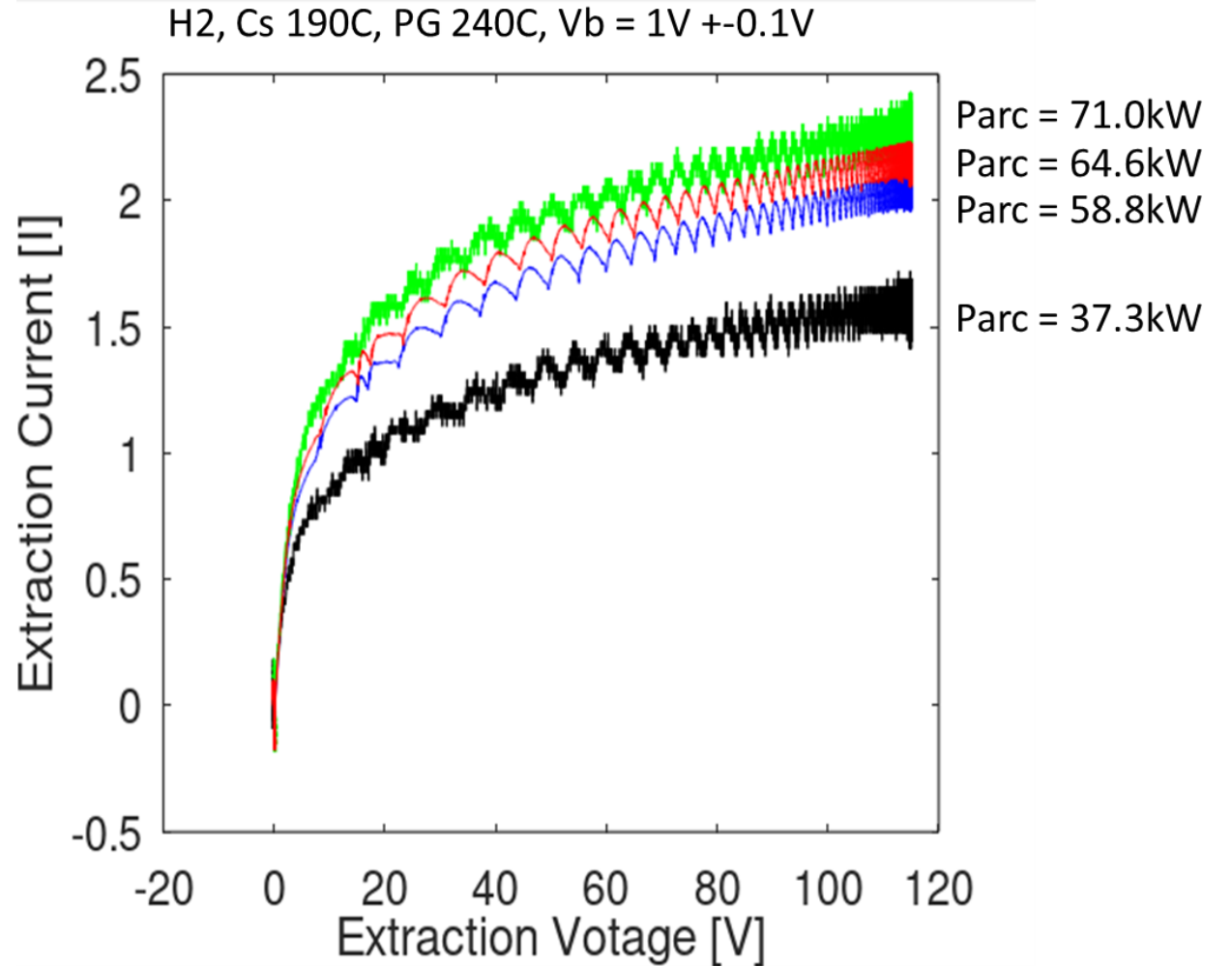
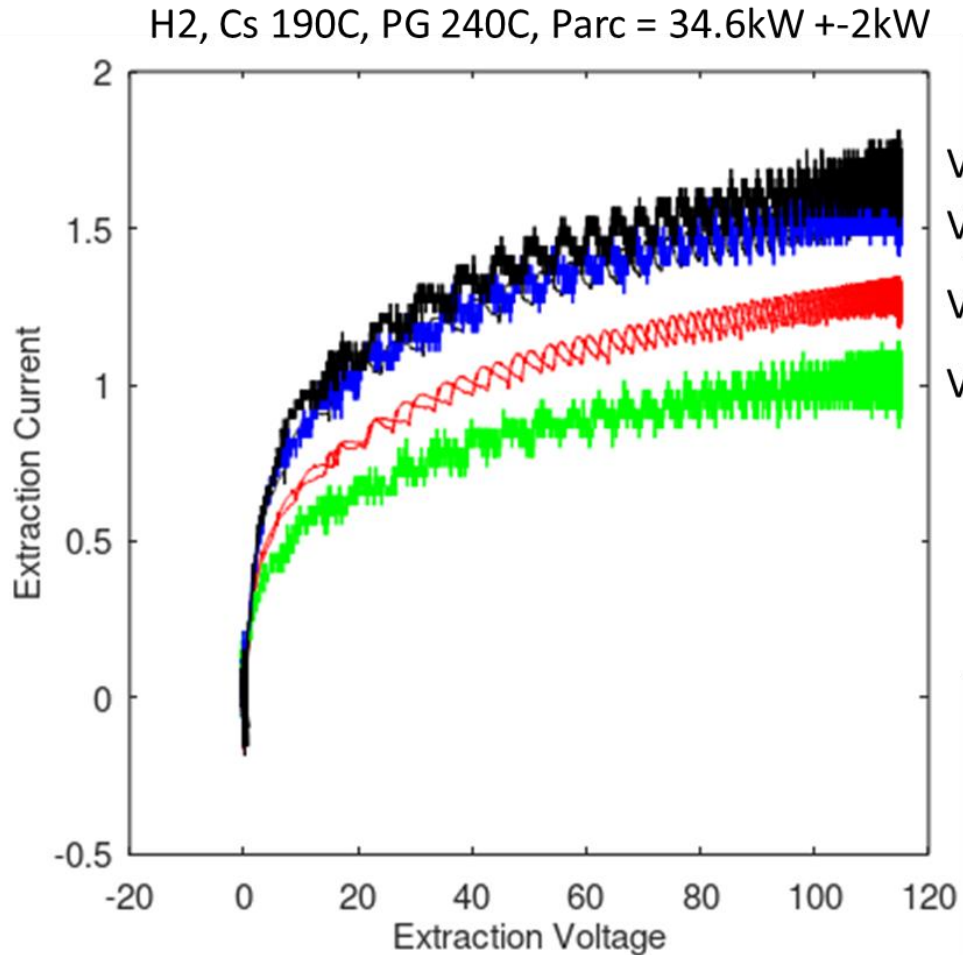


Figure 1. Electron gun and beam configuration geometry

Emission from Negative ion source



Structure of Negative Ion Source

- Hydrogen/Deuterium negative ions are produced on the **plasma grid** (PG) surface with cesium (Cs) seeding in the ion source (IS), as shown in figure 2.
- By an electrostatic field applied between the PG and the **extraction grid** (EG) called “extraction field”, the produced negative ions are extracted to form initial negative ion beams. In a single stage acceleration, An acceleration field is applied between the EG and the **grounded grid** (GG) to energize and construct the beam .

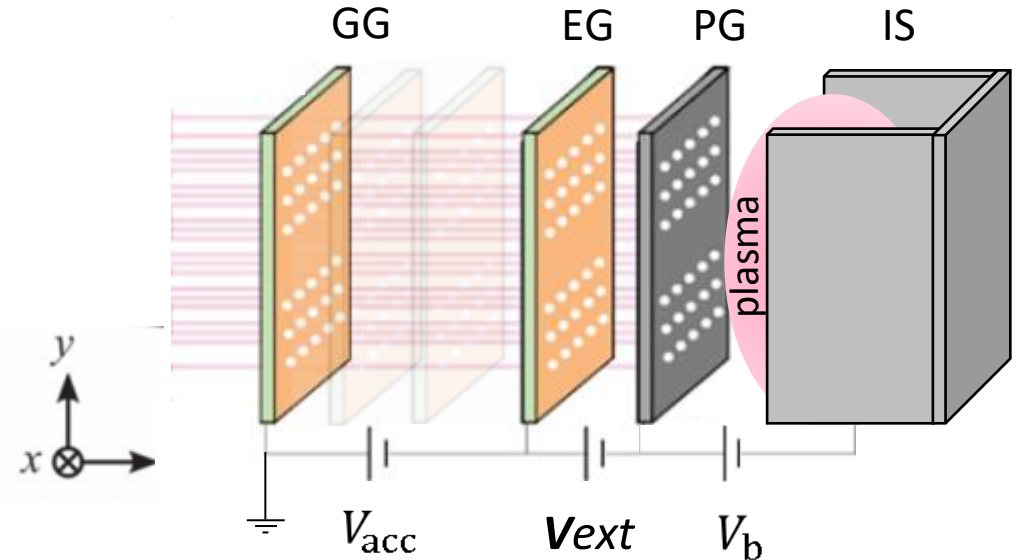


Fig. 2. Fundamental structure of the ion source with an accelerator.

Appendix 5 Cesium and isotope effect

Cesium seeding effect

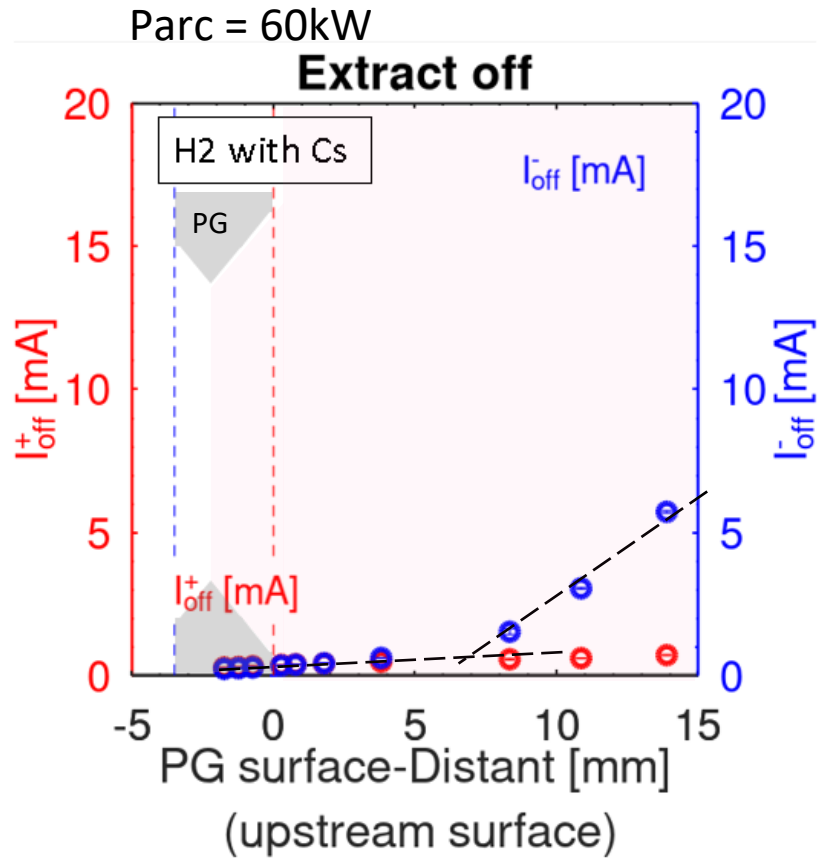


Fig. 10, Hydrogen plasma with cesium saturation current plot.

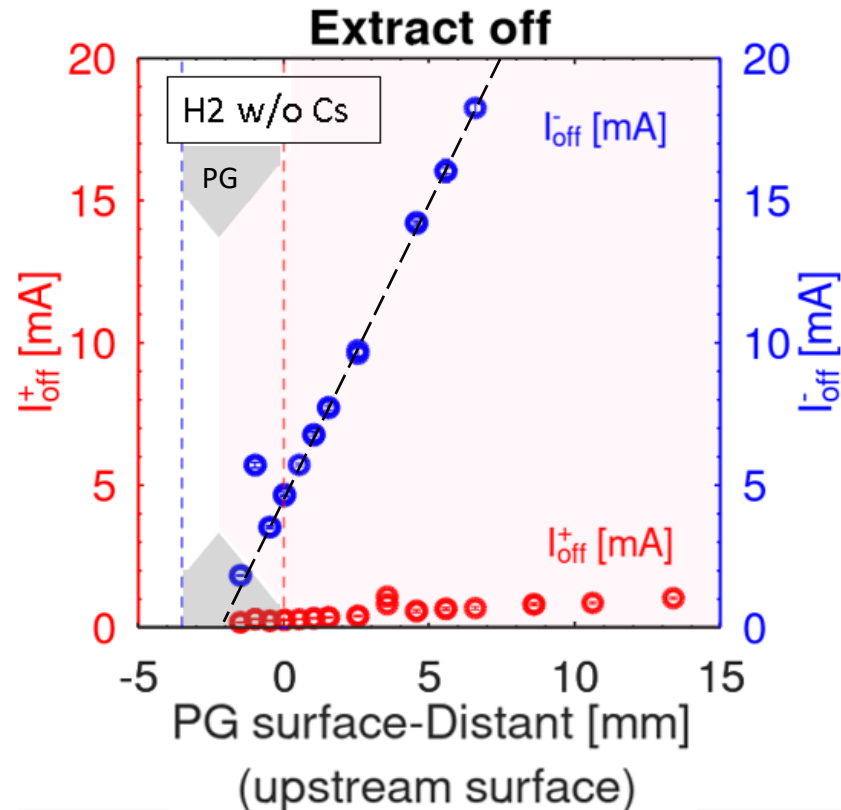


Fig. 11, Hydrogen plasma without cesium saturation current plot.

Cesium seeding effect reduce electron in plasma and nourishment negative ion at PG surface.

Isotope Effect

Parc = 50kW

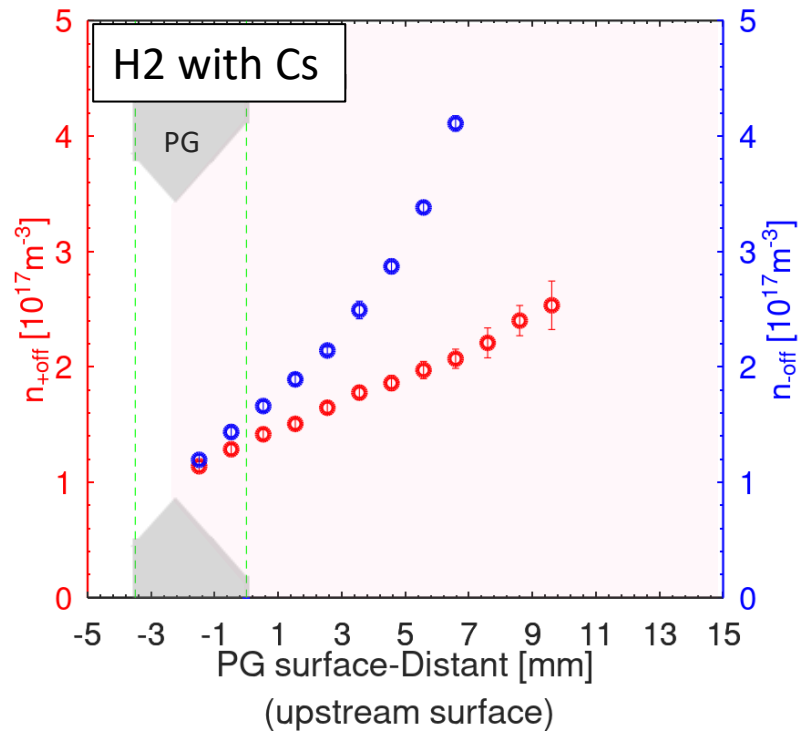


Fig. 12, Hydrogen plasma with cesium saturation current plot.

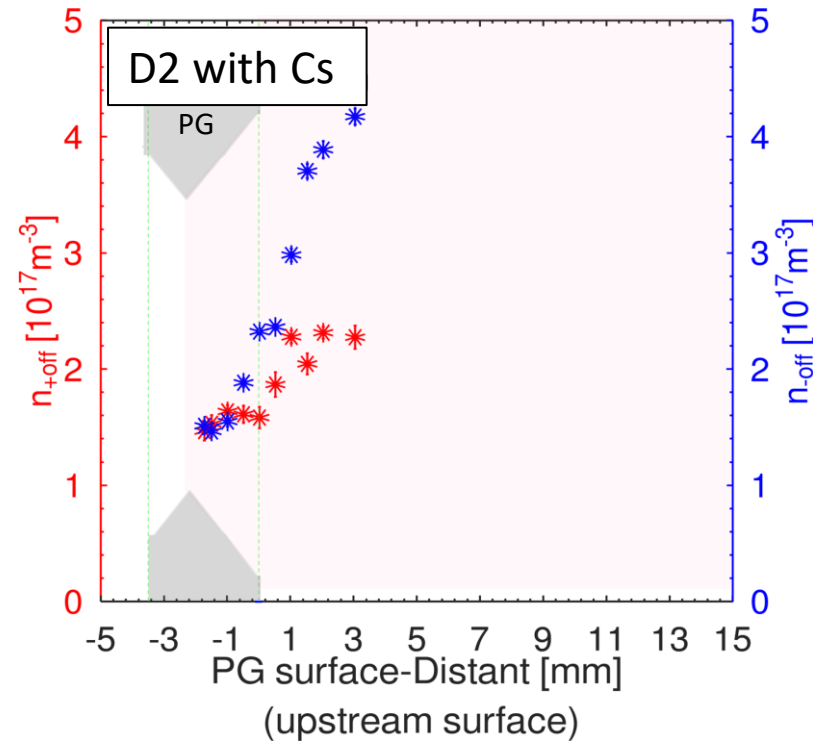


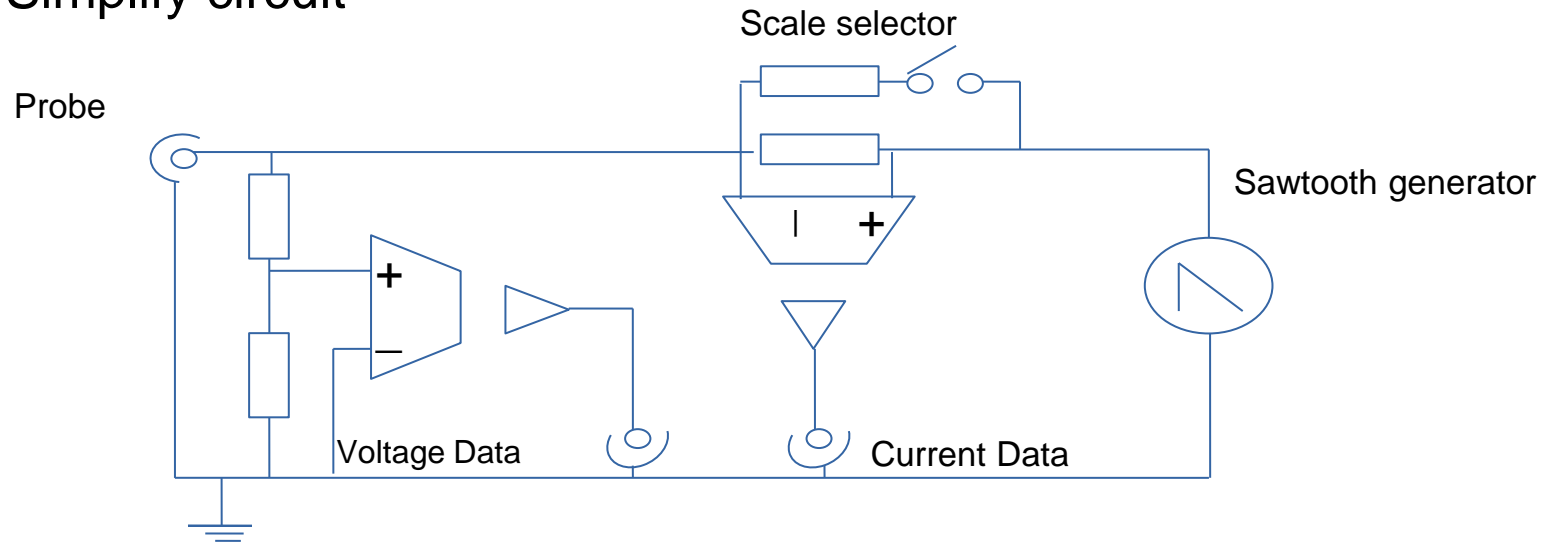
Fig. 13, Deuterium plasma with cesium saturation current plot.

Isotope effect shows that Deuterium plasma have higher density than hydrogen by seeding Cesium the density of electron is reduce and maintain charge neutrality.

Appendix 6 Detailed Setup

Current Measurement System

Simplify circuit



Sweep voltage -39.27 to 40.44 V

Voltage drop Scale 1000 : 10k to 5k load 0.3V
 Scale 100 : 10k to 2k load 1V

Voltage Calibration factor $9.79317V/V + 4.52105E-1$

Current Calibration factor Scale 1000 : $1109.42A/V + 3.16783E-5A$
 Scale 100 : $92.8616A/V + 3.78333E-5A$

Probe Structure

Meniscus measurement probe was design to have L shape provide electrode insertable into PG aperture.

The probe is installed on xy-stage to move on X and Z direction of ion source.

Probe consist of 4 electrode provide two tip measurement inside aperture (inner probe) and outside deep into plasma. Inner probe is open to touch any flow to plasma and outer probe is shaded by the probe stem but expose to lower aperture.

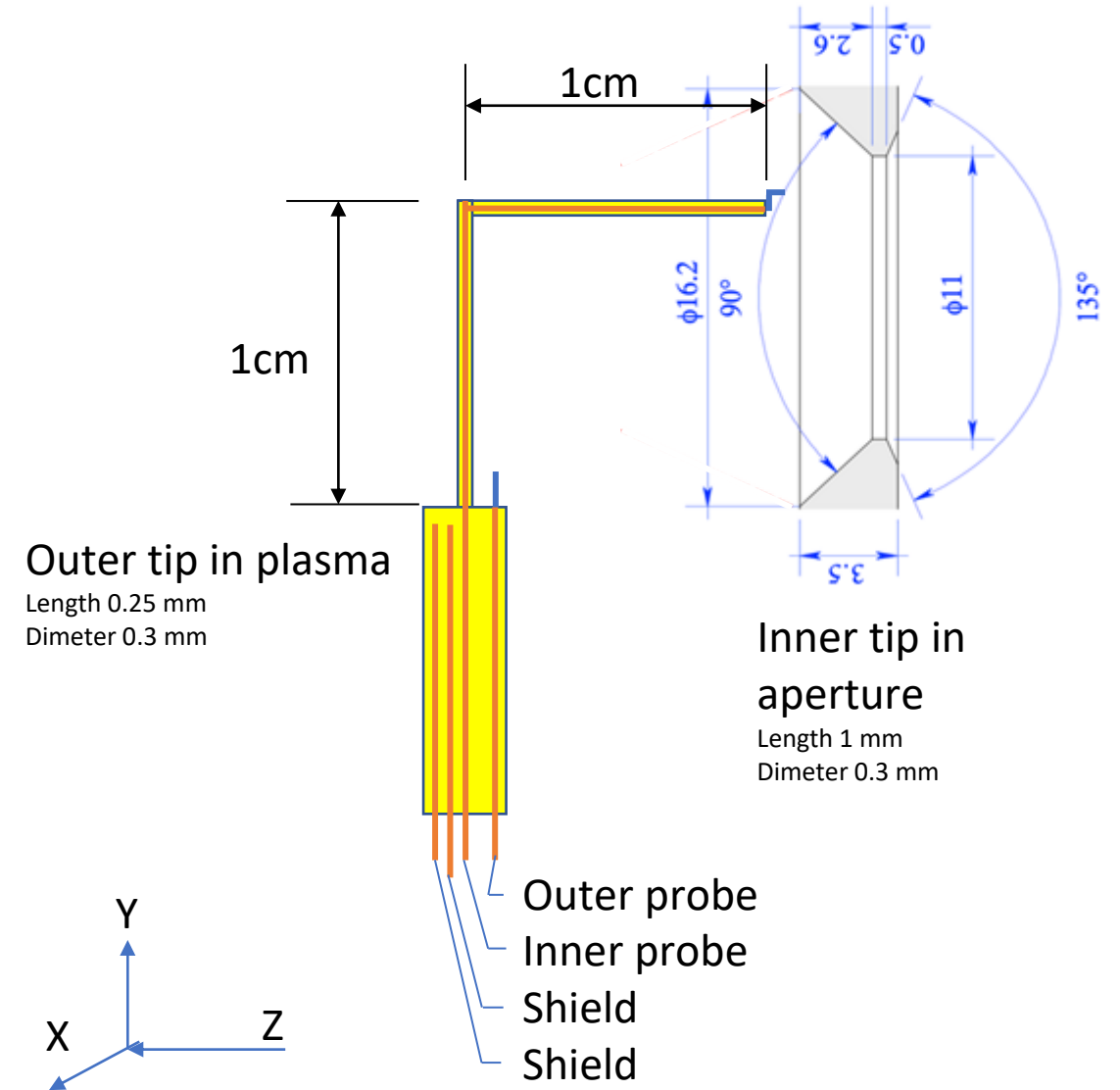


Fig. 8, probe structure description.

Installation of probe

Probe is designed as “L” shape to be able to measure the plasma in the vicinity of the plasma grid aperture.

XY-stage is installed to control the position of the probe in the Z and X directions refer to the ion source orientation.

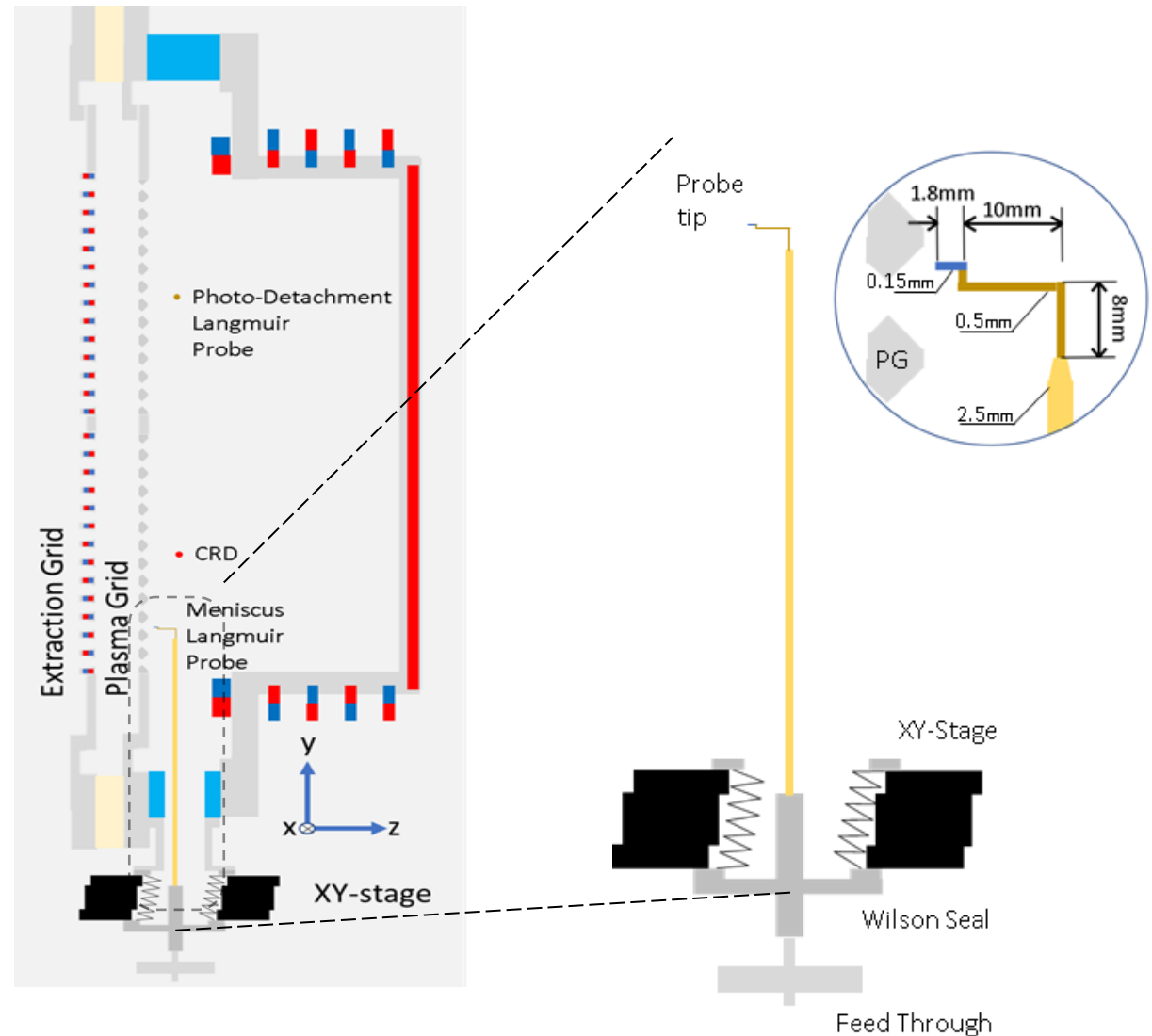
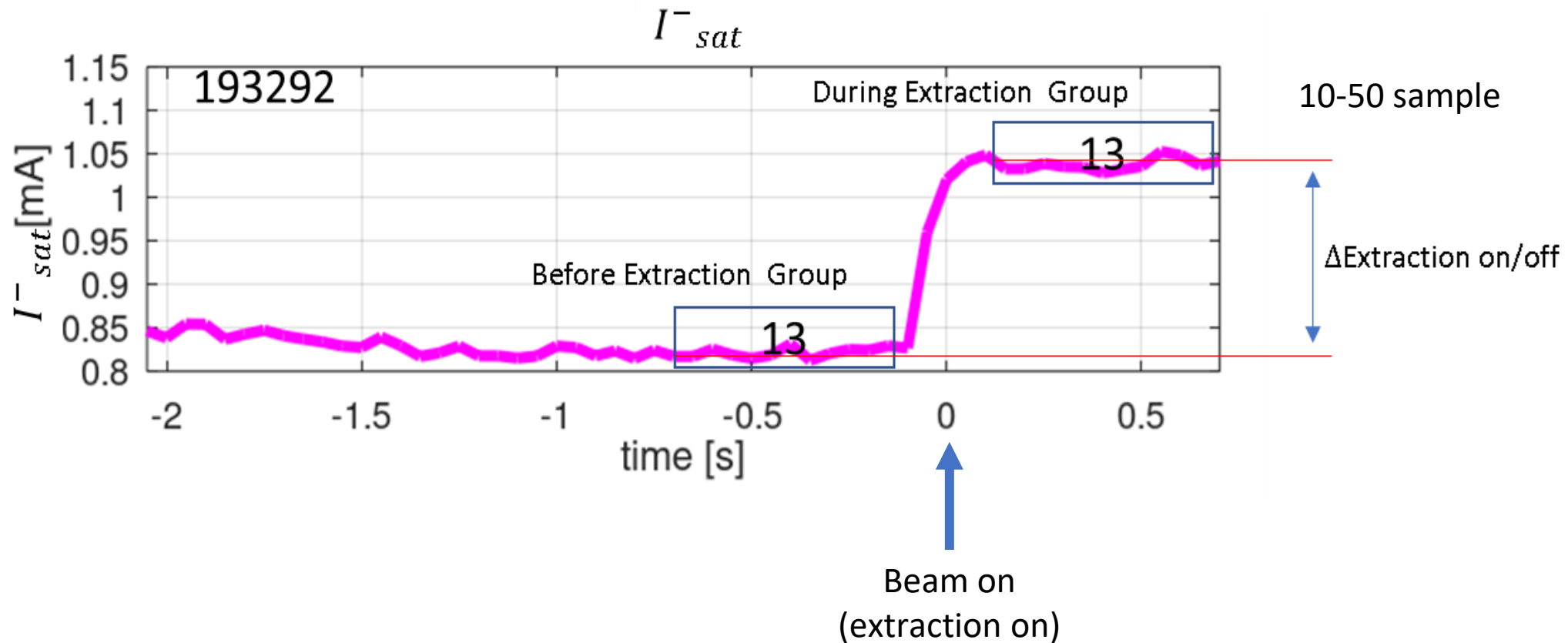


Fig. 5 Diagram of the probe moving setup.

Data averaging

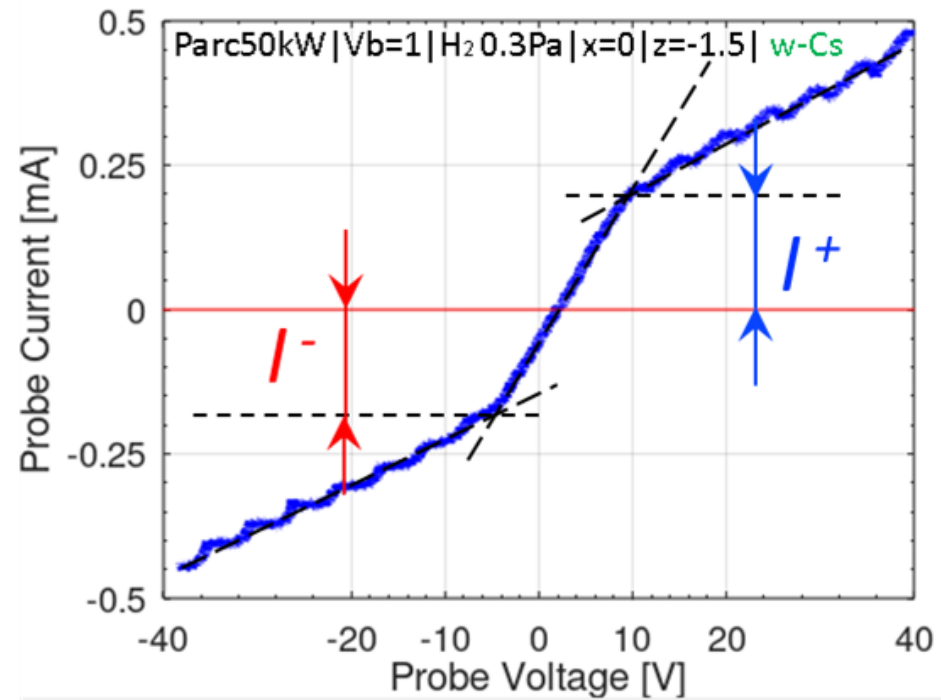


Appendix 7 General IV-curve analysis

Linear asymptotic

$$I = \frac{qn_e A}{4} \sqrt{\frac{8kT_e}{m\pi}}$$

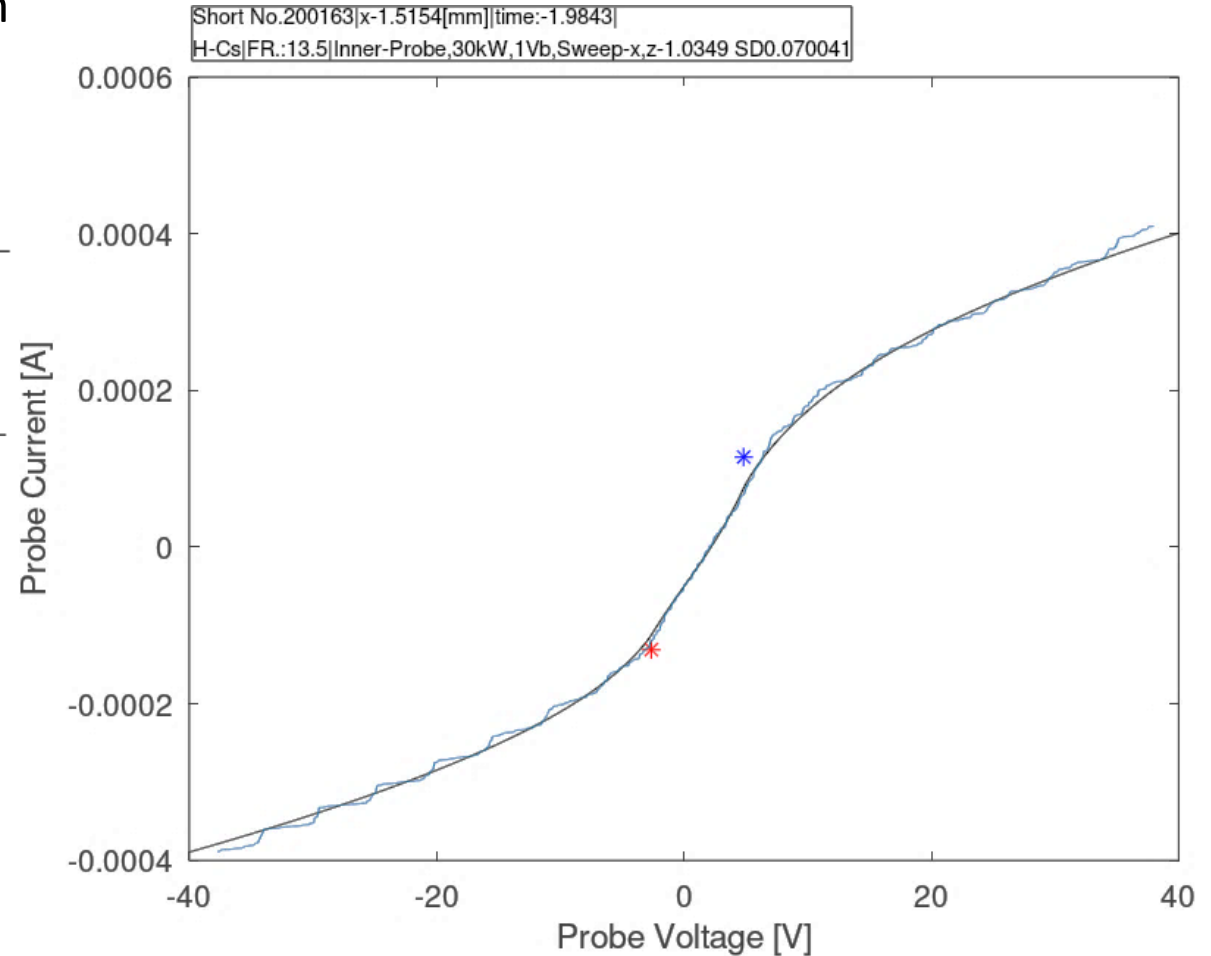
b) Ion-ion plasma



OML Fitting

From Maxwellian distribution plasma. We can obtain ideal cylindrical probe current equation here.

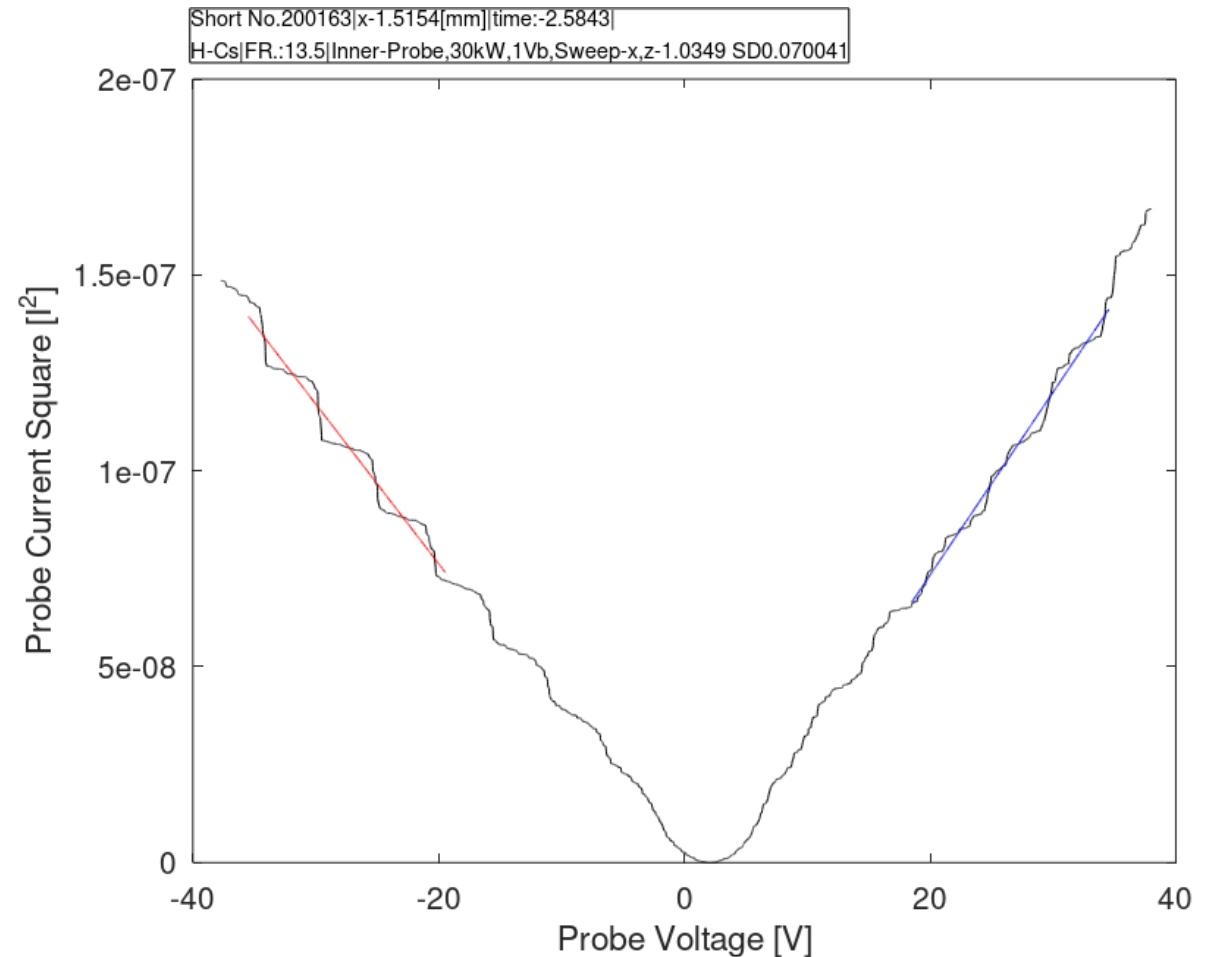
$$I_- = \begin{cases} \frac{qn_-A}{4} \sqrt{\frac{8kT_-}{m\pi}} \left[\frac{r_{s-}}{r_p} \operatorname{erf} \left(\sqrt{\frac{q(V - \phi_-)}{kT_- \left(\left(\frac{r_{s-}}{r_p} \right)^2 - 1 \right)}} \right) + e^{\frac{q(\phi_- - V)}{kT_-}} \operatorname{erfc} \left(\sqrt{\frac{q(V - \phi_-)}{kT_- \left(1 - \left(\frac{r_p}{r_{s-}} \right)^2 \right)}} \right) \right]; V > \phi_- \\ \frac{qn_-A}{4} \sqrt{\frac{8kT_-}{m\pi}} e^{\frac{q(V - \phi_-)}{kT_-}}; V < \phi_- \end{cases}$$



OML approximation

With approximation of thick sheet

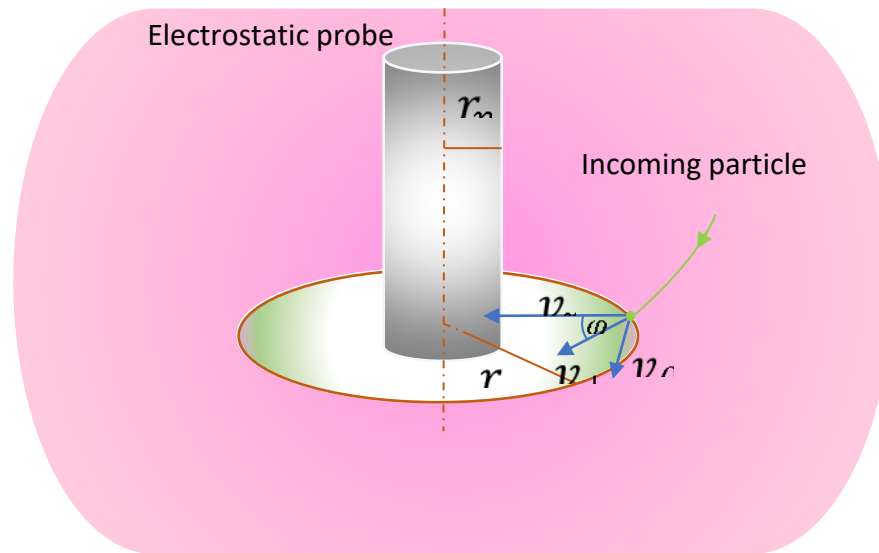
$$I_{OML} = \sqrt{\frac{2}{\pi}} A_{cy} \left(\frac{q^{3/2} n}{m^{1/2}} \right) \sqrt{V_{bias} - \phi_{plasma}} \quad ; V > \phi_-$$



Appendix 8 Langmuir probe theory

Sheath model

Langmuir probe depend on plasma shielding effect to accelerate or deaccelerate particle in vicinity of sheath (low density plasma). The effect came from appearance of electric field between plasma potential and probe potential¹. When particles enter sheath boundary, some are continued to hit probe surface and being absorbed², some are repelled and go out. With this characteristic the probe can select highest velocity and sign of charge of the incoming particle.



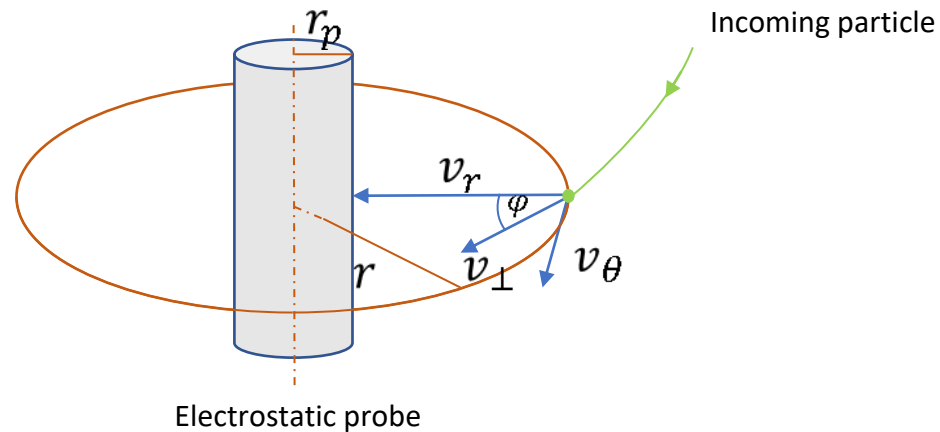
¹ Plasma potential in our study related to sheath shielding potential and wall potential the shielding potential between plasma and wall when the probe is reference to wall.

² Positive ion and negative ion might need activation energy to exchange electron to produce current.

Orbital theory

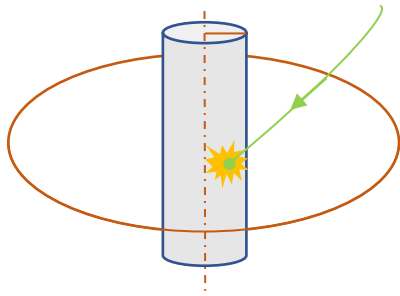
From the definition, calculation of cylindrical probe can be done by consider general initial velocity of incoming particle as v_r , which connect to distribution function of the plasma, and velocity when the particle hit the probe v_{rp} , which indicate absorption of particle is possible or not. Radius of plasma sheath provide more possible of particle to orbit around the probe.

This orbiting model coupling to plasma distribution function bring to analytical and numerical calculation of the Langmuir probe theory.

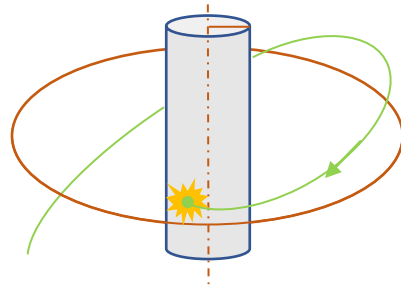


Orbital type

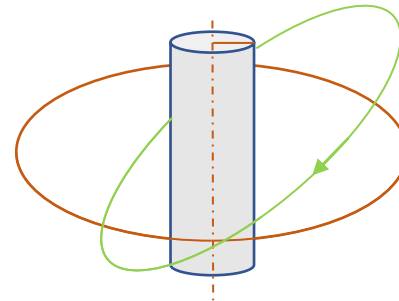
The orbiting of particle can be separate in to four category, which produce current for absorb orbit. The orbiting of particle effect to sheath potential the longer time particle spend in the sheath the increase of sheath potential depends.



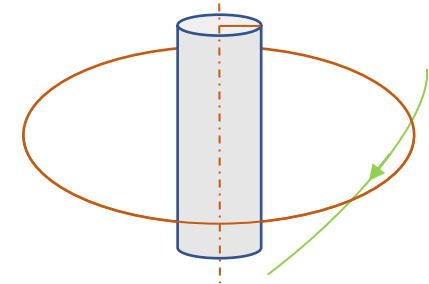
Direct absorb orbit



Absorb Orbit



Trap orbit



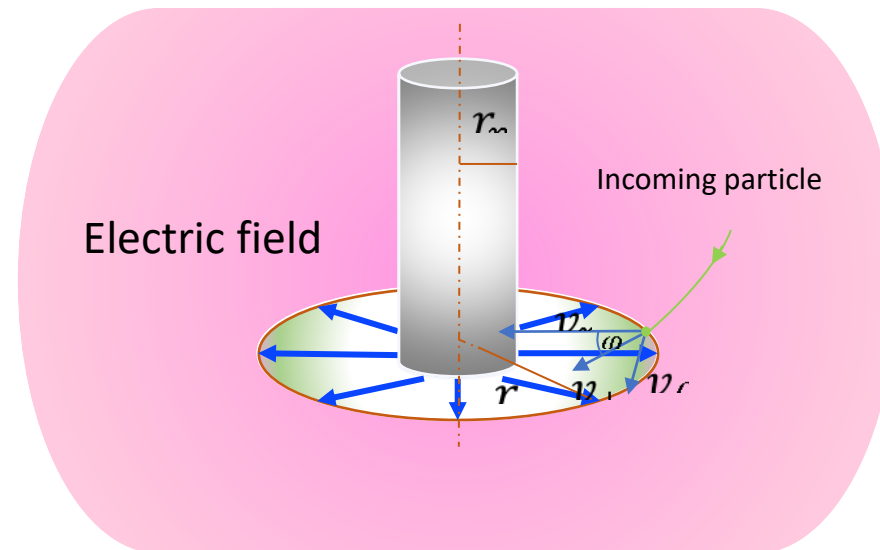
Not absorb/repel

Collision of particle in this low density is negligible.

Retard Theory

When the probe is biased below plasma potential, probe operate in repelling mode. Particle that has high enough energy to break bias blocking potential can produce current. The current produce now depend on biasing voltage and distribution of particle.

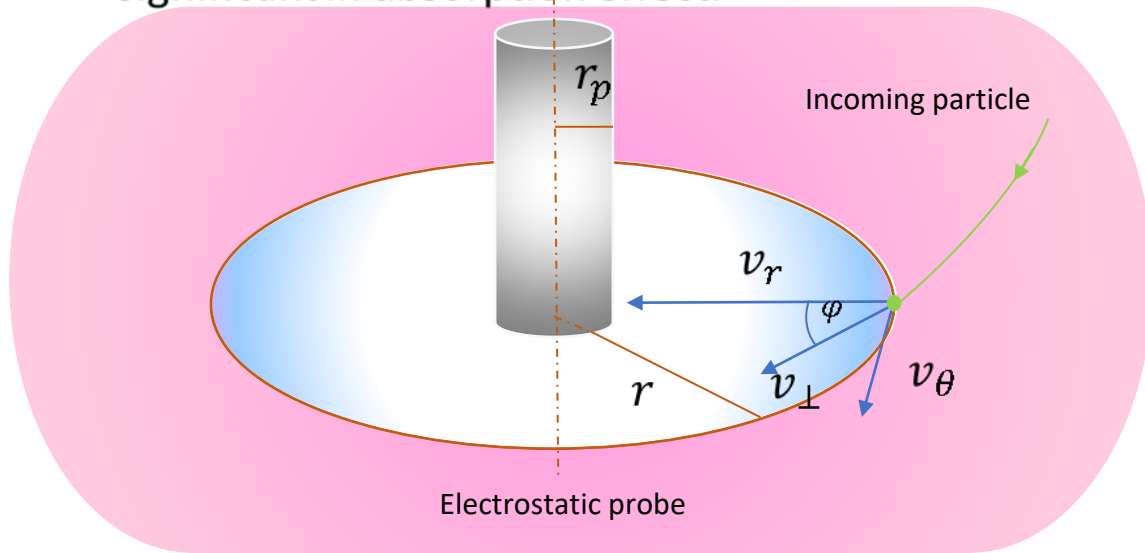
Sheath radius not directly effect to the absorption of the probe because repelling effect still occurs. Particle reaching the sheath boundary all can escape this area except some that orbit with smaller than incident angle φ limit to probe surface. In direct effect of sheath is controlling sheath potential by accumulation of charge particle. Size of sheath is approximate to thin sheath in this cause.



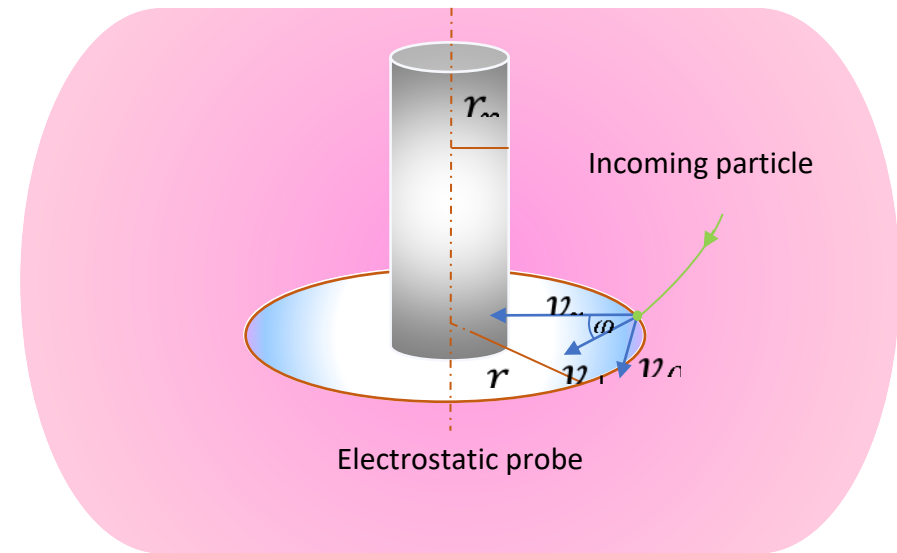
OML theory (saturation)

When the bias of probe is greater than plasma potential, probe become attracting particle.

Condition of plasma sheath are thick sheath condition and thin sheath. Thick sheath enable probe to absorb more particle because when particle reaching the sheath boundary some can be absorb when reach with higher velocity than threshold and smaller than incident angle φ limit and all that has velocity smaller than threshold can be absorbed because electric field inside the sheath is strong enough. However thin sheath has no significant in absorption effect.



Thick sheath



Thin sheath

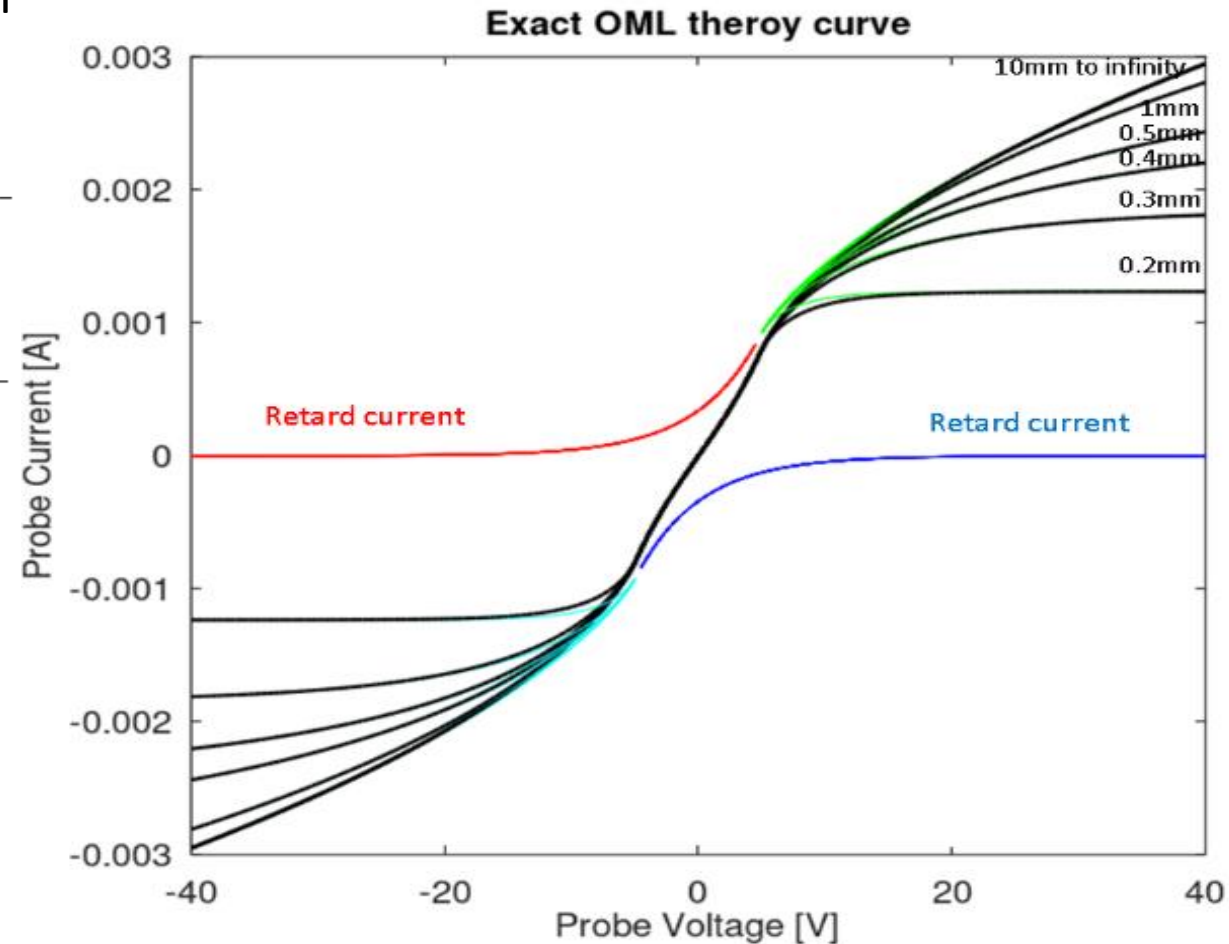
Thick sheath radius is 10 time of probe radius and thin sheath is 1.5 time of probe radius.

Summary

From Maxwellian distribution plasma. We can obtain ideal cylindrical probe current equation here.

$$I_- = \begin{cases} \frac{qn_- A}{4} \sqrt{\frac{8kT_-}{m\pi}} \left[\frac{r_{s-}}{r_p} \operatorname{erf} \left(\sqrt{\frac{q(V - \phi_-)}{kT_- \left(\left(\frac{r_{s-}}{r_p} \right)^2 - 1 \right)}} \right) + e^{\frac{q(\phi_- - V)}{kT_-}} \operatorname{erfc} \left(\sqrt{\frac{q(V - \phi_-)}{kT_- \left(1 - \left(\frac{r_p}{r_{s-}} \right)^2 \right)}} \right) \right]; V > \phi_- \\ \frac{qn_- A}{4} \sqrt{\frac{8kT_-}{m\pi}} e^{\frac{q(V - \phi_-)}{kT_-}}; V < \phi_- \end{cases}$$

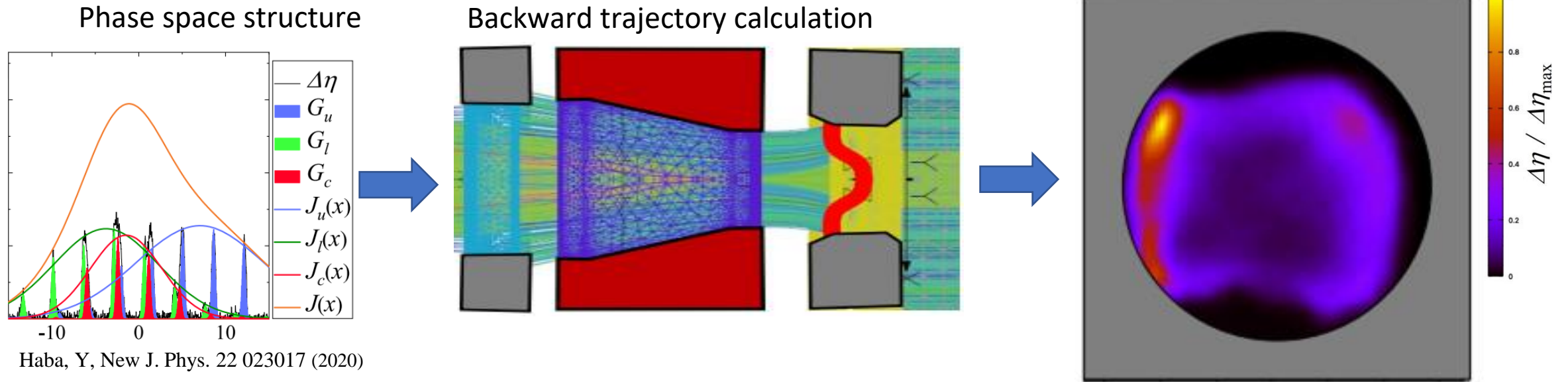
This analytical model is limit to non-distorted plasma sheath and sheath potential is not be calculated. The model is appropriate for fitting on the raw data.



Appendix 9 Backward Trajectory Calculation

Background Research

Determination meniscus shape from Beam profile



Haba, Y, New J. Phys. 22 023017 (2020)

Fig. 4. Process from experimental data to result of beam optic backward trajectory calculation.

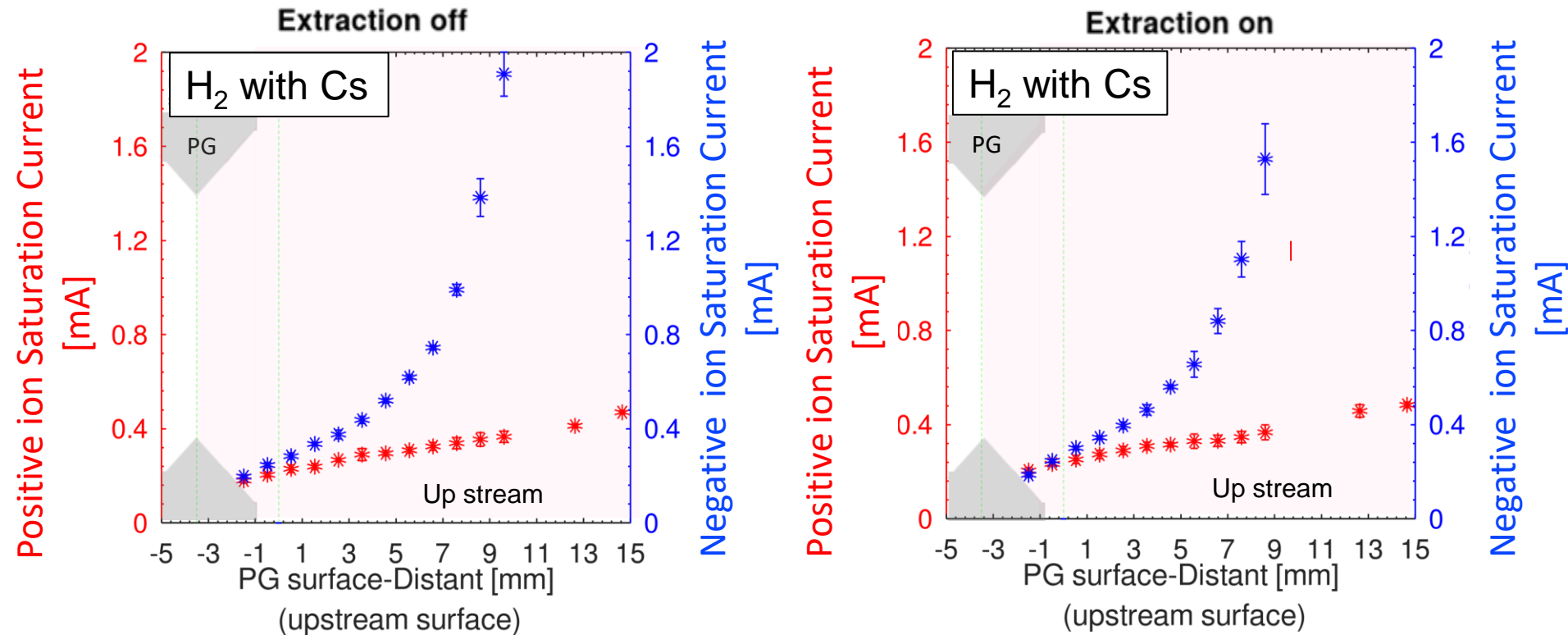
M. Kasaki et. al., IAEA-FEC conf. (2021)

Backward trajectory calculation calculated from phase space analyzer measurement is performed in our group. The result shows beam intensity map at the exit of PG aperture. With this result solely, we need confirmation from other experimental method.

Appendix 10 New analytical model

Electron contamination issue

Parc = 50kW



After apply conventional Langmuir probe evaluation (log tracing) on the raw data, we obtain the saturation current profiles.

The negative saturation current consists of the electron and negative ion currents.

However, increasing the contamination of the electrons should result in misunderstanding of the negative ion behavior.

Fig. 11. Saturation currents in the hydrogen plasma with cesium.

Negative ion evaluation from I - V curve

- Electrons and negative hydrogen-ions co-exist in the extraction region.
- Conventional Langmuir-probe theory applied to electron plasma is not possible. The theory is extended to apply two species in this research.
- Two-step procedure: (1) Separation of negative ion and electron and (2) density evaluation based on Orbital Motion limit (OML) theory.

(1) Electron separation

Separation module

$$\begin{cases} I_{pos} = I^- \\ I_{neg} = \frac{I^- + \gamma I^+}{\gamma - 1} \\ I_e = [I^+ + I^-] \frac{1}{1 - \gamma} \end{cases}$$

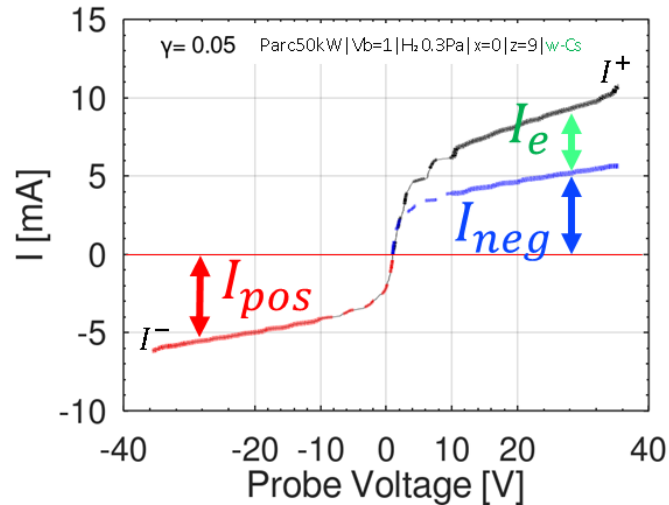
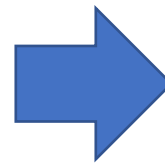


Fig. 11. separated I - V curve



(2) OML density evaluation

$$I_{OML} = \sqrt{\frac{2}{\pi}} A_{cy} \left(\frac{q^{3/2} n}{m^{1/2}} \right) \sqrt{V_{bias} - \Phi_{plasma}}$$

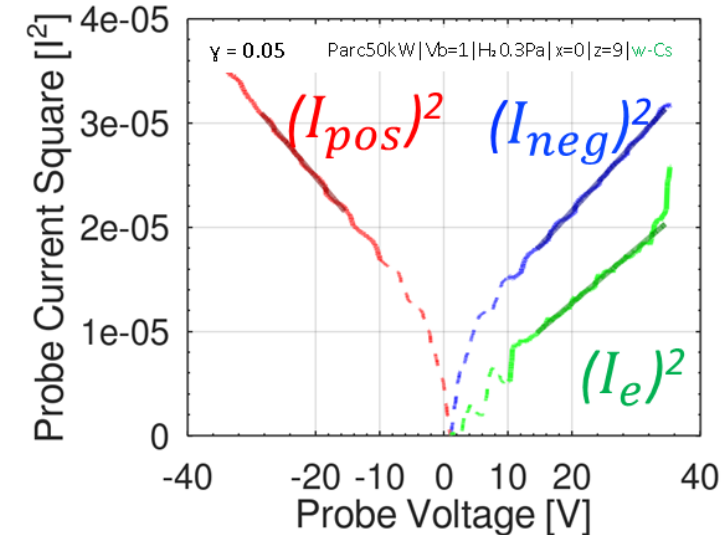


Fig. 12. I^2 - V curve evaluation

OML density evaluation

Conventional Langmuir probe evaluation (asymptotic method) is complicated to interpret the ion density. The OML approximation, which focuses on the saturation regions as shown in figure 13, is introduced to directly evaluate the ion density as described in the equation below.

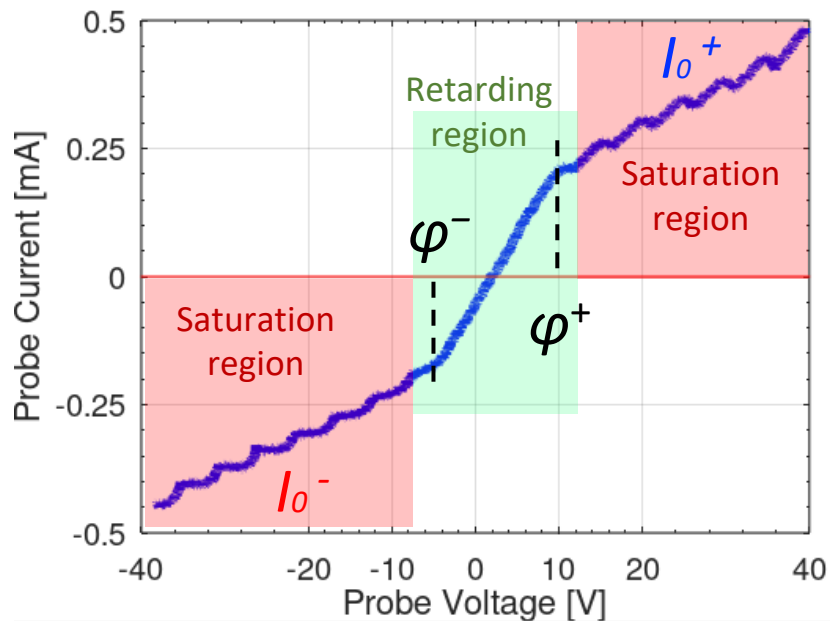


Fig. 13. IV-curve region description.

$$I_0^{+,-} = \sqrt{\frac{2}{\pi}} \eta^{ion,e} n^{+,-} \sqrt{|V_{probe} - \phi^+|} ; V_{probe} > \phi^+ \\ ; V_{probe} < \phi^-$$

where $\eta = A_{cy} \left(\frac{q^{3/2}}{m^{1/2}} \right)$, proton and hydrogen negative ion have same η value.

OML approximation density evaluation for cylindrical probe
 $I_0^{+,-}$: probe current at saturate region, A_{cy} : probe area, q : charge of the species, m : mass of the species, V_{probe} : probe voltage, $\phi^{+,-}$: potentials at bending points in I - V curve.

Separation of electron and negative ion

Separation of electron is solved from the conservation of charge neutrality.

To correct the influence of magnetic field, the ratio, γ , of electron to ion saturation currents is measured empirically using hydrogen plasma (electron-positive ion plasma).

Basic assumption

$$n_{neg} + n_e = n_{pos} \text{ ---(1) charge neutrality}$$

Experimental data

$$I^+ = I_{neg} + I_e \text{ ----(2) negative saturation current}$$

$$I^- = I_{pos}; \text{ ----(3) positive saturation current}$$

$$\gamma = \eta_i / \eta_{ele} \text{ ----(4) electron to positive ion current ratio}$$

obtain from non-caesiated cause

OML theory

$$I_{neg} = \eta_{neg} n_{neg} \sqrt{V_{probe} - \phi^-} \text{ ----(5.1).}$$

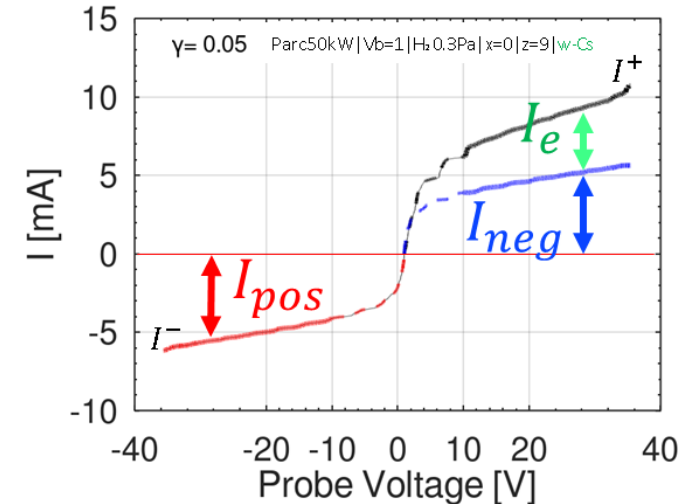
$$I_e = \eta_{ele} n_{ele} \sqrt{V_{probe} - \phi^e} \text{ ----(5.2).}$$

$$I_{pos} = \eta_{pos} n_{pos} \sqrt{|V_{probe} - \phi^+|} \text{ ----(5.3).}$$

Additional assumption

$$\eta_{neg} = -\eta_{pos} = \eta_i \text{ ----(6.1)}$$

$$\phi^e = \phi^- = \phi^+ \text{ ----(6.2) ion limit probe sheath boundary}$$



Finally, the module equations become
Separation modules

$$\begin{cases} I_{pos} = I^- \text{ ----(7.1)} \end{cases}$$

$$\begin{cases} I_{neg} = \frac{I^- + \gamma I^+}{\gamma - 1} \text{ ----(7.2)} \end{cases}$$

$$\begin{cases} I_e = [I^+ + I^-] \frac{1}{1 - \gamma} \text{ ----(7.3)} \end{cases}$$

Derivation of electron separation equation

Starting equation

Experimental data

$$I^+ = I_{neg} + I_e \text{ ----(1) negative saturation current}$$

$$I^- = I_{pos}; \text{ ----(2) positive saturation current}$$

$$\gamma = \eta_i / \eta_{ele} \text{ ----(3) electron to positive ion current ratio}$$

obtain from non-caesited cause

OML theory

$$I_{neg} = \eta_{neg} n_{neg} \sqrt{V_{bias} - \Phi_{plasma}} \text{ ---(4.1).}$$

$$I_e = \eta_{ele} n_{ele} \sqrt{V_{bias} - \Phi_{plasma}} \text{ ---(4.2).}$$

$$I_{pos} = \eta_{pos} n_{pos} \sqrt{|V_{bias} - \Phi_{plasma}|} \text{ ---(4.2).}$$

Assumption,

$$\eta_{neg} = -\eta_{pos} = \eta_i \text{ ---(5.1) ion sheath radius and mass equal}$$

$$n_{neg} + n_e = n_{pos} \text{ ---(5.2) charge neutrality}$$

$$\phi^e = \phi^- = \phi^+ \text{ ----(5.3) ion limit sheath (of probe) boundary}$$

Derivation

Given that $f = \sqrt{V_{bias} - \Phi_{plasma}}$
 (4.1&4.2)---(1): $I^+ = \eta_{neg} n_{neg} f + \eta_{ele} n_{ele} f \text{ ----(1')}$

(3&5.1)---(1') $I^+ = \eta_i n_{neg} f + \frac{\eta_i}{\gamma} n_{ele} f \text{ ----(2')}$

(5.1)---(2') $I^+ = \eta_i (n_{pos} - n_e) f + \frac{\eta_i}{\gamma} n_{ele} f$
 $= \eta_i n_{pos} f + \eta_i \frac{1-\gamma}{\gamma} n_{ele} f \text{ ----(3')}$

(5.1&4.2&2)---(3') $I^+ = -I^- + \eta_i \frac{1-\gamma}{\gamma} n_{ele} f \text{ ----(4')}$

(4.2&3)---(4') $I_e = [I^+ + I^-] \frac{1}{1-\gamma} \text{ ----(5')}$

(1)---(5') $I_{neg} = \frac{I^- + \gamma I^+}{\gamma - 1} \text{ ----(6')}$

(2) $I_{pos} = I^-$

Derivation of electron separation ratio

This procedure derives the electron to negative ion ratio. The ratio is used for the electron separation process.

Based on the OML approximation, the current signal components for electrons and negative hydrogen ions are defined as I_{ele} and I_{neg} , respectively;

Considering the current in the saturation region where the plasma sheath exits at a single average potential, the Langmuir probe current composed of multiple negative-charged particles (I_+) can be written as;

From the definition of η , r can be expressed as;

The ratio is experimentally obtained from a non-cesiased plasma as shown in table 1, keeping the charge neutrality. It is assumed that the positive and negative ions have the same behavior due to equal mass. In this case the ratio is 1/20.

$$I_{ele} = \eta_{ele} n_{ele} \sqrt{V_{bias} - \Phi_{plasma}} \quad \text{---(2)},$$

$$I_{neg} = \eta_{neg} n_{neg} \sqrt{V_{bias} - \Phi_{plasma}} \quad \text{---(3)}.$$

$$\eta = A_{cy} \left(\frac{q^{3/2}}{m^{1/2}} \right)$$

$$\begin{aligned} I_+ &= I_{ele} + I_{neg} \\ &= (\eta_{ele} n_{ele} + \eta_{neg} n_{neg}) \sqrt{V_{bias} - \Phi_{plasma}} \\ &= \eta_{neg} \left(\frac{1}{\gamma} n_{ele} + n_{neg} \right) \sqrt{V_{bias} - \Phi_{plasma}} \quad \text{---(4)}. \end{aligned}$$

$$\gamma = \frac{\eta_{neg}}{\eta_{ele}} = \left(\frac{m_{ele}}{m_{neg}} \right)^{1/2} \left(\frac{A_{neg}}{A_{ele}} \right) \cong \frac{1}{43} \left(\frac{A_{neg}}{A_{ele}} \right) \quad \text{---(5)}.$$

1/ γ ratio x: 0mm

30kW wo-cs	
z: -1.5mm	r=6.4431 +-0.0012051
z: 2mm	r=14.9866 +-0.00010461
z: 10.5mm	r=17.0309 +-0.00019948
z: 13mm	r=15.9293 +-0.0002157

Mr.Masaki 50kW	
z: 9mm	r=22.5467 +-0.0008493

Table 1, Non-cesiased case

Beam Extraction Boundary

- In the vicinity of the PG aperture called “extraction area”, a meniscus is formed as a boundary between plasma and beam regions as shown in Fig. 2.
- Beamlet focusing is strongly affected by the meniscus shape, which depends on the variations of negative-ion density and applied extraction voltage

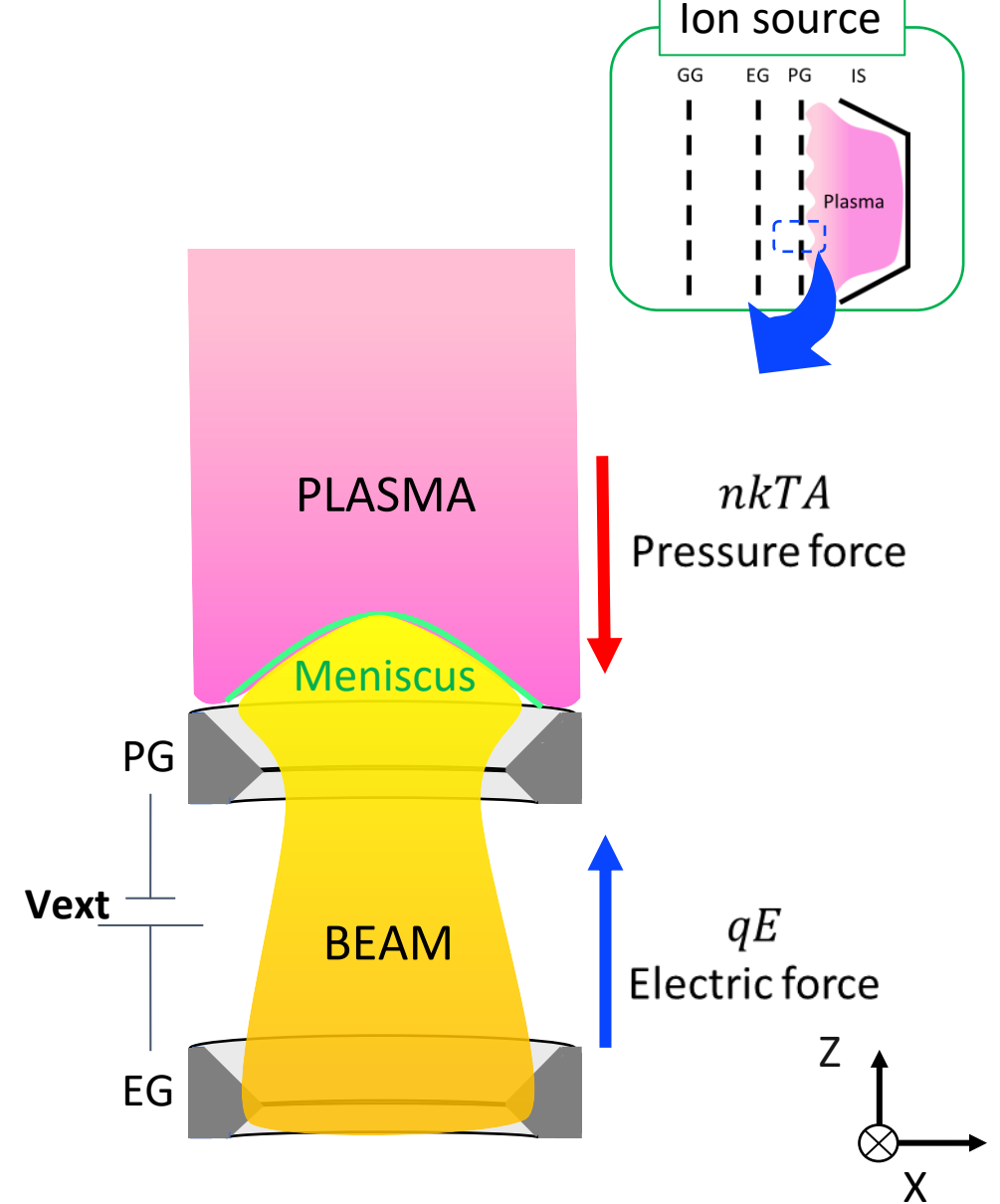


Fig. 2. Definition of the meniscus in the vicinity of the PG aperture.

Ion Source Condition

Research and development Negative ion source at NBI-Test Stand is a single stage acceleration. We define extraction voltage V_{ext} and don't apply acceleration voltage in this experiment.

- Ion Source : filament-arc type
- Input discharge power: 50kW
- Plasma density: $2 \times 10^{17} \text{ m}^{-3}$
- Puffing gas H_2 :0.8 Pa
- with and without Cs seeding

- Accelerator Grid: PG, EG, and GG
- Bias voltage 0.4V
- Extraction voltage 0,150,250,300,500V

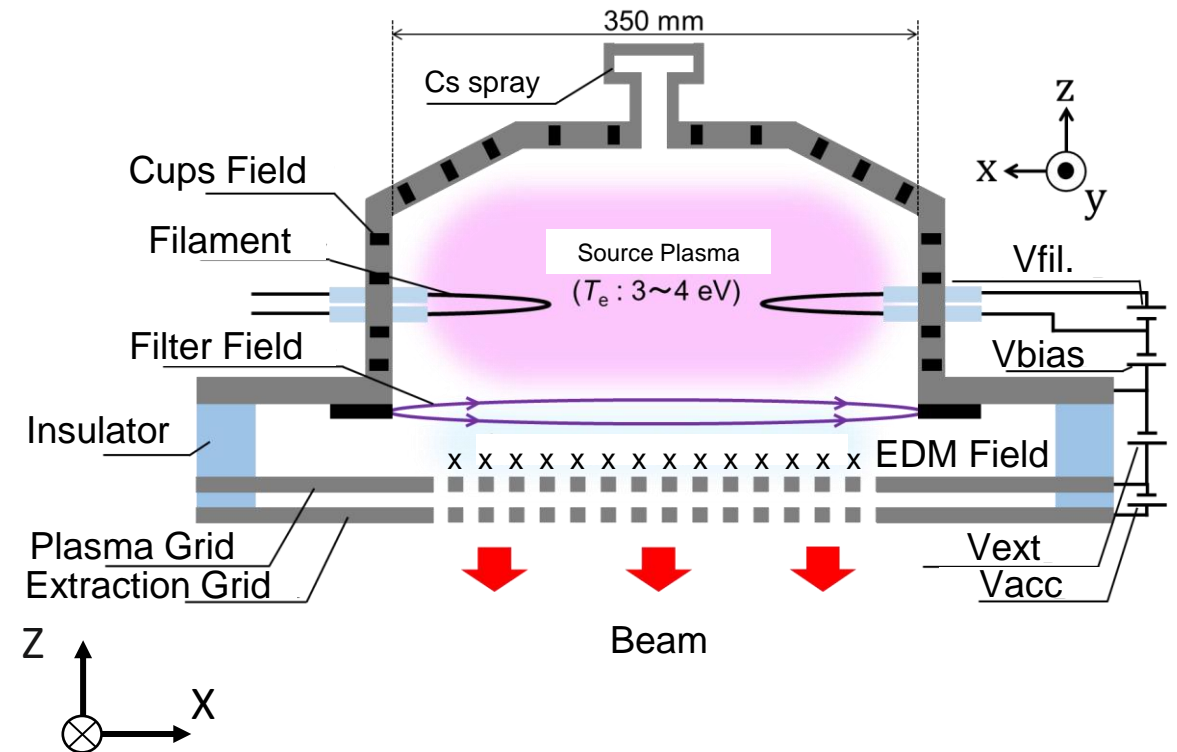
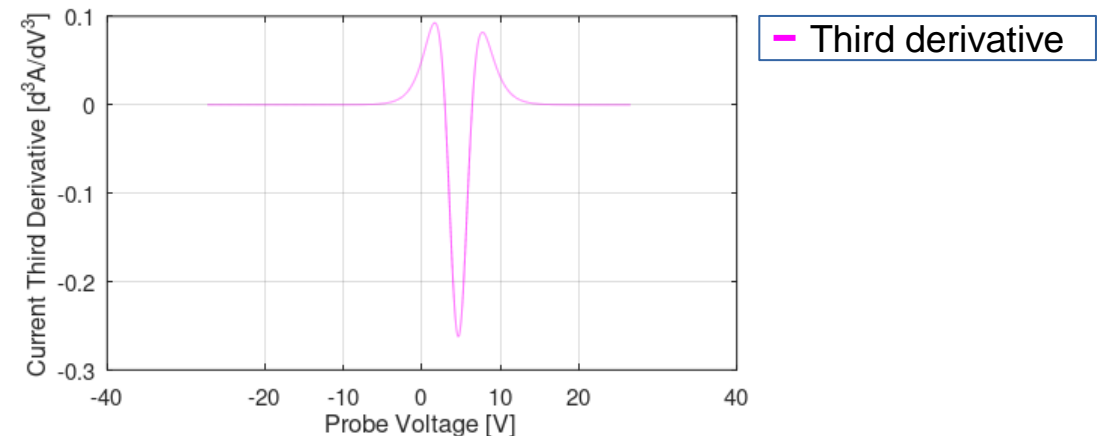
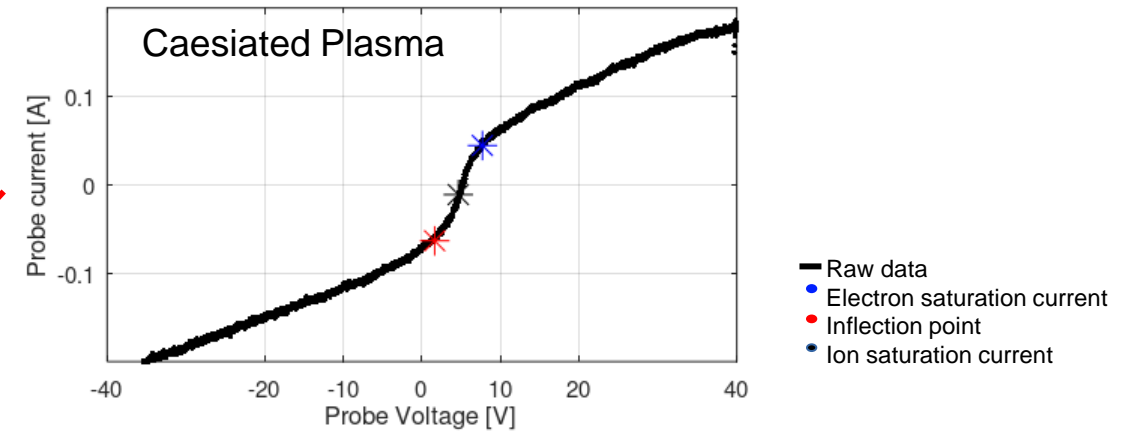
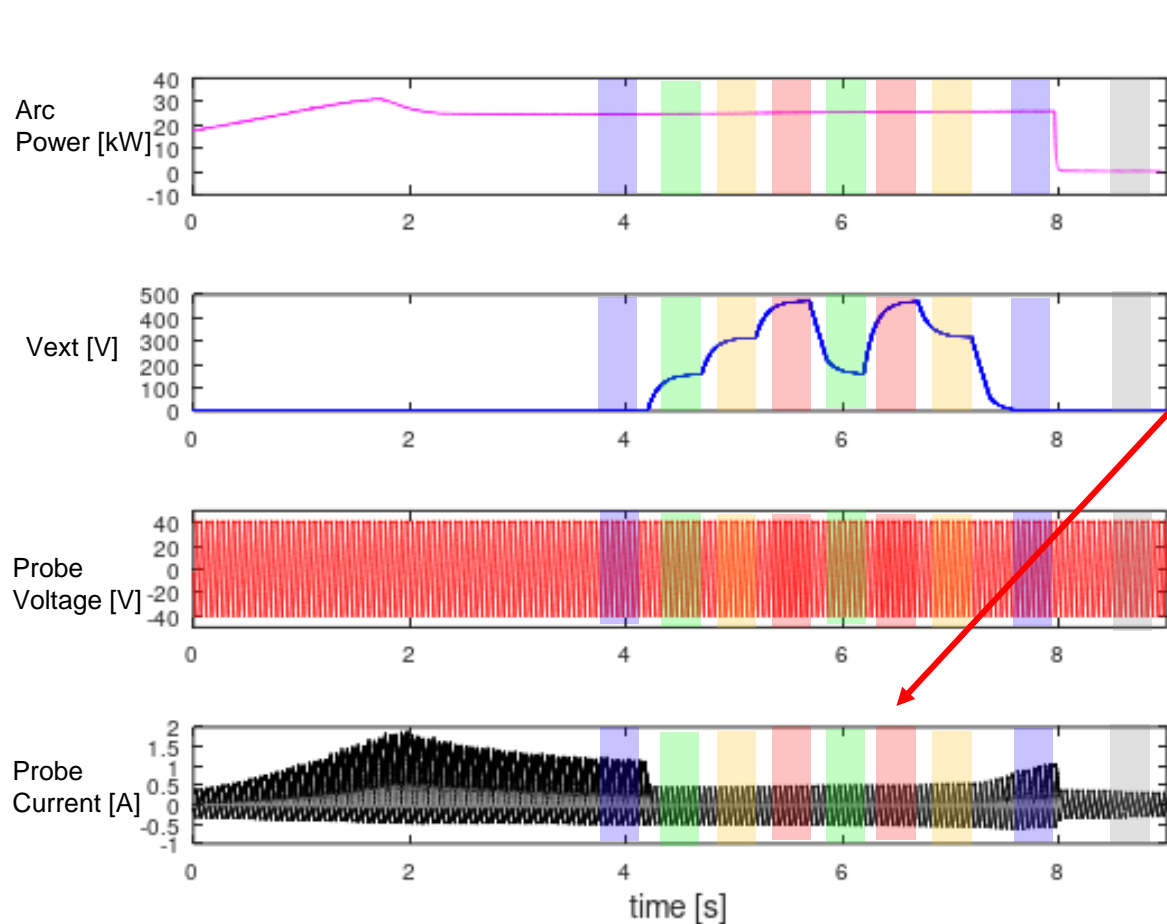


Fig. 4. Diagram of the ion source setup.

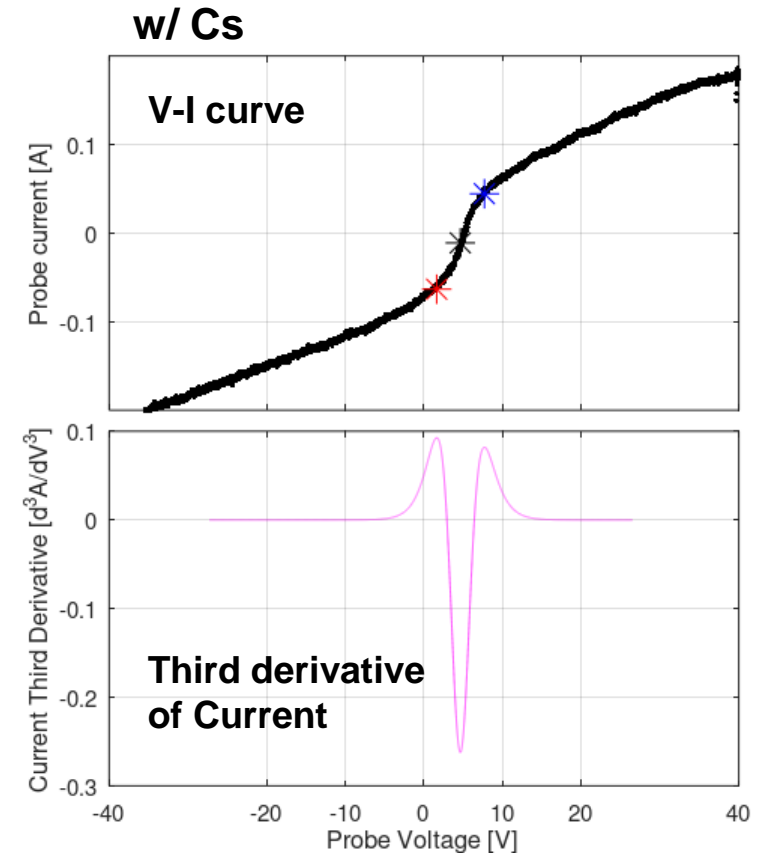
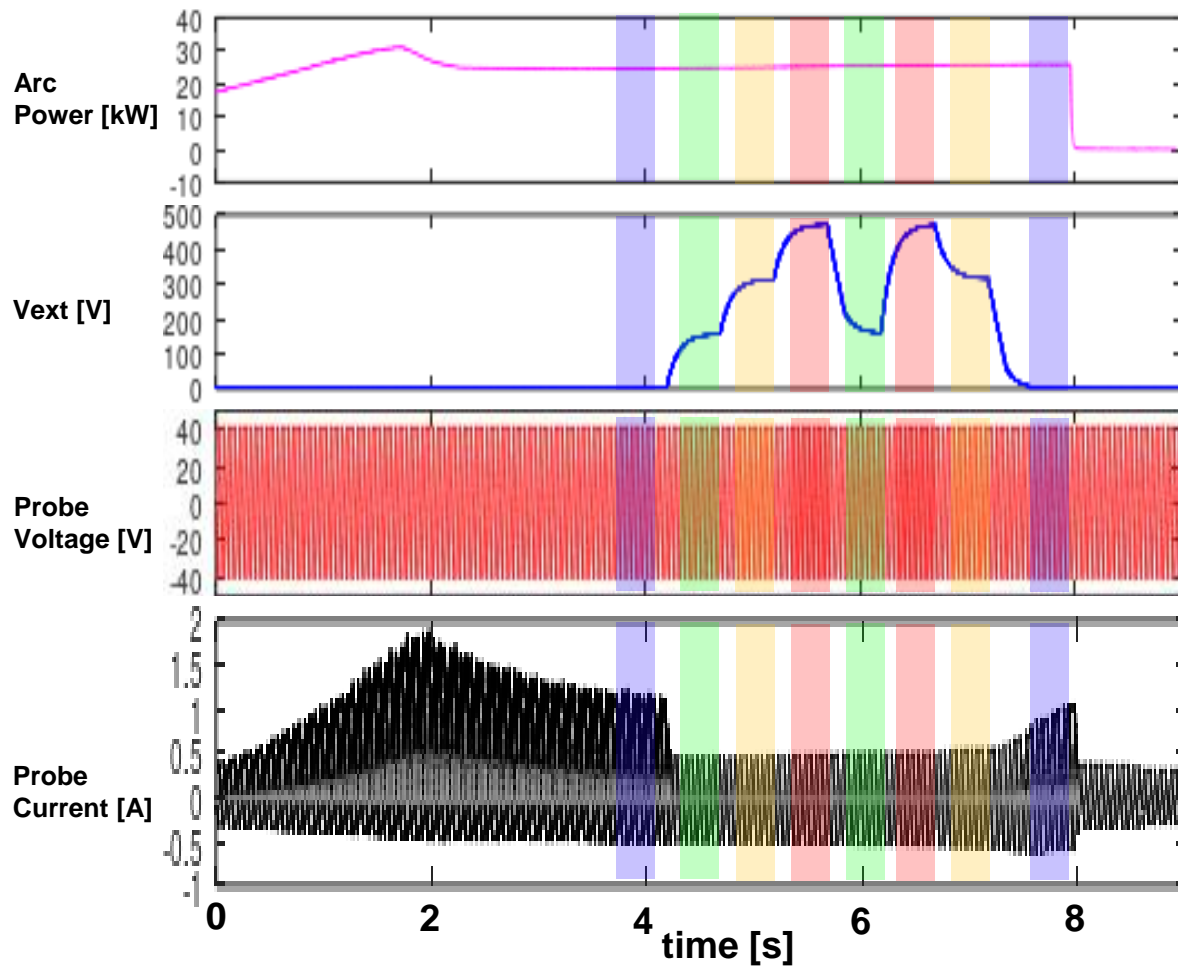
Typical discharge waveform and Langmuir probe signal



Probe bias is sweeping for diagnostic through out the time of discharge.

The color hatch on the trace indicate group of sample we take for each Vext level.

Each I-V curve sample are fitted by specific curve. The function will track voltage position of the retard region. Third derivative is calculated from the fitted function. The positive peak of third derivative on lower value and higher probe bias voltage is use as saturation voltage for electron saturation current and location of ion saturation current.



Calculation

Starting Equation

1 Momentum balance equation is use with approximation that magnetic field is not strong, and collision is not significant.

$$mn_j \left(\frac{\partial}{\partial t} + v_i \cdot \nabla \right) v_i = -q_j n_j E_i - \nabla p_j \quad : \quad i \in \{x, y, z\}, \quad j \in \{-i, +i, e\}$$

2 Continuity equation is use because plasma is incompressible fluid.

$$\frac{\partial n_j}{\partial t} + \nabla \cdot (n_j v_i) = S \quad : \quad i \in \{x, y, z\}, \quad j \in \{-i, +i, e\}$$

3 Poisson equation is use for extraction and plasma shielding.

$$\nabla^2 \phi = \frac{e}{\epsilon_0} (n_{+i} - n_{-i} - n_e) \quad E = -\nabla \cdot \phi$$

4 Pressure term come from ideal gas because hydrogen is light enough to neglect Van Der Waals term.

$$p_j = n_j T_j$$

Solving

Momentum Equation

$$mn_j \left(\frac{\partial}{\partial t} + v_i \cdot \nabla \right) v_i = -q_j n_j E_i - \nabla p_j$$

$$X: mn \left(\frac{\partial v_x}{\partial t} + v_x \frac{\partial v_x}{\partial x} + v_y \frac{\partial v_x}{\partial y} \right) = nqE_x - \left(kn \frac{\partial T}{\partial x} + kT \frac{\partial n}{\partial x} \right) \text{ --- } Mx$$

$$Y: mn \left(\frac{\partial v_y}{\partial t} + v_x \frac{\partial v_y}{\partial x} + v_y \frac{\partial v_y}{\partial y} \right) = nqE_y - \left(kn \frac{\partial T}{\partial y} + kT \frac{\partial n}{\partial y} \right) \text{ --- } My$$

Continuity Equation

$$\frac{\partial n_j}{\partial t} + \nabla \cdot (n_j v_i) = S \quad \text{sheath boundary (net in = net out) } S = 0$$

$$\frac{\partial n}{\partial t} + v_x \frac{\partial n}{\partial x} + v_y \frac{\partial n}{\partial y} + n \frac{\partial v_x}{\partial x} + n \frac{\partial v_y}{\partial y} = 0 \text{ --- } C1$$

1D solving

Flux Balance Equation

$$(v \cdot \nabla) \frac{1}{2} m v^2 = kT \nabla v + q(v \cdot E)$$

Whole species population velocity

Pressure

induced electric field

From this equation we can determined extraction from balance of the pushing pressure and pulling electric field. When we determined curvature of the sheet is low ($V_x \gg V_y$) in cartesian then we can determine one-dimension sheath.

$$\frac{v_x^2}{2} = \frac{kT}{m} \ln(|v_x|) + \int_{x_v}^{x_n} \frac{q}{m} E_x dx$$

Determination of Boundary Condition

Due to effect of plasma shield, acceleration field in the system is determined by appearance field.

$$E_{appear} = E_{applied} + E' = \frac{1}{\epsilon_r \epsilon_0} E_{applied}$$

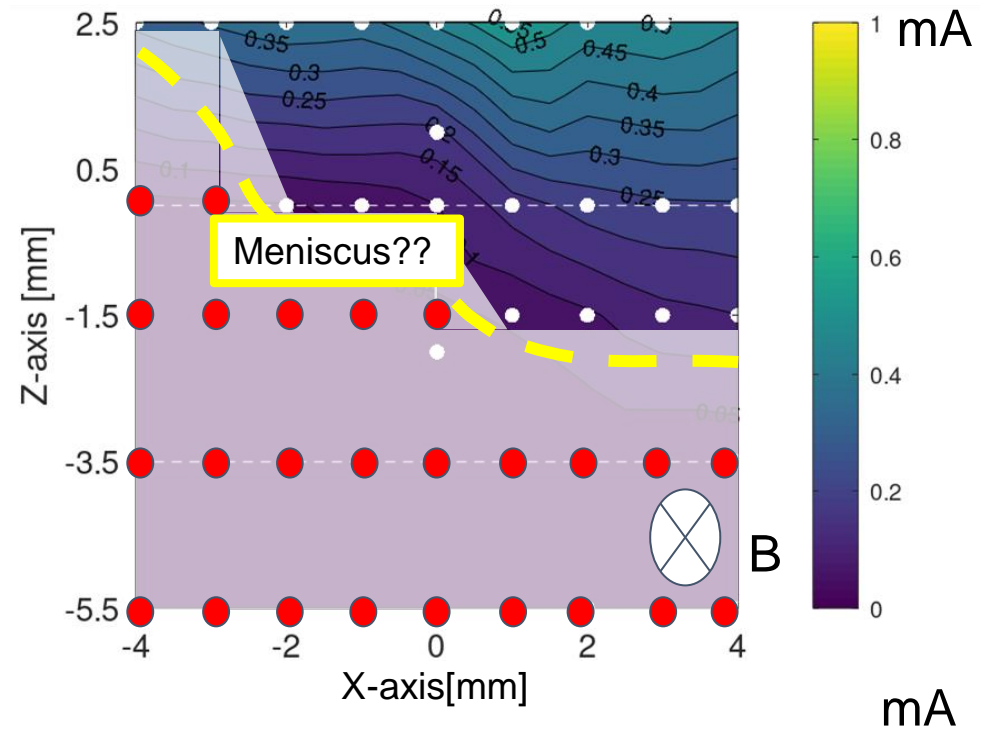
then

$$\frac{kT}{m} \ln(v_+(x)) = \int_{x_v}^{x_n} \frac{q}{m} \left(E_{applied} + \frac{1}{\epsilon_0} \int_{x_v}^{x_1} \frac{n_0^+ v_0^+}{v^+(x)} dx_2 \right) dx_1$$

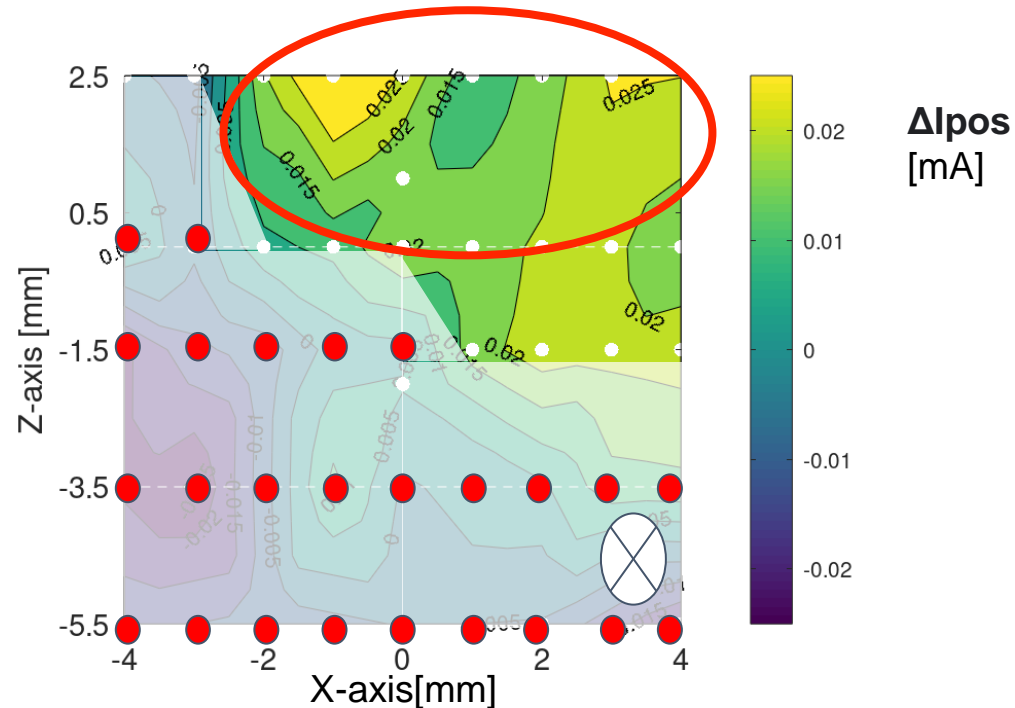
This equation must be solved to determine the boundary x_n of the meniscus. In other means, v_+ will be obtained when balanced from v_+0 to v_+ at x_v and x_v is decided by uniform electric field region.

Beam Extraction Boundary

The boundary of beam-plasma can be considered by the appearance of anomaly I-V curve, which might correspond to no-plasma or failure of Maxwellian assumption region.

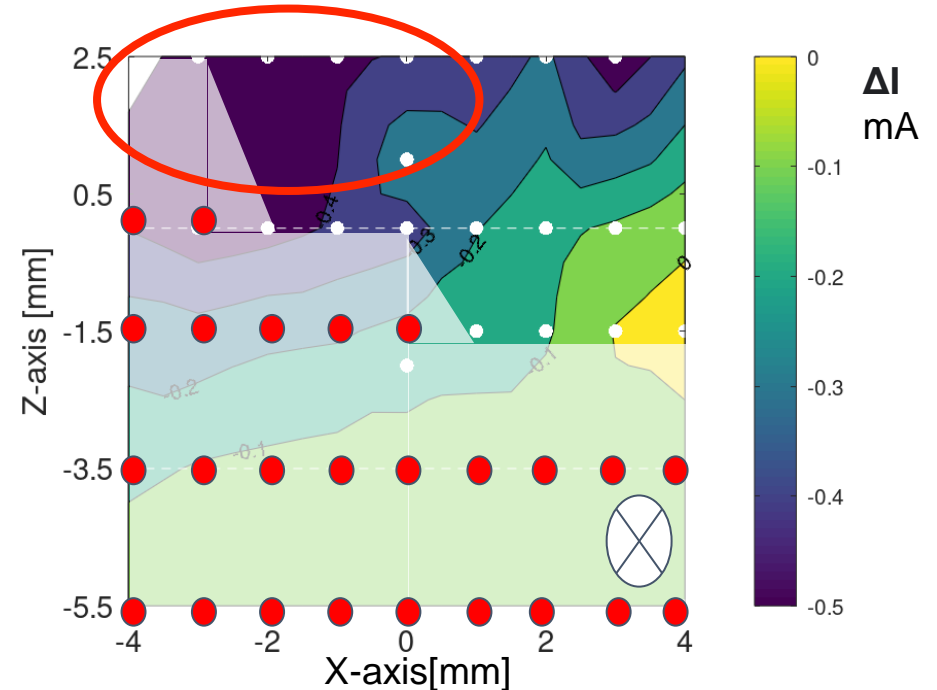


Accumulation of charged particles



The difference of Positively charged saturation current between $V_{ext} = 450V$ and $V_{ext} = 0V$

$$\Delta I = I_{pos_sat_V450} - I_{pos_sat_V0}$$



The difference of Negative charged saturation current between $V_{ext} = 450V$ and $V_{ext} = 0V$

$$\Delta I = I_{neg_sat_V450} - I_{neg_sat_V0}$$

The difference of current shows accumulation of charge particle